

Thesis: A Climatology of Inversions

Submitted by
George J. Schewe

Department of Atmospheric Science
Colorado State University
Fort Collins, Colorado

A partial fulfillment of the requirements for the Degree of Master Science.
Fall 1975

**Colorado
State
University**

**Department of
Atmospheric Science**

Paper No. 238

THESIS

A CLIMATOLOGY OF INVERSIONS

Submitted By

George J. Schewe

In partial fulfillment of the requirements

for the Degree of Master of Science

Colorado State University

Fort Collins, Colorado

Fall, 1975

ABSTRACT

A CLIMATOLOGY OF INVERSIONS

Stratifications and analysis of acoustic radar* records are performed for the Ft. Collins area of Colorado. Two months of daily continuous data are utilized from the winter of 1975. Procedures carried out on this data are designed to set up techniques of study that will be of value to climatologists and air pollution specialists, as well as describing a short climatology of Ft. Collins' inversions. Frequencies of occurrence of inversions in time and space are found and stratified in several ways. These include stratification by time of day, thickness, persistence and type of inversion (elevated or surface based). Associations with routine meteorological measurements such as wind speed, wind direction, cloud cover, etc., are also performed. These were done in order to establish relationships and possible control mechanisms and to show the advantages of using acoustic radar in association with other measurements to monitor lower boundary layer phenomena. Finally, CO concentrations, available on a fairly routine basis, were associated with inversion occurrences. This was carried out to show the value of acoustic radar in possible future research and operational pollution studies.

George J. Schewe
Department of Atmospheric Science
Colorado State University
Ft. Collins, Colorado 80523
Fall, 1975

* See Appendix A

ACKNOWLEDGMENTS

The author gratefully acknowledges the guidance and helpful criticisms and suggestions of Dr. Elmar R. Reiter during the preparation of the work described herein. Very special thanks go to Dr. Myron L. Corrin, Dr. Teizi Henmi, Mr. Paul Katen, Mr. Robert Banta and Mr. David Wackter for their many and varied contributions, especially the numerous thought-provoking discussions and technical suggestions.

Mr. Scott Ryden aided significantly in the drafting and data reduction. Mrs. Alice Fields did the majority of the computer programming. Photographic assistance was done by Mr. Duayne Barnhart. The typing of the manuscript was done by Mrs. Grace Holt. A special thanks is also extended to my wife, Mary, for her patience and understanding during this time.

This research was sponsored by Grant GI-44423, National Science Foundation.

TABLE OF CONTENTS

	<u>Page</u>
TITLE PAGE	i
ABSTRACT	ii
ACKNOWLEDGMENTS	iii
LIST OF TABLES	v
LIST OF FIGURES	vi
LIST OF SYMBOLS	x
1. INTRODUCTION	1
2. BASIC CONCEPTS AND PROBLEMS	4
3. MAIN FEATURES OF INVERSION CLIMATOLOGY AT FT. COLLINS	17
4. ASSOCIATIONS WITH METEOROLOGICAL PARAMTERS	40
5. CASE STUDY	65
6. DISCUSSIONS AND CONCLUSIONS	70
REFERENCES	72
APPENDIX A: ACDAR	74
APPENDIX B: χ_{RI}^2 AND χ_{RC}^2	101

LIST OF TABLES

<u>Table</u>	<u>Page</u>
3.1 Thickness of Inversions Versus Base Heights in Categories	31
3.2 Inversion Episodes Longer than 48 Hours	37
4.1 Inversion Parameters Displayed as Functions of Meteorological Variables for Subsequent Analysis	40
4.2 Summary of χ^2_{R1} and χ^2_{RC} for January and February, 1975	42
4.3 Inversion Probabilities with a Given Wind Category	43
4.4 January-February Contingency Table for Elevated Inversions	44
4.5 Thickness vs. Wind Direction for Surface Inversions	46
4.6 Wind Speed Versus Inversion Occurrence	53
4.7 Summary of χ^2 for January and February, 1975	53
4.8 χ^2 Results for 3-Way ANOVA of Wind Speeds, Cloud Cover and Inversion Occurrence	56
4.9 χ^2 Results for 3-Way ANOVA for Wind Speeds, Wind Directions, and Inversion Occurrences	57
4.10 χ^2 Results for 3-Way ANOVA of CO Concentrations, Wind Speeds, and Inversion Occurrences	61
B.1 χ^2_{R1} (Test for Homogeneity)	102
B.2 χ^2_{RC} (No Inversion - Inversion)	103

LIST OF FIGURES

<u>Figure</u>	<u>Page</u>
2.1 Acdar record, November 29, 1974	6
2.2 Nocturnal formation of a valley slope drainage wind	8
2.3 Surface and elevated temperature profiles	9
2.4 Approximate location of Larimer County in northern Colorado	10
2.5 a) Cross Section of Larimer County; b) Topographical map of Larimer County	11
2.6 Annual wind rose, Ft. Collins, Colorado	12
2.7 Streamlines and wind speeds for Ft. Collins for night and day	14
2.8 Acdar records from Ft. Collins, 1-22-75	15
2.9 Computer derived output of analyzed acdar records	16
3.1 Daily frequencies of all inversion occurrences, January and February, 1975	18
3.2 Daily frequencies of surface inversions, January and February, 1975	18
3.3 Daily frequencies of elevated inversions, January and February, 1975	19
3.4 Daily frequencies of elevated inversions, January and February, 1975	19
3.5 Average base heights by month of all inversions	21
3.6 Average thicknesses of all inversions by month	22
3.7 Surface inversion thickness changes (1600-2400 MST)	24
3.8 Surface inversion thickness changes (0000-1600 MST)	25
3.9 Average changes for 0800-1400 MST elevated inversions	27
3.10 Average changes for 1400-2000 MST elevated inversions	28
3.11 Frequencies of occurrence of each base height category, January, 1975	29

LIST OF FIGURES (Cont'd)

<u>Figure</u>	<u>Page</u>	
3.12	Frequencies of occurrence of each base height category, February, 1975	29
3.13	Frequencies of occurrence of thicknesses in the 0-30 meter base height category	32
3.14	Frequencies of occurrence of thicknesses in the 31-50 meter base height category	32
3.15	Frequencies of occurrence of thicknesses in the 51-100 meter base height category	33
3.16	Frequencies of occurrence of thicknesses in the 101-150 meter base height category	33
3.17	Frequencies of occurrence of thicknesses in the 151-200 meter base height category	34
3.18	Frequencies of occurrence of thicknesses in the 201-250 meter base height category	34
3.19	Frequencies of occurrence of thicknesses in the 251-300 meter base height category	35
3.20	Frequencies of occurrence of thicknesses in the 301-350 meter base height category	35
3.21	Frequencies of occurrence of thicknesses in the 351-400 meter base height category	36
3.22	Frequencies of occurrence of thicknesses in the 401-450 meter base height category	36
3.23	Frequencies of occurrence of thicknesses in the 451-500 meter base height category	36
3.24	Frequencies of occurrence of all inversions of certain durations	38
3.25	Frequencies of occurrence of elevated inversions of certain durations	38
3.26	Frequencies of occurrence of surface inversions of certain durations	39
4.1	Wind directions in categories for January and February, 1975	41

LIST OF FIGURES (Cont'd)

<u>Figure</u>	<u>Page</u>
4.2 All inversions counted by associated wind direction and averaged. a) January	47
b) February	48
4.3 Surface inversions counted by associated wind direction and averaged. a) January	49
b) February	50
4.4 Cloud cover, wind speeds and frequency of inversion occurrence	55
4.5 Windspeeds, wind directions and frequency of occurrence of thin and thick inversions associated with them	59
4.6 Windspeeds, wind directions and frequency of occurrence of thin and thick inversions associated with them from 1700 to 0800 MST	60
4.7 Association of [CO], wind speeds and surface inversion occurrences from 1700 to 0800 MST, January, 1975	62
4.8 Association of [CO], wind speeds and surface inversion occurrences from 0800 to 1700 MST, January, 1975	62
4.9 Association of [CO], wind speeds, and elevated inversions from 0800 to 1700 MST, January, 1975	64
4.10 Association of [CO], wind speeds, and elevated inversions from 1700 to 0800 MST, January, 1975	64
5.1 Surface weather map, January 31, 1975	66
5.2 Surface weather map, February 1, 1975	67
5.3 CO concentrations, inversions, and wind field for January from 1600 to February 1 at 0800, 1975	68
A.2.1 Angle dependence of the acoustic backscattering cross section	79
A.3.1 Aerovironment Model 300 module	80
A.3.2 Side view of the antenna, transducer and horn configuration	81
A.3.3 Acoustic transducer	82
A.3.4 Fiberglass cone	83

LIST OF FIGURES (Cont'd)

<u>Figure</u>	<u>Page</u>
A.3.5 Top view of acdar antenna	84
A.3.6 Side view of the acoustic enclosure	85
A.3.7 Convoluted methane foam	86
A.3.8 Acoustic enclosure in operational position	87
A.3.9 Aerovironment Model 300 controls	88
A.4.1 Atmospheric conditions. a) superadiabatic, b) neutral and c) stable	90 91
A.4.2 Daytime convective plumes	92
A.4.3 Nocturnal radiation inversion	94
A.4.4 Subsidence inversion	95
A.4.5 Fog	97
A.4.6 Wind	97
A.4.7 Frontal inversion	98
A.4.8 Diurnal inversion - convective plume cycle	100

LIST OF SYMBOLS

[CO]	Carbon dioxide concentrations
H	Base height of inversions
$\sigma(t)$	Standard deviation as a function of time
σ	Sample standard deviation from regression
β	Slope of regression line
α	y-intercept of regression line
χ_{R1}^2	Chi square test for homogeneity
χ_{RC}^2	Chi square test for multiple rows and columns
\hat{p}_i	Inversion probabilities with directions
$\chi_{critical}^2$	Chi square at a particular confidence level
d.f.	Degrees of freedom
α'	Confidence level
H_0	Initial hypothesis
H_α	Alternate hypothesis
\vec{V}	Total velocity of sound
\vec{C}	Velocity of sound relative to the air
\vec{W}	Velocity of sound relative to the observer
T	Absolute temperature of air
$\sigma(\theta)$	Acoustic backscattering cross section
λ	Acoustic wavelength
θ	Scattering angle
C_v^2	Velocity structure parameter
C_T^2	Thermal structure parameter
$u(x),$ $u(x+r)$	Velocities of different scatterers separated by distance r
$T(x+r)$	Temperatures of different scatterers separated by distance r

LIST OF SYMBOLS (Cont'd)

P	Received power
P_t	Transmitted power
t	Time duration of acoustic pulse
A	Area of antenna
r	Distance to scatterers
τ	Transmittance of atmosphere for acoustic energy
G	Gain factor for acdar unit

1. INTRODUCTION

Slade (1968) describes the atmosphere as a turbulent fluid with a wide variety of perturbations on all space and time scales. Such characteristics as latitude, location within land mass, altitude, slope of the ground, type of soil, nature of ground cover, and proximity to areas of different geographical properties determine the evolution of meteorological changes at a given site in response to large-scale perturbations to which that location is exposed. The response and interrelated nature of changes in several meteorological aspects permit certain of these perturbations that repeat themselves sufficiently often to be studied and categorized.

For the air pollution meteorologist the most important consequence of large-scale fluctuations in the atmosphere occur in the lowest 1 or 2 kilometers, that is, in the planetary boundary layer. Hoxit (1973) defines the planetary boundary layer (PBL) as that portion of the atmosphere in which the wind deviates from gradient or geostrophic flow as a result of the retarding influence of surface friction. The PBL plays a vital role in exchanging momentum, water vapor, and sensible heat between the earth's surface and the free atmosphere above.

Friction-induced vertical motions provide the triggering mechanism for both large scale and mesoscale vertical exchange processes, while local scale events can act as important controls on the dispersion and mixing of atmospheric pollutants in the planetary boundary layer.

One such atmospheric planetary boundary layer phenomenon is the temperature inversion. This can be defined as an atmospheric state in which temperature increases with height. Such a vertical variation

tends to inhibit turbulence and thus to reduce the extent of atmospheric mixing. Temperature inversions are most frequently associated with high pressure regions which are a direct cause of subsiding air and other stability enhancing features.

Because of their direct influence on suppressing the mixing of air-borne pollutants, meteorologists have studied inversion characteristics at several locations. Baynton et al. (1965) associated two soundings of the atmosphere per day at Point Arguello to local wind and temperature regimes. Holzworth (1971) utilized primary station soundings for the contiguous United States and arrived at rough estimates of mixing heights,* and wind speeds, again based on 2 soundings per day. Details of inversion height variations, persistence, coupling with local winds, etc., are lacking and these are details that the air pollution meteorologist needs. In order to increase the resolution of inversion studies many more profiles of the atmosphere are needed per day.

The objective of this study will be to obtain a description of the variations in height and thickness of local inversion events. Once these patterns of occurrence are established, association of low level inversions with wind direction, wind speed, cloud cover and CO concentrations will be performed to specify coupling mechanisms with other meteorological parameters, and point out possible local inversion climatological controls.

The method employed is the collection of data by a monostatic Acoustic Echo Sounder (see Appendix A), with subsequent analysis of

* Maximum heights to which environmental air from the earth's surface is mixed into the air above.

chart recordings. Half-hour average heights of low-level inversions are used giving 48 possible readings per day per event. Wind and temperature analog records from the Ft. Collins weather station are analyzed and processed by computer. Contingency tables, frequency distributions, and correlation statistics are carried out by computer. Interpretations and conclusions concerning the climatology of inversions and local climatic controls are based on results of these data stratifications.

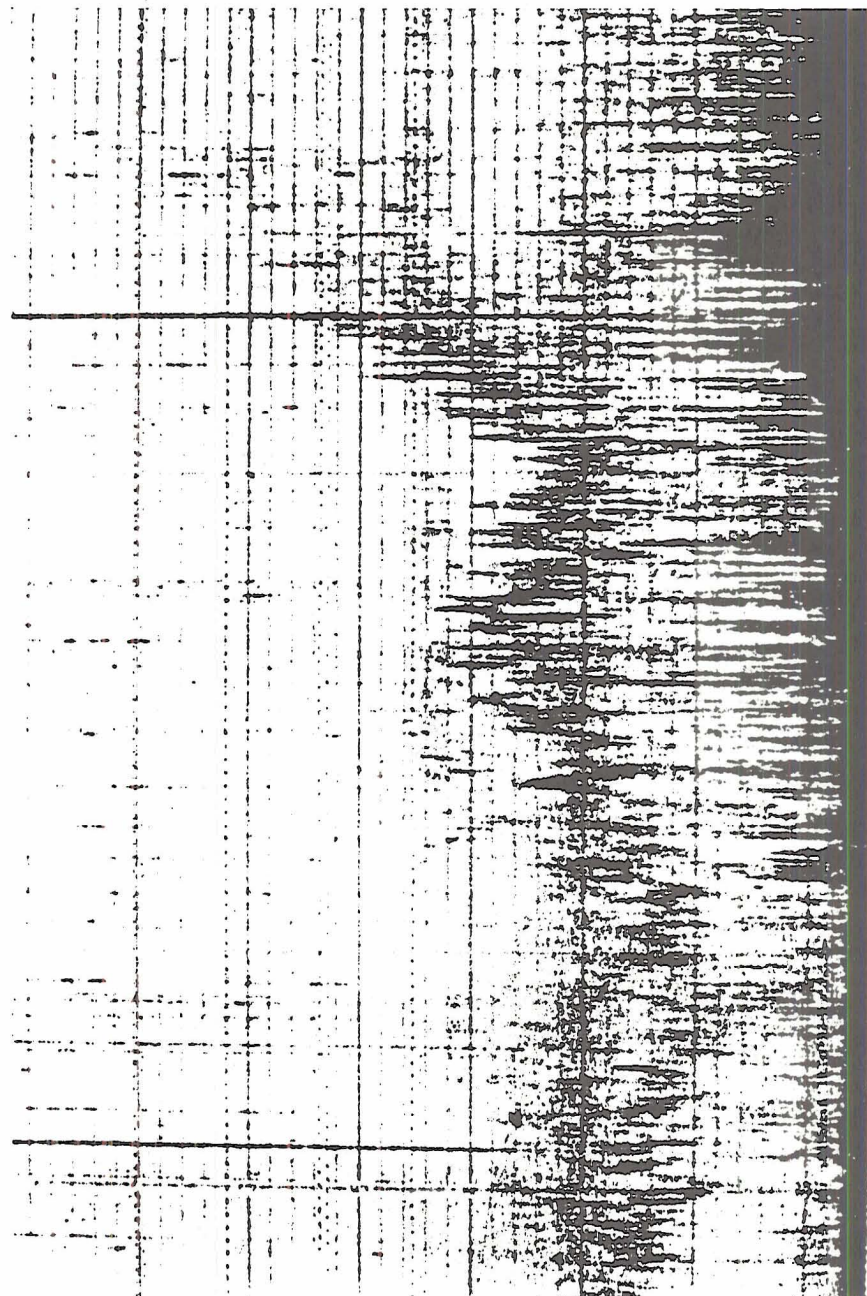
2. BASIC CONCEPTS AND PROBLEMS

Hosler (1961) shows the percentage frequency (percent of total hours) of inversion conditions in the contiguous United States, with the Larimer County region of Colorado near the 48% isopleth in winter. With the presence in Larimer County of other factors (light winds, snow cover, clear nights) which can enhance stability, inversion estimates of Hosler based on extrapolated radiosonde flights are at best rough. Because these estimates are inadequate for air pollution modelling and forecasting, increased resolution of daily profiles would be required.

On-site continuous monitoring of the lower boundary layer would be the most desirable way of examining inversion and non-inversion events. With radiosonde soundings not available and too costly for the scope of the proposed study, an Acoustic Echo Detection and Ranging system (acdar) was utilized to give continuous real time estimates of inversion and convective plume characteristics up to a height of 500 meters. A monostatic acdar unit typically emits a short audible pulse of sound collimated by an antenna and transmitted into the atmosphere. Temperature variations then scatter the acoustic waves which the system recollects and records as the intensity and time delay of the returned signal. Because acoustic echoes actually result from index of acoustic refraction changes in the atmosphere (which can be related to temperature changes), acdar "sees" volumes of air where temperature variations are the greatest. Strong temperature gradients induced by turbulence can be found in thermal plumes; similar gradients occur in temperature inversions. Both can be monitored by acdar. A typical acdar record is shown in Figure 2.1, where the abscissa is marked in hours and the ordinate,

Figure 2.1. Acdar record (time in hours, height in meters): At 0700 three layers are distinguishable, a surface radiation inversion and two slightly separated elevated inversions near 125 m and 150 m, respectively. The stable layer at the surface joins the two layers aloft at around 0800 as ground thermals begin to appear and drive the inversion aloft. The convection also advects the warm turbulent air from the surface into the cooler stable air aloft. The consistent waviness pattern from 0800 to 1030 indicates good mixing beneath the inversion layer which is caused by the presence of vertical thermal structures pushing up the inversion intermittently. Finally, about 1130 the surface convective activity has succeeded in penetrating and mixing the inversion aloft with environmental air enough that the inversion lid is broken, and free mixing to higher levels can occur. The dark vertical lines at 0715 and 1045 are caused by noise from low flying aircraft over Fort Collins, and the short dark vertical lines which appear from time to time are from barking dogs, birds or occasional nearby automobiles.

Figure 2.1. Acdar record (time in hours, height in meters): At 0700 three layers are distinguishable, a surface radiation inversion and two slightly separated elevated inversions near 125 m and 150 m, respectively. The stable layer at the surface joins the two layers aloft at around 0800 as ground thermals begin to appear and drive the inversion aloft. The convection also advects the warm turbulent air from the surface into the cooler stable air aloft. The consistent waviness pattern from 0800 to 1030 indicates good mixing beneath the inversion layer which is caused by the presence of vertical thermal structures pushing up the inversion intermittently. Finally, about 1130 the surface convective activity has succeeded in penetrating and mixing the inversion aloft with environmental air enough that the inversion lid is broken, and free mixing to higher levels can occur. The dark vertical lines at 0715 and 1045 are caused by noise from low flying aircraft over Fort Collins, and the short dark vertical lines which appear from time to time are from barking dogs, birds or occasional nearby automobiles.



400-

300-

200-

100-

Height above Surface(meters)

0700

0800

0900

1000

1100

Time of Day(hours M.S.T.)

(November 29, 1974)

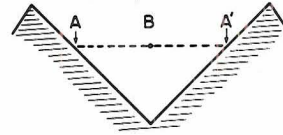
height, in meters. Cronenwett (1972), Hall (1972), Little (1969), and McAllister (1968) give good reviews of acdar and its flexibility in monitoring lower atmospheric phenomena. (For more details see Appendix A.)

Acadar, then, is able to yield a great deal of information about the temporal variation of inversions. To make use of this information beyond the accumulation of inversion statistics, associations with winds on a local scale will be developed in this dissertation. Synoptic and regional influences can have a definite effect on inversion climatology (especially along the Front Range of the Rockies).

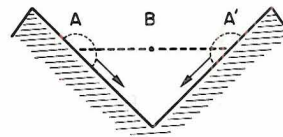
Paddock (1959) describes several common weather types along the Front Range, with emphasis on wind regimes, moisture, time of year, and pressure system positions. Slade (1968) and Schroeder and Buck (1970) suggest how general features of terrain can effect inversion characteristics in mountainous and hilly surroundings. Banta et al., (1975), Buettner (1967), Paddock (1959), and Riehl and Herkhof (1970a,b) put forth detailed descriptions of the influences of terrain and synoptic events on local wind patterns, temperatures, etc.

According to Defant (1951) a typical nocturnal wind in a mountainous region occurs when the slopes of the valley sides become cooler than the free air at the same level over the valley (see Figure 2.2a). The slopes cool by radiation (IR loss) and the air adjacent to the slopes cools by conduction and convection from the surface. The cooler air sinks katabatically down the slopes of the valley because of its negative buoyancy (denser air with respect to the free air at its own level) (Fig. 2.2b) and a downslope wind is established (Fig. 2.2c). If in

a) Air at slopes (A') cool by IR loss through convection and conduction at the surface, while free air at the same level does not cool (B).



b) Cooler air (A') sinks down the slopes because of negative buoyancy with respect to the free air (B).



c) Downslope wind is established.

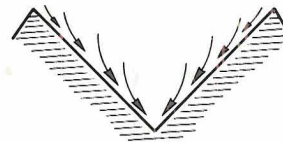


Figure 2.2. Nocturnal formation of a valley slope drainage wind (after Defant, 1951).

addition the valley is sloped, the sinking air will continue in the same fashion toward the lower end of the valley.

When this cold sinking air drains into a basin or valley that does not have good outflow or does not "leak" rapidly, there is a buildup of cooler air in the basin. Coupled with radiational cooling at the surface, the layer of dense cool air can build up and create a temperature inversion. Typical temperature profiles and resultant stable layers for this condition are shown in Figure 2.3.

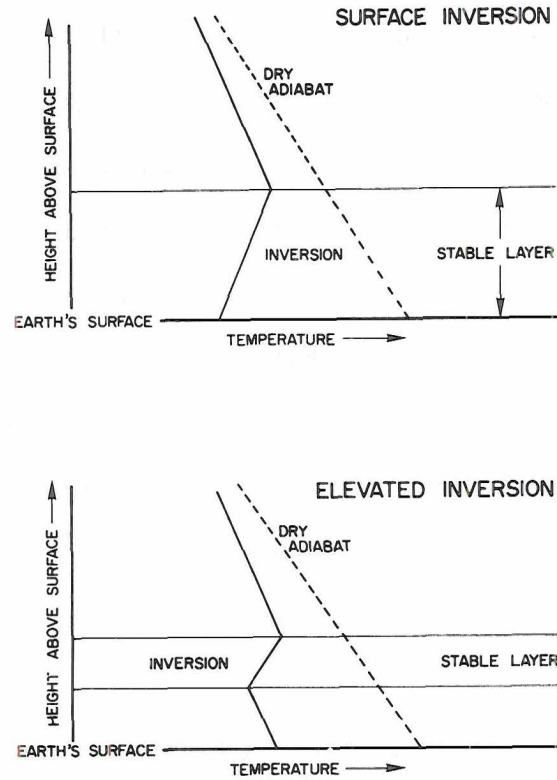


Figure 2.3. Generalized surface and elevated temperature profiles and stable layers. Dotted line is adiabatic.

This mountain-valley wind flow and the resultant nocturnal inversions are influenced by synoptic conditions. Under anticyclonic conditions (strong subsidence and light winds) local meteorological regimes are best developed, while cyclonic systems may or may not change local regimes depending upon the associated synoptic features.

Local Terrain and Climate

Fort Collins is located in the northern part of central Colorado near the Colorado-Wyoming border (See Figure 2.4). It is situated at

approximately 5000 ft. above sea level with the front range of the Rocky Mountains to the west and gently sloping farmlands to the east (see Figures 2.5a and b). Rainfall is sparse with the majority coming in the form of summertime convective storms. The high plains meteorological picture simplifies in winter, which is dominated by an anticyclonic pattern over the western states with associated light winds, subsidence and clear skies. Under these conditions the atmosphere tends to be stably stratified (vertical turbulence suppressed), with temperature inversions near the ground at night. Marked warming near the surface on clear days (the mean daily temperature range even in mid-winter is near 30°F over the Colorado plains) causes increased convective activity and, therefore, increased winds and turbulence as the stable stratification is weakened.

Seasonal wind patterns shown in Figure 2.6 indicate that preferred directions are the north-north-west (335°) and south-south-east (155°).



Figure 2.4. Approximate location of Larimer County in northern Colorado.

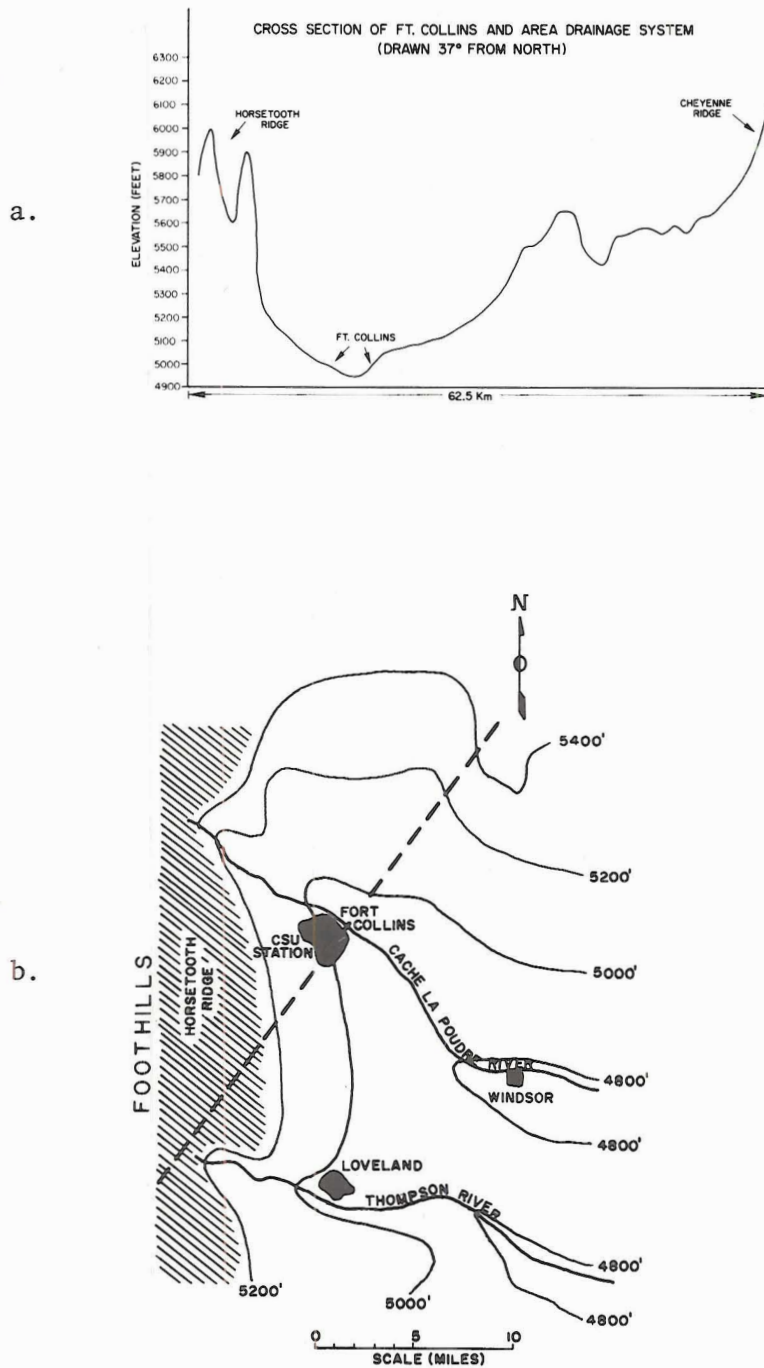


Figure 2.5. (a) cross section of Larimer County taken at the dotted line in b. showing the front range of the Rockies to the west and gradual rise of high plains to the east. (b) map showing main terrain features and contours around Ft. Collins, and location of adcar site (CSU Station in map)(after Riehl and Herkhof, 1970b).

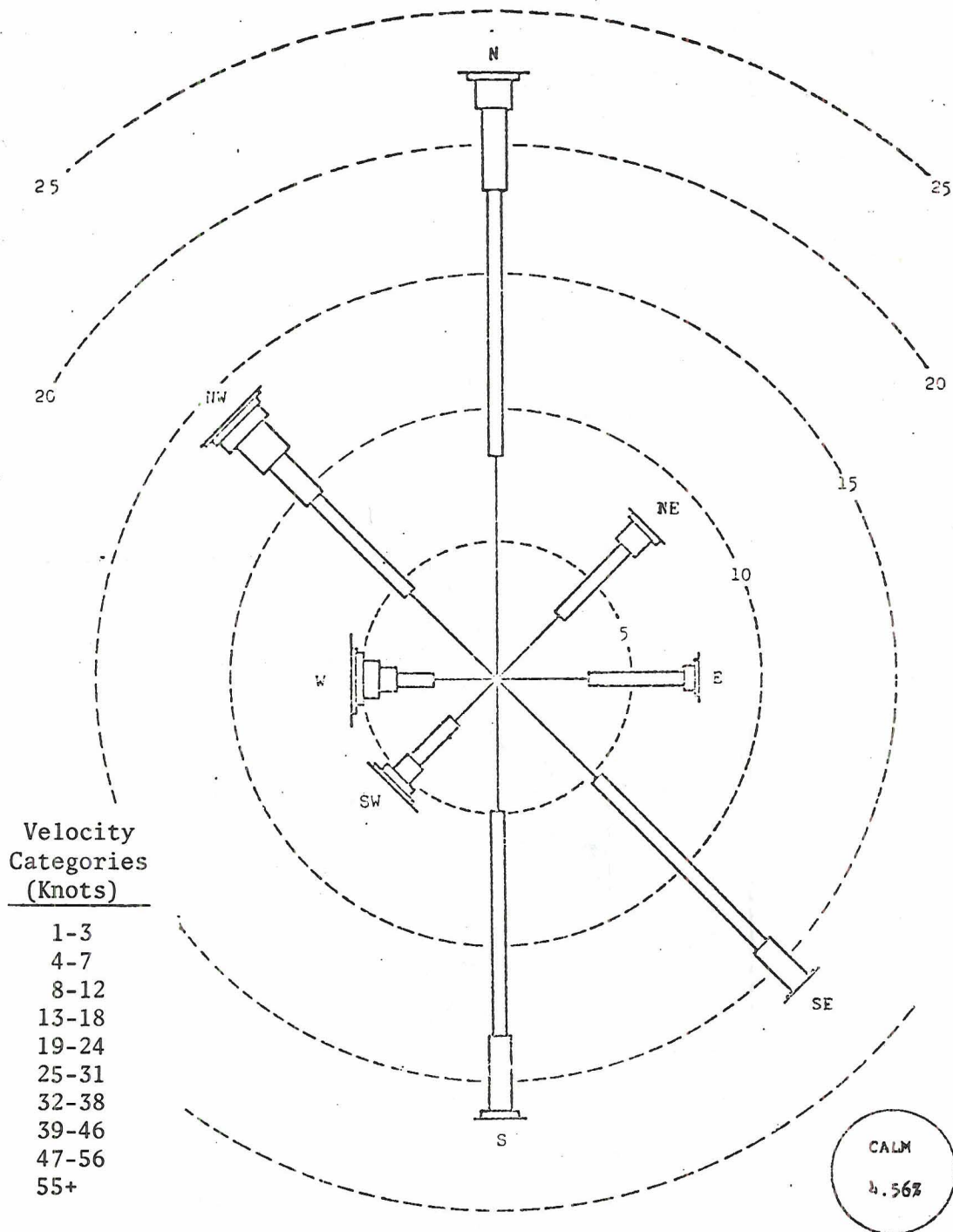


Figure 2.6. Annual wind rose, Ft. Collins, Colorado, 1954-1963 (42,510 observations). Wind speed classes as indicated in the diagram (Samson, 1965).

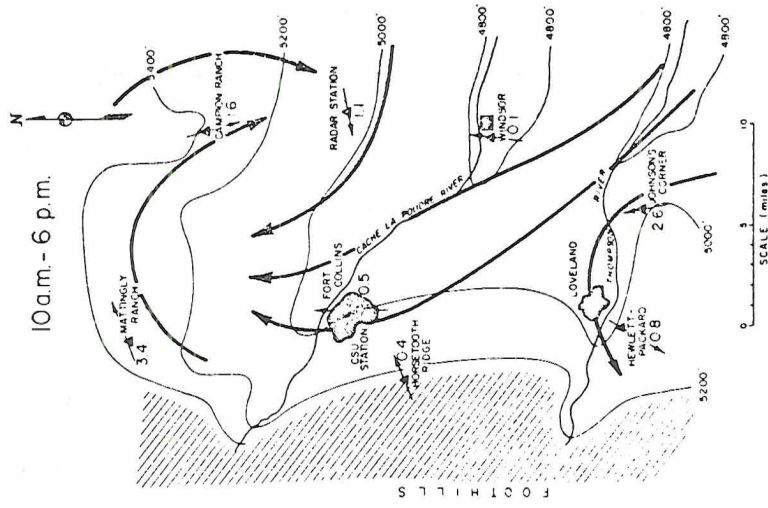
This agrees with the pendulum-type of reversal from day to night in wind direction as proposed for Larimer County by Riehl and Herkhof (1970) (see Figure 2.7a and b) and discussed as the drainage winds system by Buettner (1967). Other dominating wind systems are from chinook winds characteristically flowing in the lee of the Rockies from the west and northwest, and from synoptic frontal passages.

Data Collection and Reduction

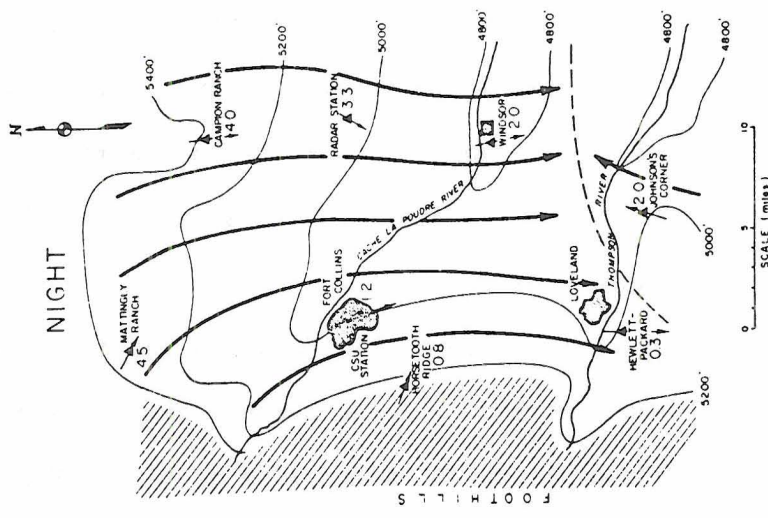
The instrument employed to obtain all acdar measurements was the Aerovironment Model 300 Acoustic Echo Sounder (see Appendix A, Section 3). The period from 1-9-75 to 2-28-75 was used as the primary acdar data source for analysis. This period was relatively noise free because of the location, whereas several other locations were very noisy and acdar records were uninterpretable (acoustic screen used around antenna did a better job of damping out side lobes and ambient noise than did bales of hay).

The data consists of charts of returned echoes from temperature variations aloft with the height and time of relative intensities of the echo region being displayed. The time axis is continuous with one sounding up to 500 meters approximately every 7 seconds. Intensity of echo regions could not be used because of calibration and mechanical difficulties inherent to the instruments. For this reason height and time are the only two elements utilized.

Figure 2.8 shows an acdar record. This data was reduced by averaging heights over half-hour periods. These average heights were recorded on the computer and plotted as a function of time. Figure 2.9 shows the results of such a data reduction. The region between the dotted lines in Figure 2.9 corresponds to the whole of Figure 2.8.



b.



a.

Figure 2.7. Resultant streamlines and wind speeds for: a) nighttime (8 p.m. - 8 a.m.); and b) daytime (10 a.m. - 6 p.m.). (After Riehl and Herkhof, 1970b).

All other data used in this study including wind speeds, wind directions, cloud cover, and CO concentrations were collected from routine measurements at Ft. Collins stations.

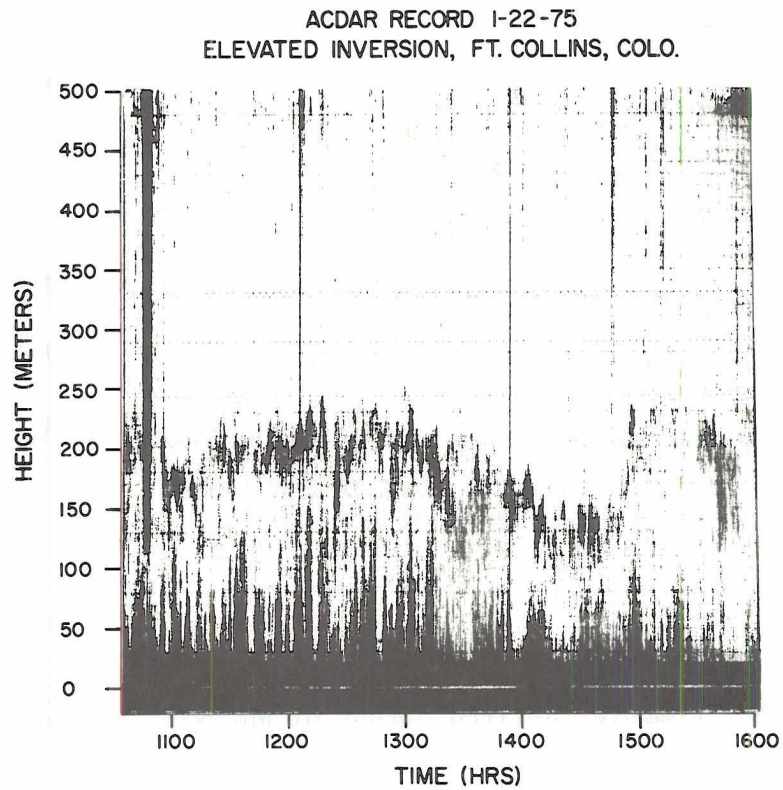


Figure 2.8. Typical record from acdar system, Ft. Collins, Colorado.

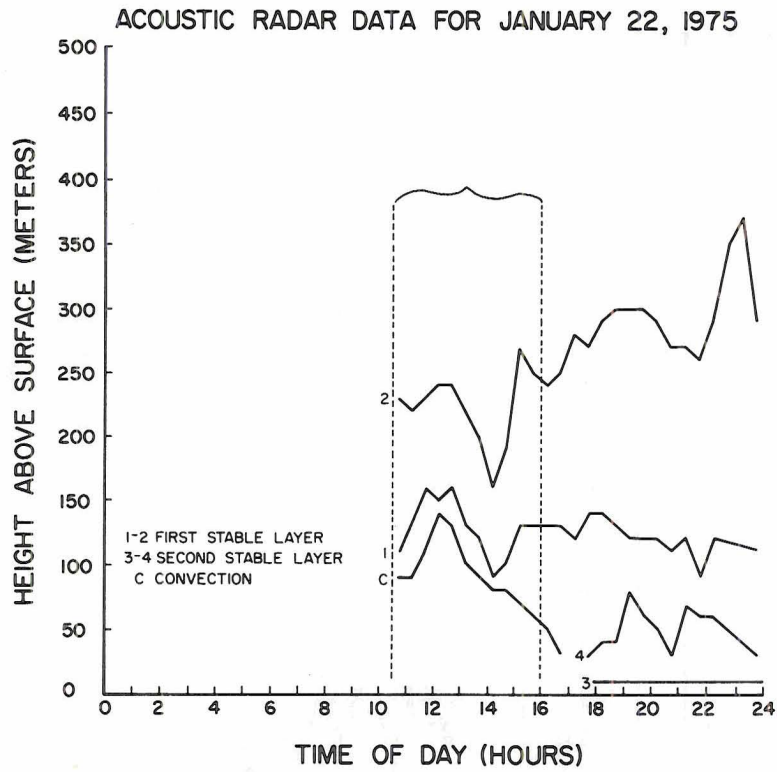


Figure 2.9. Computer derived output of analyzed acdar records.

3. MAIN FEATURES OF INVERSION CLIMATOLOGY AT FT. COLLINS

Average frequencies of inversions at Ft. Collins, are presented in Figures 3.1 through 3.4 for January and February 1975. Daily trends of all inversion occurrences indicate higher frequencies of events in the nighttime hours than in the daytime (Figure 3.1). This agrees well with physical considerations. Nocturnal inversions in wintertime occur as ground cooling and general subsidence are more frequent. Daytime convection, however, associated with clear skies tends to reduce the frequency of occurrence of daytime inversions. Figure 3.1 exhibits similar daily trends for both months, but February shows a higher frequency of occurrence of nighttime inversions than January, while January has slightly higher frequencies of daytime inversions.

Analysis was performed to further differentiate between elevated and surface based inversions. Results are presented in Figure 3.2 and 3.3. In the surface based inversion distributions we can see the effects of nocturnal cooling in that the surface inversion frequencies are high. Also evident is the near absence of surface inversions from 1000 to 1600 hours showing the influence of convective cells which break or push up surface based inversions. Likewise, February had a higher frequency of nocturnal inversion events.

With the high frequency of surface inversions at night and low frequency in day we can expect a peak of elevated inversions sometime near midday. As can be seen in Figure 3.3, the highest frequencies of elevated inversions occur slightly before midday, at 1100 hours. This can be explained by close examination of acdar soundings and noting that as early morning thermals begin to push surface or low lying inversions

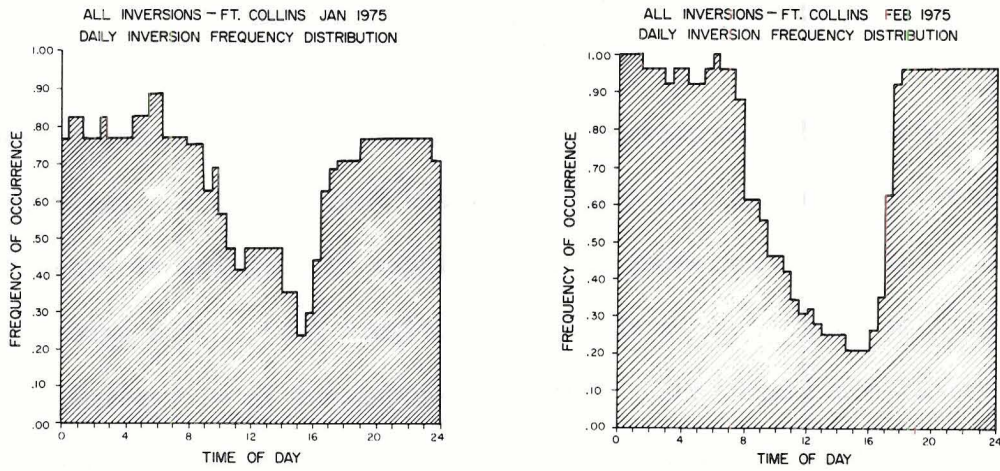


Figure 3.1. Daily frequencies of all inversions (elevated and/or surface) based on January and February, 1975 occurrences.

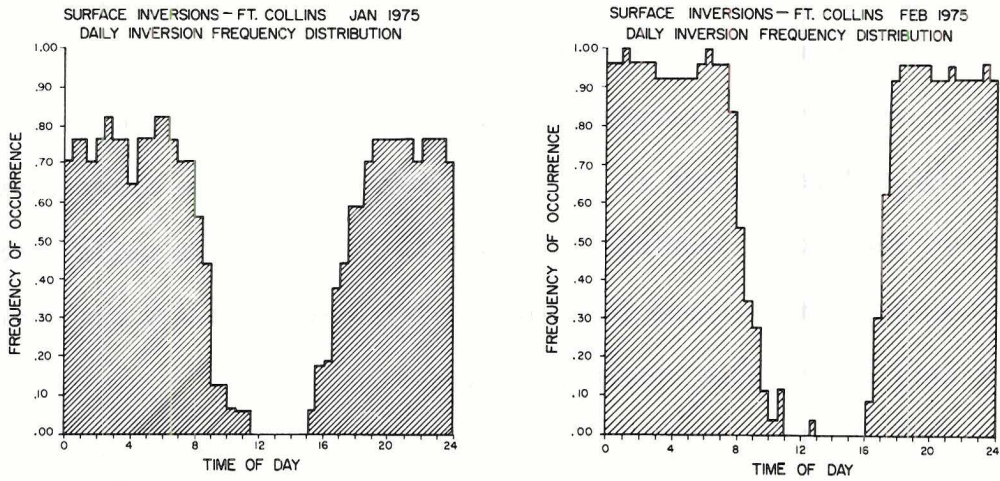


Figure 3.2. Daily frequencies of surface inversions based on January and February, 1975 occurrences.

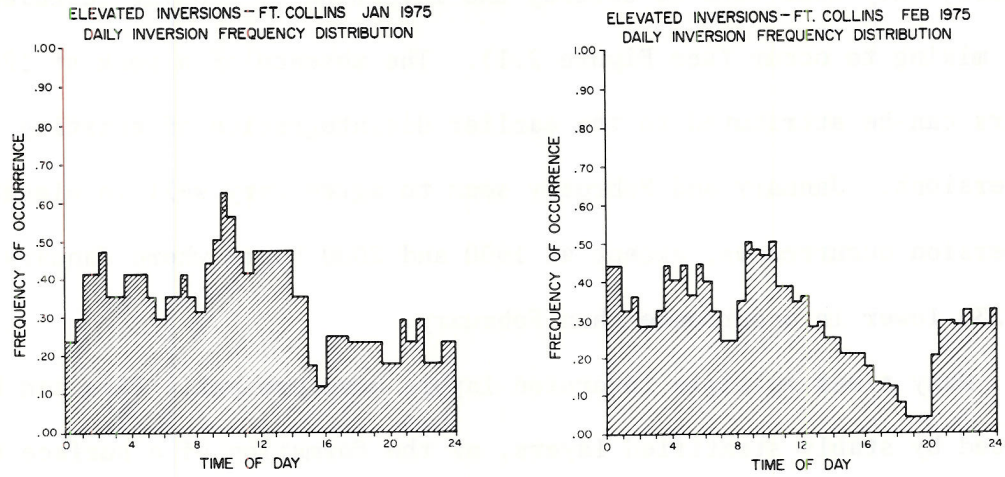


Figure 3.3. Daily frequencies of elevated inversions based on January and February, 1975 occurrences.

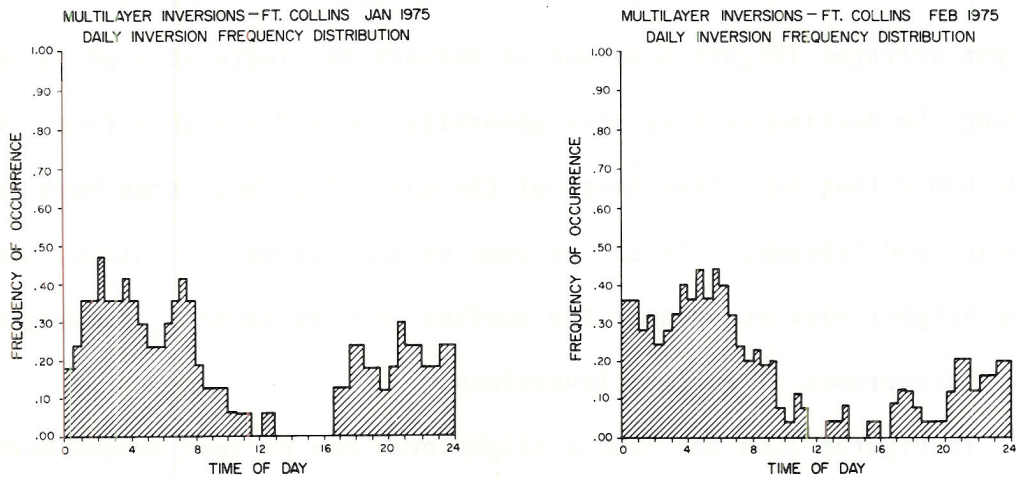


Figure 3.4. Daily frequencies of multilayer inversions based on January and February, 1975 occurrences.

upward, they also tend to destroy the inversion by causing turbulence and mixing to occur (see Figure 2.1). The absence of a peak at 1200 hours can be attributed to the earlier disintegration of existing inversions. January and February seem to agree very well in elevated inversion occurrences, except at 1900 and 2000 hours where January is 20-23% lower in occurrence than February.

Many times multiple inversion layers were present. This can be caused by stably stratified layers, or the formation of a surface based inversion below an elevated inversion. Figure 3.4 shows the frequency of occurrence of these types of multilayer inversions. For both January and February a maximum occurred near 0400 hours and a minimum in the early afternoon.

For each month of data, average base heights and average inversion thicknesses were calculated. These were founded on all inversion events each half-hour, that is, surface inversions and elevated inversions. Averages for each half-hour are shown in Figures 3.5 and 3.6. The base height averages (Figure 3.5a and b) reflect the influences of thermals during the daytime as they were generally 100-150 m higher from 1100 to 1600 hours than all other hours of the day. This held true both for January and February. As can be seen by the scatter of points, many base heights were at or near the surface ($H < 30$ meters), showing the heavy occurrence of surface inversions.

In Figures 3.6a and 3.6b a slight peak can be seen around early afternoon in inversion thicknesses. Because there were almost no surface inversions occurring at this time (see Figure 3.2) one possible conclusion is that afternoon elevated inversions were thicker than nocturnal surface inversions. Generally the difference, however, was

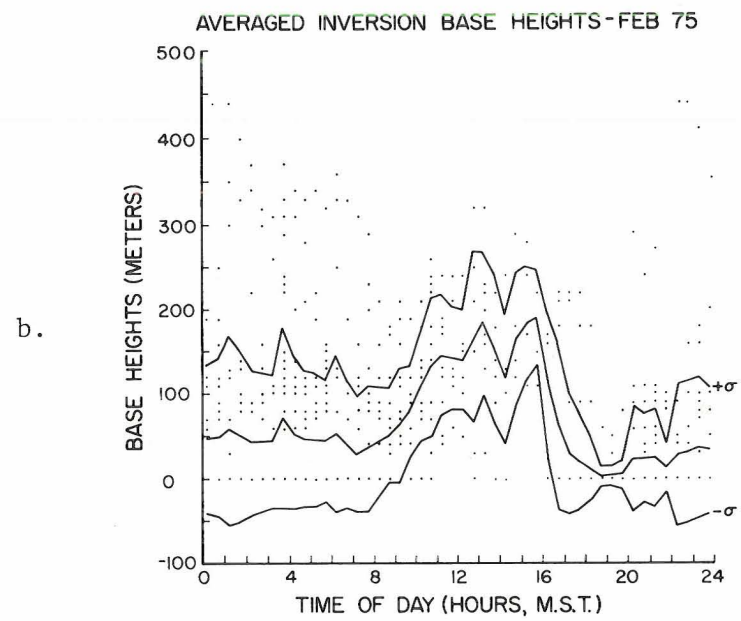
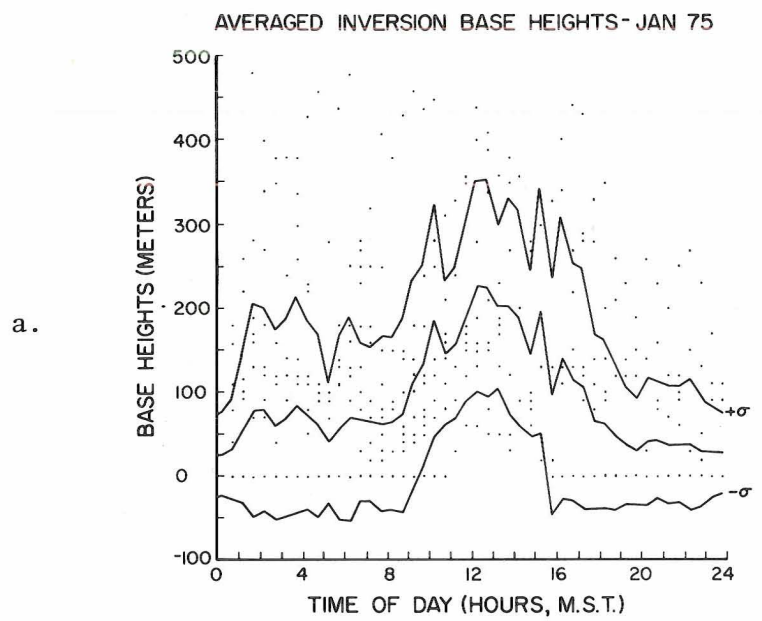


Figure 3.5. Average base heights of all inversions (solid center line) and $\pm\sigma(t)$ from each average height. Individual data are plotted as points. Points at 0 meters can represent more than one point.
 a) January, 1975. b) February, 1975.

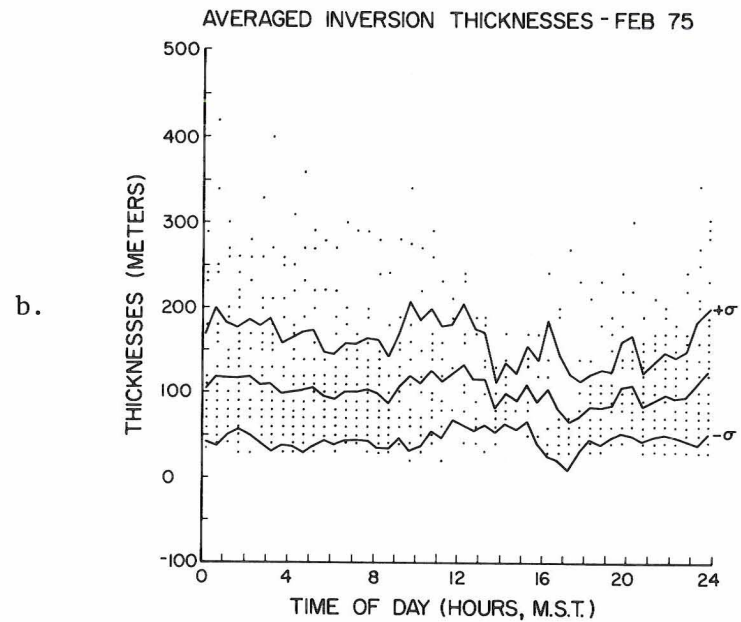
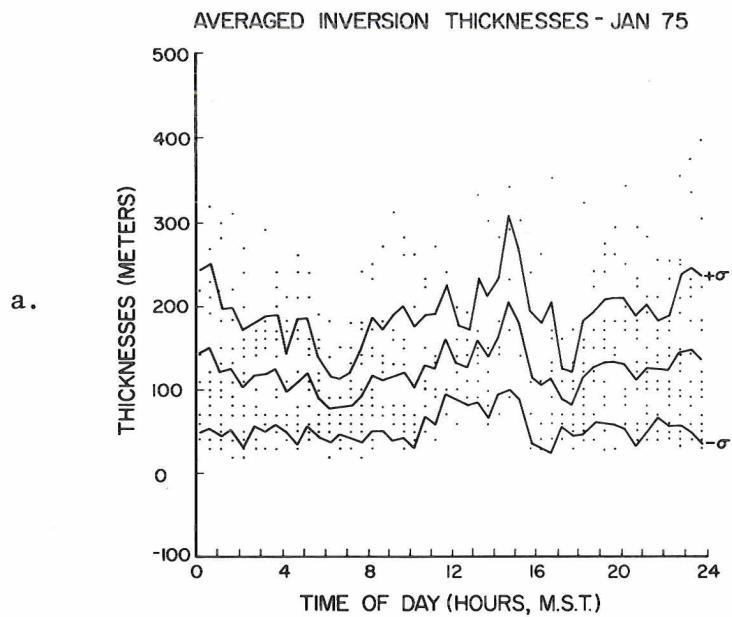


Figure 3.6. Average thicknesses of all inversions (solid center line) and $\pm\sigma(t)$ lines. Actual thickness data are plotted as points. a) January, 1975. b) February, 1975.

only on the order of 50-75 meters and this was within the $\pm\sigma$ values calculated (see $\pm\sigma$ lines on each figure).

Of major interest in the establishment of an inversion climatology is the growth or decay of surface inversions whether caused by surface radiation or cold air drainage. Regression lines and $\pm\sigma$ lines were solved for the early evening and early morning time periods. Figures 3.7 and 3.8 give the results of average thicknesses and regression lines of thickness changes.

Early evening plots (Figure 3.7a and b) for January and February show similar results, where surface inversion thickness increases with time. These increases can be attributed to radiational cooling or the descending and reconnection of elevated daytime inversions with the surface as seen at times in the acdar records. Slopes, y-intercepts and σ values are indicated in each figure.

For the 0000 to 0800 MST plots (Figures 3.8a and b) negative slopes are noted showing a decrease in surface inversion thickness toward sunrise. In many acdar records with inversions present in this time period, surface inversions often split into a surface and an elevated inversion thereby accounting for the apparent decrease in surface inversion thicknesses. The σ 's calculated here and in subsequent regression analyses are called the "sample standard deviation from regression". These σ 's are found by dividing the sum of the squares of deviations from regression by $m-2$ (degrees of freedom) and then taking the square root.

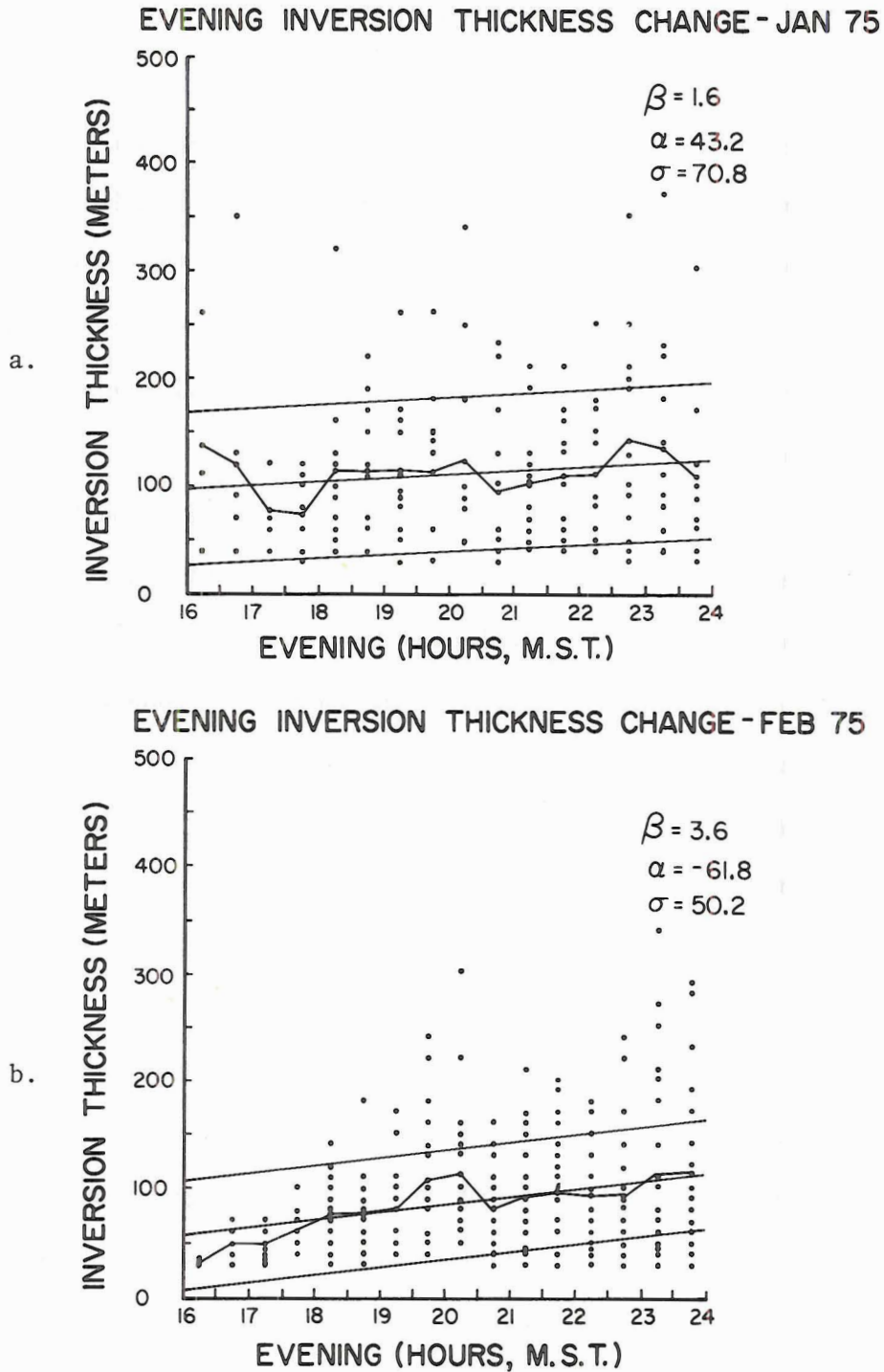


Figure 3.7. Surface inversion thickness changes including average heights (crooked line), regression lines (of all data), $\pm\sigma$ lines for: a) January, 1975 and b) February, 1975, from 1600 to 2400 MST, Ft. Collins. (β , m/.5 hr; α , meters; σ , meters).

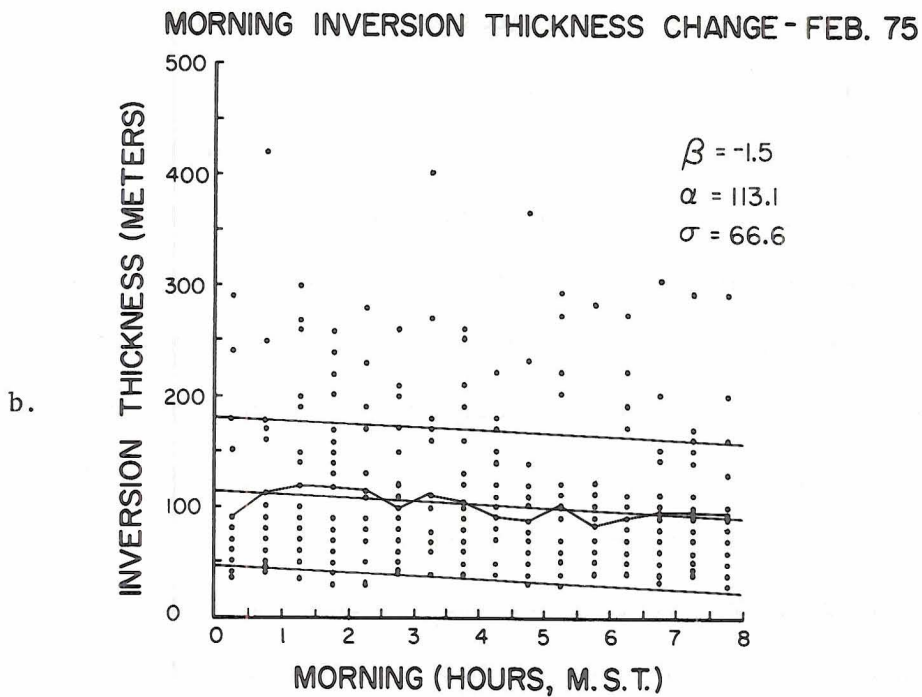
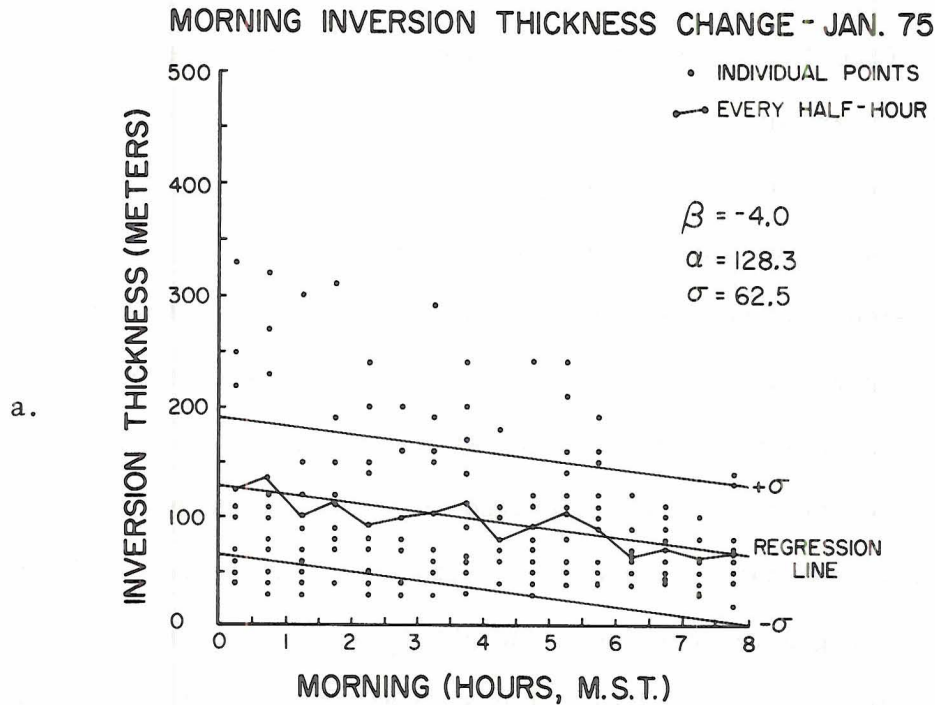


Figure 3.8. Surface inversion thickness changes including average heights (crooked line), regression lines (of all data), $\pm\sigma$ lines for: a) January, 1975 and b) February, 1975, from 0000 to 1600 hours MST, Ft. Collins. (β , m/.5 hr; α , meters; σ , meters).

Another characteristic feature of inversion behavior is the early morning (0800-1300) and late afternoon (1400-2000) rise and fall of elevated inversions. Figures 3.9a and b and 3.10a and b show the results for January and February at Fort Collins of an analysis of elevated inversion base heights in daytime.

Apparent for each month in Figures 3.9a and b is the rise of the elevated inversions in the morning. For January the rise is approximately 19 meters per hour starting at an average of 90 meters.

In the afternoon fewer elevated inversions occurred but nevertheless sufficient data was accumulated to note that here the elevated inversions begin to decrease in height (Figure 3.10a and b). This is probably due to increased cloudiness in afternoons and decreased thermal activity at the surface. The regression lines for afternoon elevated inversions displayed negative slopes of approximately -6.5 meters per hour for January and -10.8 meters per hour for February.

In previous sections no joint consideration was given to thickness and height above surface. In order to find events which occur most frequently in terms of base height and thickness, the acdar analysis included counting events within categories. Categories were every 50 meters up to 500 meters, except for 0-50 base height category which was subdivided into 0-30 and 30.1-50 meters.

The 0-30 meters category for base heights was counted as surface inversions because of detection limits on the acdar system. Figures 3.11 and 3.12 show the frequency of occurrence of each base height category described above for January and February 1975. The surface

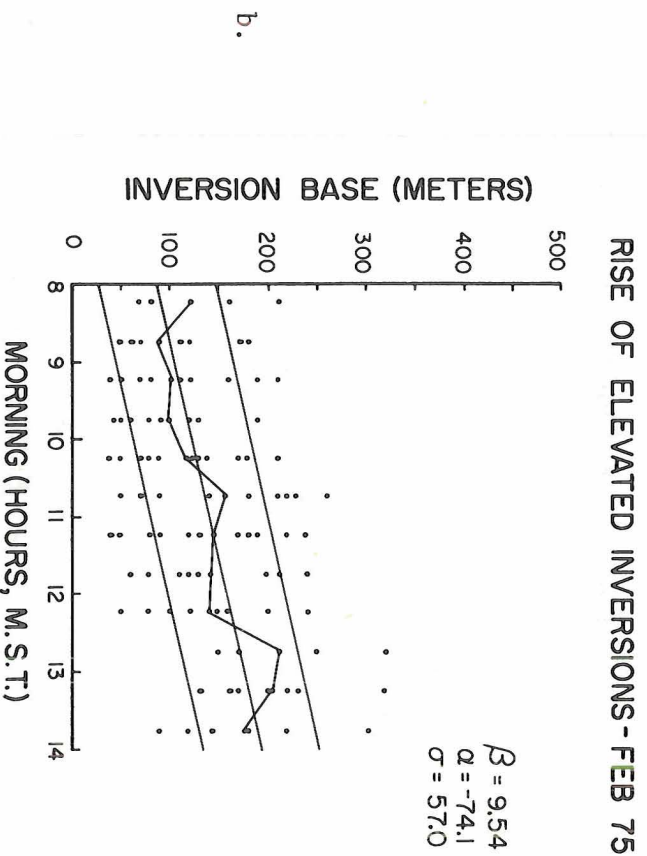
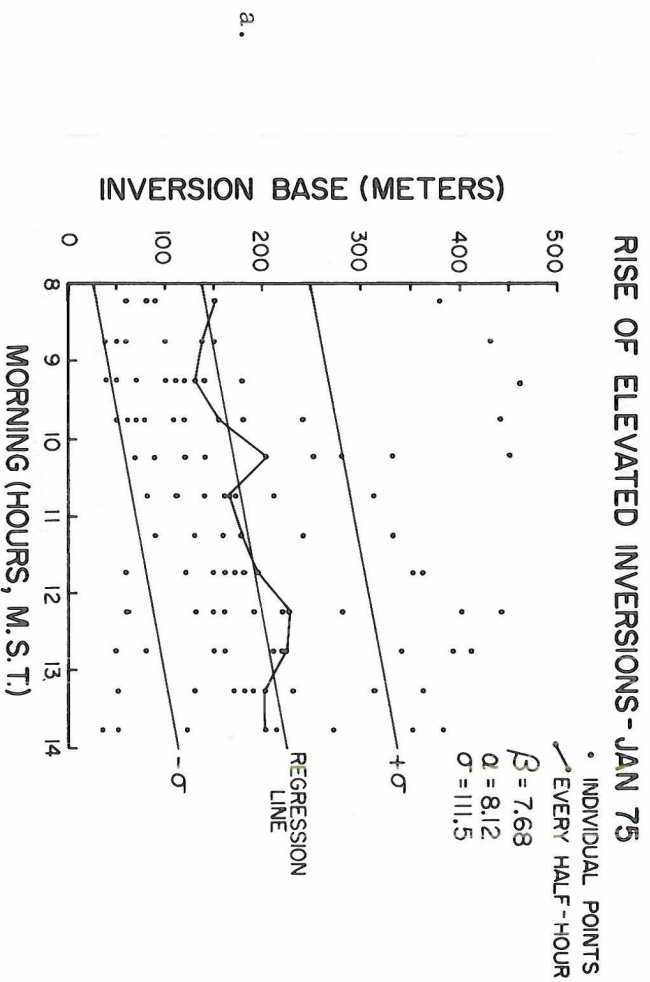
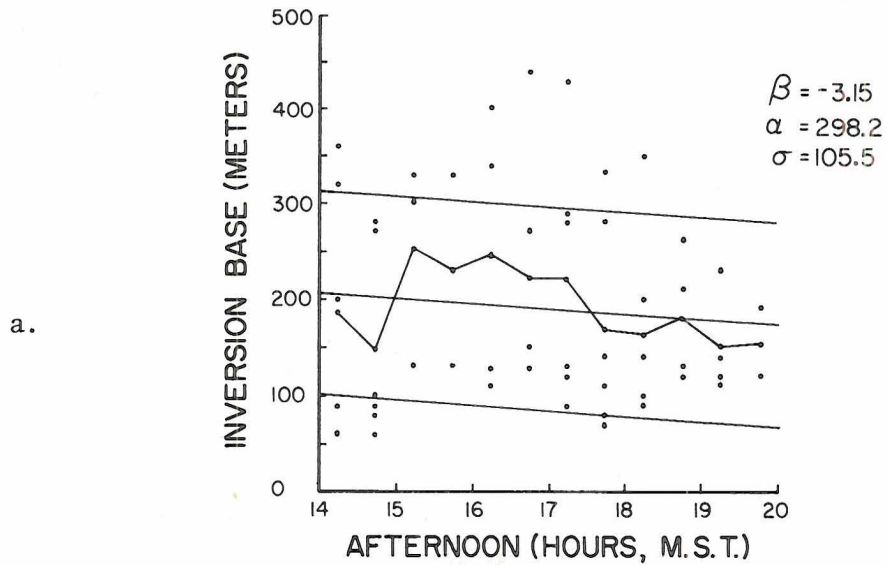


Figure 3.9. Averages changes, regression lines (for all data), to and data points for morning elevated inversion base heights for: a) January, 1975 and b) February, 1975. (β , meters/.5 hr; α , meters; σ , meters).

FALL OF ELEVATED INVERSIONS - JAN 75



FALL OF ELEVATED INVERSIONS - FEB 75

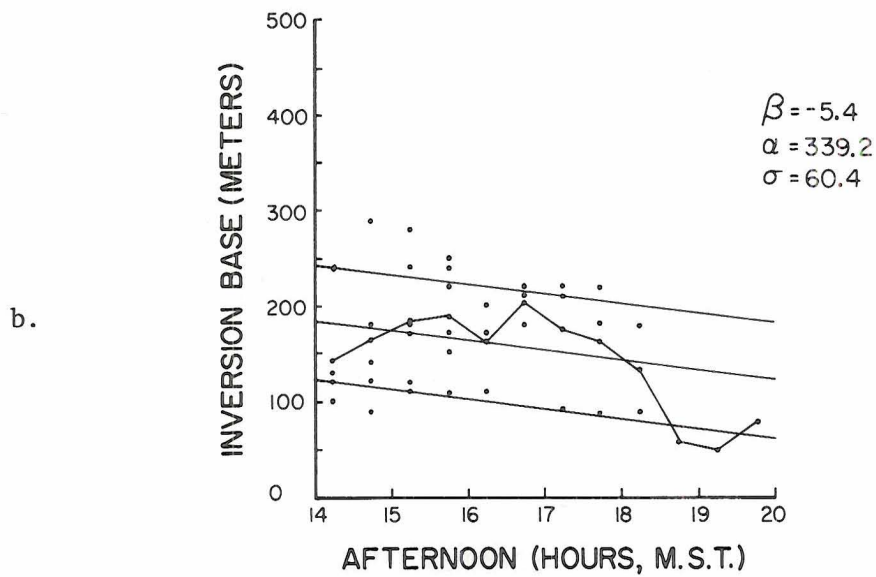


Figure 3.10. Average changes, regression lines (for all data), $\pm\sigma$ and data points for afternoon elevated inversion base heights for: a) January, 1975 and b) February, 1975. (β , meters/.5 hr; α , meters; σ , meters).

inversion frequencies were 58% for January and 67% for February. Both histograms tail off similarly with very few inversions occurring at the higher base heights.

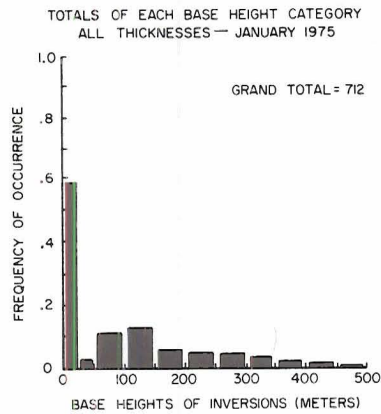


Figure 3.11. Frequency of occurrence of each base height category, January.

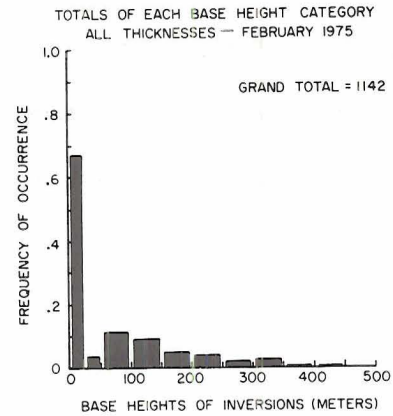


Figure 3.12. Frequency of occurrence of each base height category, February.

Table 3.1 shows the actual values tabulated for each month in each cell. Again evident is the great number of inversions based below about 200 meters and less than 250 meters in thickness. Hourly tables for January (not presented) indicate that most of the surface inversions occur in the early morning and late evening with few elevated inversions in these hours. Elevated, mid-thickness category inversions are the usual type seen in daytime hours. In February, however, the pattern of inversion occurrence is slightly different. Early morning surface events are generally capped by 50-150 m elevated inversions, which cause thicker elevated inversions in the daytime hours.

Histograms of all inversions in each base height category are shown in Figures 3.13 through 3.23. For each frequency plotted, the total

number of cases in that base height category is used as the normalizing factor. These totals and also the contribution of the category to the total number of inversions for the month are presented in each figure.

For both months of data, even with a differing number of events for each histogram, the general patterns match very well for every base height. Peaks of thickness occurrence for each plot lie between 50-200 meters showing the predominance of this thickness of inversion over thicker ones at almost every base height.

TABLE 3.1
 Thickness of Inversions Versus Height of Base of Inversions in Categories
 With Number of Occurrences in Each Cell

January	Thickness Categories (meters)									
	0-50	50-100	101-150	151-200	201-250	251-300	301-350	351-400	401-450	451-500
0-30	107	152	69	39	23	10	7	1	0	0
31-50	2	3	7	1	1	1	1	0	0	0
51-100	4	26	18	9	7	6	1	0	0	0
101-150	10	25	22	21	7	2	0	1	0	0
151-200	1	10	16	3	2	3	4	0	0	0
201-250	0	4	10	6	2	4	0	0	0	0
251-300	1	6	4	4	5	0	0	0	0	0
301-350	0	5	3	10	0	0	0	0	0	0
351-400	0	1	11	0	0	0	0	0	0	0
401-450	0	10	0	0	0	0	0	0	0	0
451-500	4	0	0	0	0	0	0	0	0	0
February										
0-30	199	341	103	63	23	23	2	2	1	0
31-50	3	11	10	6	4	3	0	0	0	0
51-100	8	44	31	21	9	4	1	0	0	0
101-150	20	41	20	12	5	0	2	0	0	0
151-200	5	20	19	5	3	0	0	0	0	0
201-250	8	19	12	1	0	0	0	0	0	0
251-300	2	4	3	1	1	0	0	0	0	0
301-350	2	6	4	4	0	0	0	0	0	0
351-400	0	1	4	0	0	0	0	0	0	0
401-450	0	6	0	0	0	0	0	0	0	0
451-500	0	0	0	0	0	0	0	0	0	0

Base Height Categories (meters)

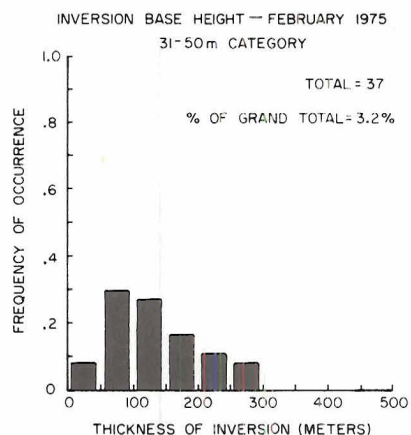
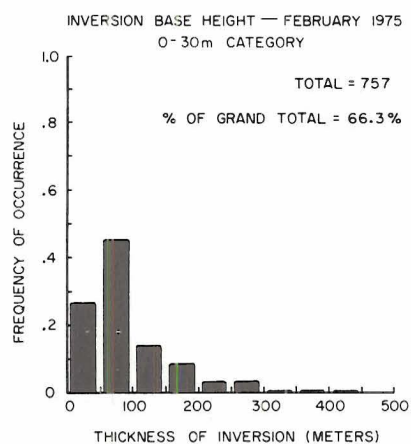
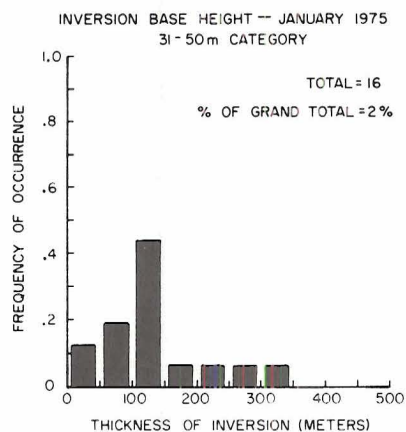
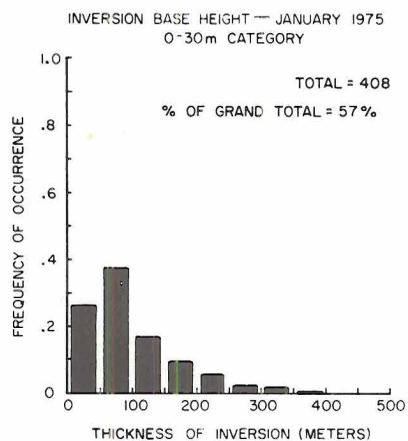


Figure 3.13: Frequencies of occurrence of thicknesses in the 0-30 meter base height category.

Figure 3.14: Frequencies of occurrence of thicknesses in the 31-50 meter base height category.

Figures 3.13 through 3.23: These are graphical representations of each row of Table 3.1. "TOTAL" is the number of occurrences of thicknesses in the base height category defined at the top of each figure. "% of Grand Total" is the percent of all inversions each month that occurred in each base height category.

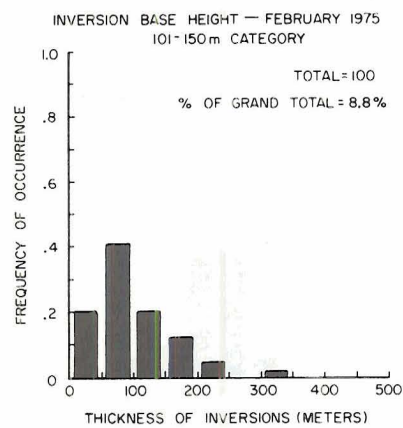
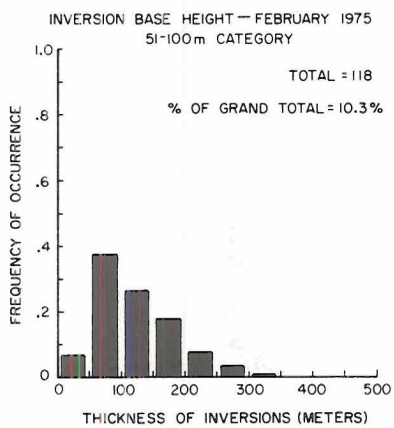
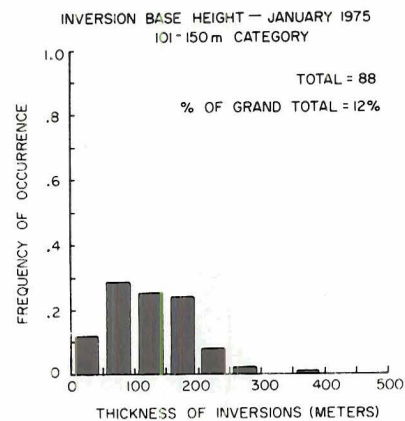
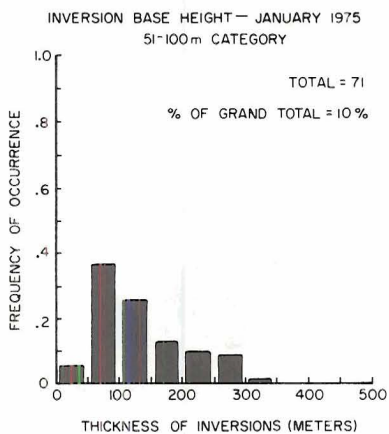


Figure 3.15. Frequencies of occurrence of thicknesses in the 51-100 meter base height category.

Figure 3.16. Frequencies of occurrence of thickness in the 101-150 meter base height category.

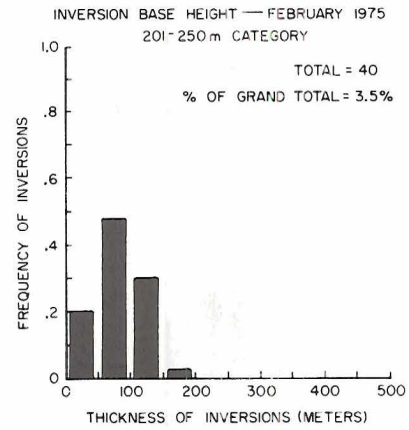
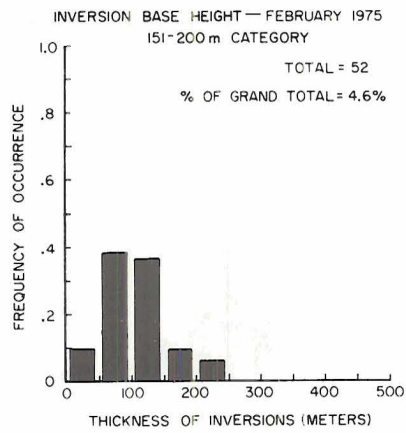
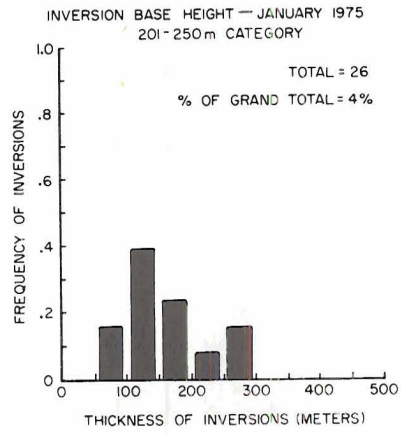
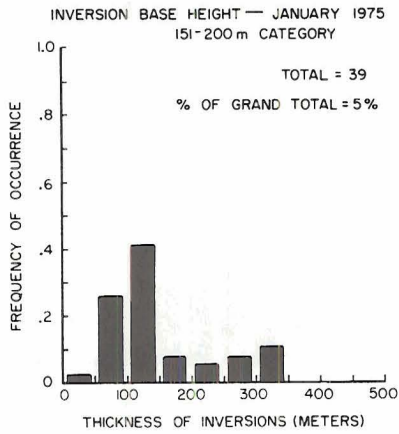


Figure 3.17. Frequencies of occurrence of thicknesses in the 151-200 meter base height category.

Figure 3.18. Frequencies of occurrence of thickness in the 201-250 meter base height category.

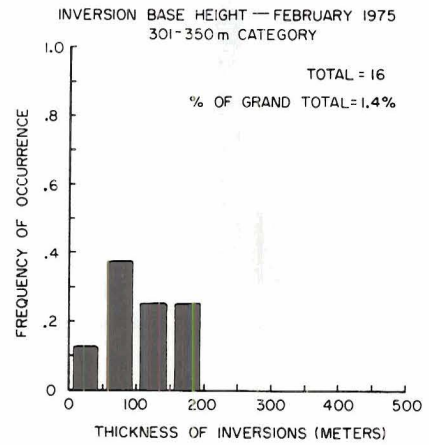
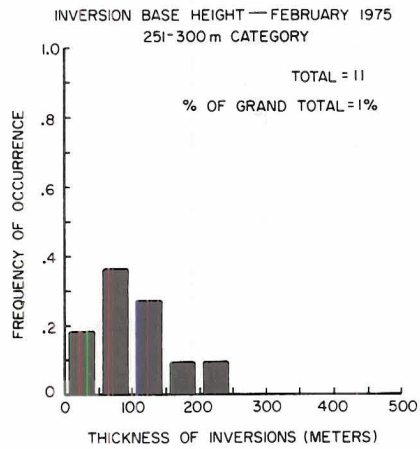
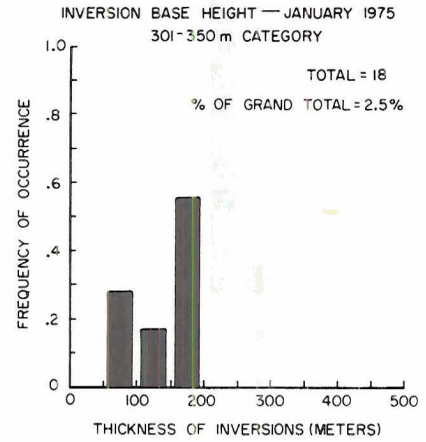
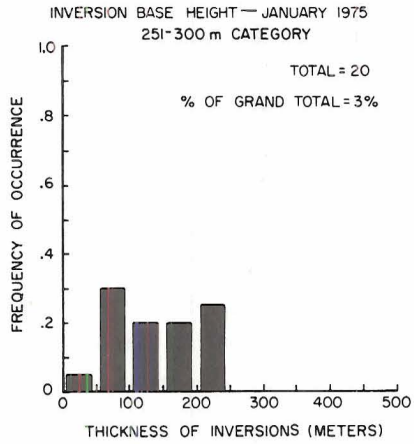


Figure 3.19. Frequencies of occurrence of thicknesses in the 251-300 meter base height category.

Figure 3.20. Frequencies of occurrence of thickness in the 301-350 meter base height category.

Figure 3.21

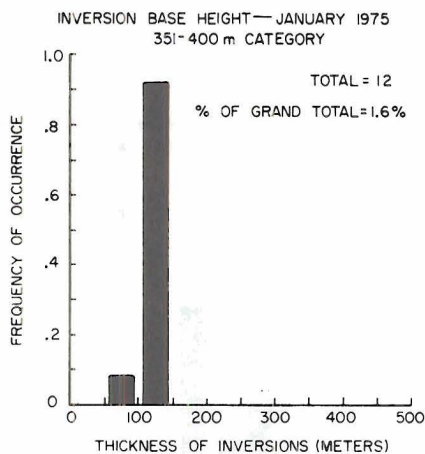


Figure 3.22

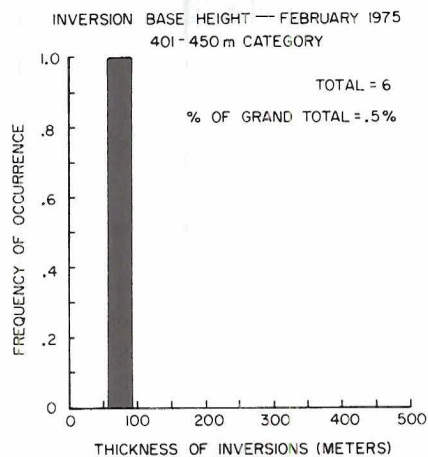
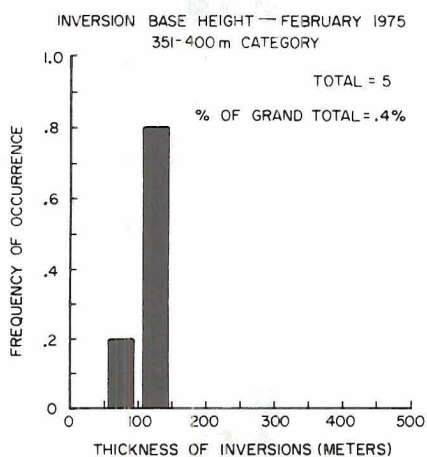
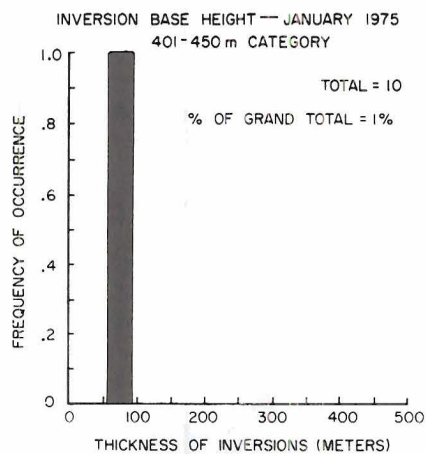
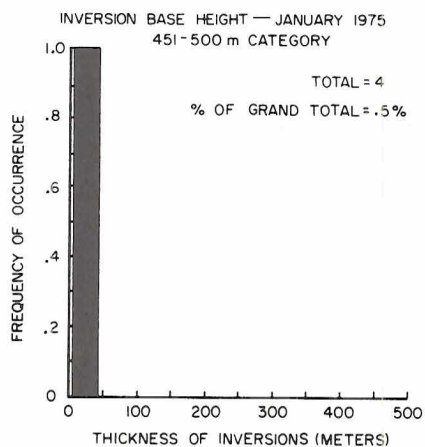


Figure 3.23



Figures 3.21, 3.22, 3.33. Frequencies of occurrence of thicknesses in the base height category specified above each histogram.

January and February acdar soundings were also analyzed for persistencies of all, surface only, and elevated only inversion frequencies. Figures 3.24 through 3.26 show the results of such an analysis. For "all inversions", both surface and elevated were tabulated if they followed each other in succession. The inversion period was deemed to have terminated when no inversion was present. Figure 3.24a,b agrees to some extent in inversion persistencies for January and February. Shown below is a tabulation of longer episodes not plotted:

TABLE 3.2

<u>Ending Date</u>	<u>Episode Duration (Hours)</u>
Jan. 14, 1975	82
Jan. 23, 1975	57
Feb. 7, 1975	88
Feb. 10, 1975	70
Feb. 17, 1975	78

Four of these episodes were three days or longer. Ft. Collins, under the influence of these stagnating conditions, was therefore prone to possible air pollution threats.

To determine further which kind of inversion event was longer lived, Figures 3.25 and 3.26 show January and February surface and elevated inversion frequencies. Elevated inversions for both months tended to be short in duration while surface inversions were more evenly distributed from short to approximately 16 hour durations. Both of these frequency distributions stemmed from active daytime thermals and long winter nights with radiational cooling and subsidence. This accounts for short-lived elevated inversions that either persisted during the daytime and sunk to connect later with the surface, or were

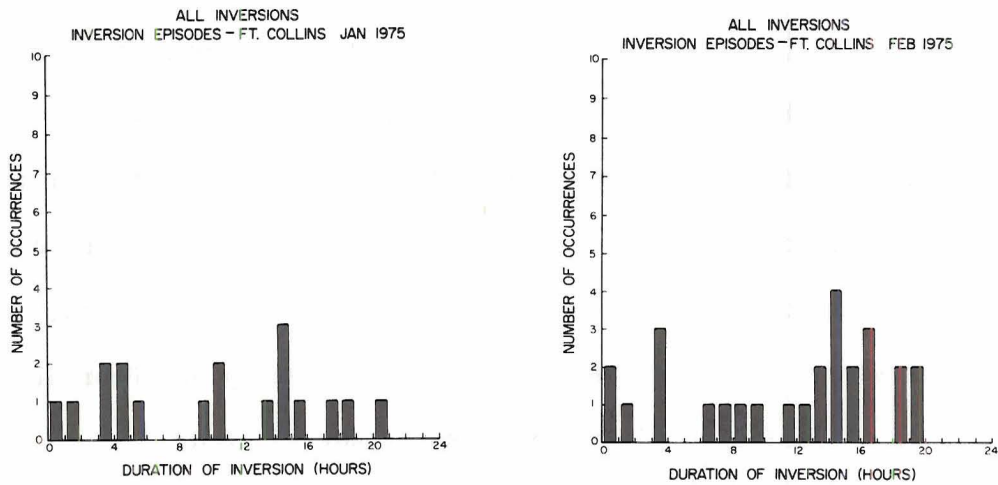


Figure 3.24. Frequencies of occurrence of all inversions of specified numbers of hours (persistence).

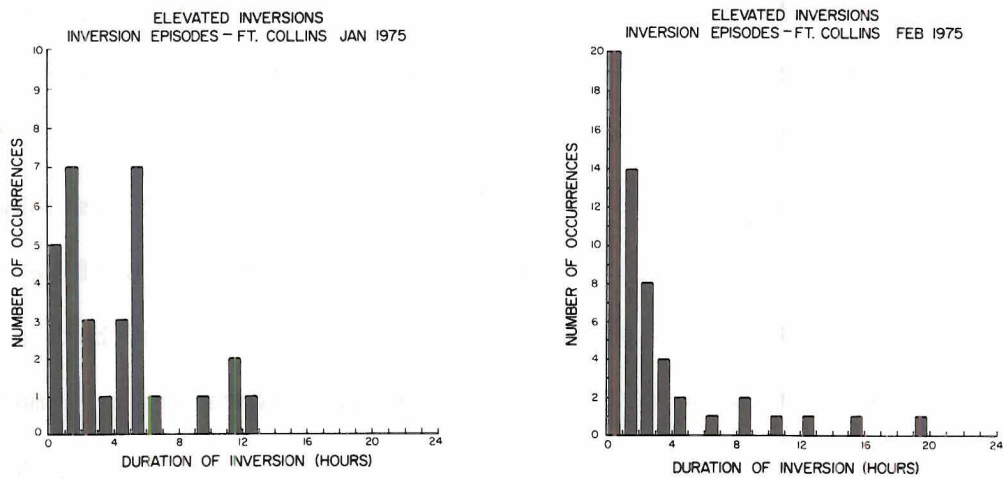


Figure 3.25. Frequencies of occurrence of elevated inversions of specified numbers of hours (persistence).

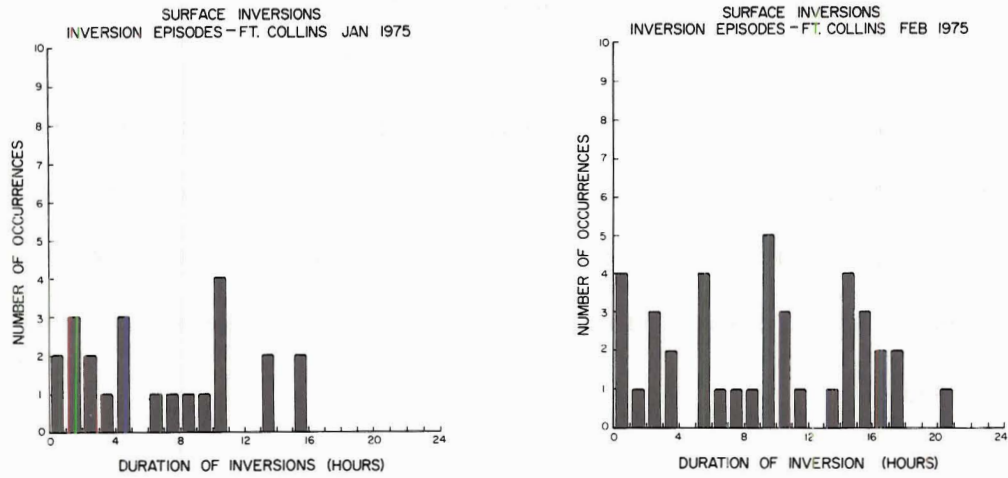


Figure 3.26. Frequencies of occurrences of surface inversions of specified numbers of hours (persistence).

mixed and dispersed with environmental air by thermals in the daytime. Surface inversions frequently were dispersed in the early evening by wind shear or persisted several hours after late night formation. Many surface inversions were pushed from the surface in the early morning by convective activity and were no longer surface based.

4. ASSOCIATIONS WITH METEOROLOGICAL PARAMETERS

The major portion of the remainder of this thesis will be devoted to associating inversions to meteorological parameters. The following table describes relationships that are to be investigated (the presence or absence of an inversion is determined by the presence or absence of a base height).

TABLE 4.1

Inversion Parameters Displayed As Functions of
Meteorological Parameters for Subsequent Analysis

Inversions		
<u>Base Heights</u>	<u>Thicknesses</u>	<u>Type of Analysis</u>
f(wind direction)	f(wind direction) f(wind direction)	2-way ANOVA averages, plots
f(wind speed)		2-way ANOVA
f(cloud cover, wind speed)	f(cloud cover, wind speed)	3-way ANOVA plots
f(wind speed, wind direction)	f(wind speed, wind direction)	3-way ANOVA plots
f([CO], wind speed)	f([CO], wind speed)	3-way ANOVA plots

Confidence levels in all cases will be at the 5% level.

Analysis of variance (ANOVA) was used in all cases.

Association of Inversion Occurrence with Wind Direction

In order to study the association of inversion occurrences with wind direction, it is first necessary to count the number of cases of wind in categories. This was done by looking at the wind field for each month. Figure 4.1 gives the results for January and February 1975 in 7 classes.

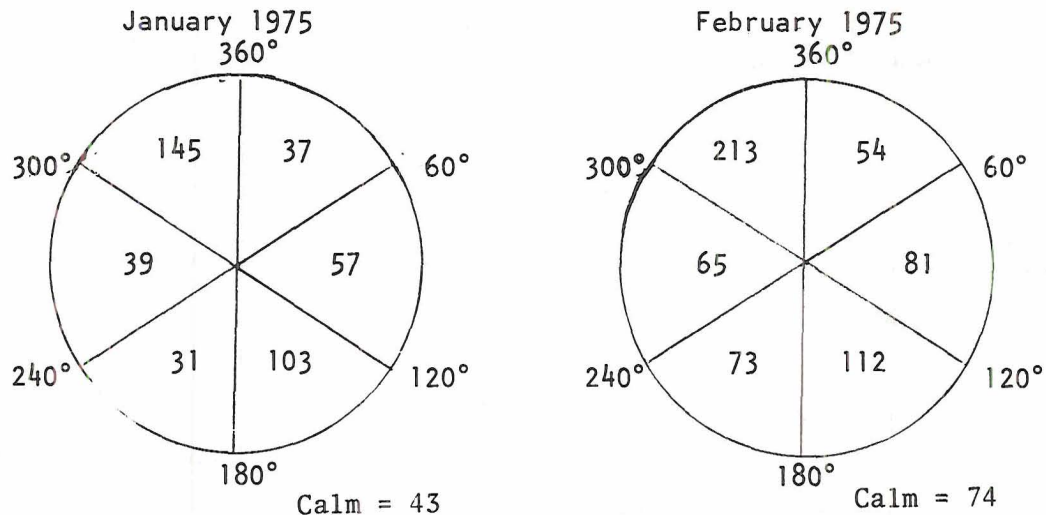


Figure 4.1. Cases of wind per wind direction category (each case is a 1 hour mean wind).

Referring to Figure 2.6 it can be seen by comparison that January and February, 1975 agreed well with the annual wind rose in terms of dominant wind regimes from the northwest and southeast indicating the up-valley down-valley diurnal flow discussed by Buettner (1967) and Riehl and Herkhof (1970). These two months were relatively calm, however, in comparison to annual means. This could be attributed to the less frequent occurrence of chinook type winds this year.

Calms will be defined in this paper as periods of highly variable wind directions usually associated with low wind speeds.

ANOVA of Wind Direction and Inversions

χ_{R1}^2 and χ_{RC}^2 (see Appendix B) were tabulated for surface inversions and elevated inversions using categories of wind as on the previous page. Table 4.2 gives the results of those tests. (Examples of the contingency tables can be found in Appendix B.)

TABLE 4.2

Summary of χ_{R1}^2 and χ_{RC}^2 for January and February, 1975

$$\chi_c^2 = 12.59$$

$$\text{d.f.} = 6$$

Type of Inversion	Date	χ_{R1}^2	χ_{RC}^2	Reject?
Surface	Jan	15.24		Yes
	Jan		30.42	Yes
Surface	Feb	34.02		Yes
	Feb		88.28	Yes
Elevated	Jan	7.04		No
	Jan		10.54	No
Elevated	Feb	13.28		Yes
	Feb		18.87	Yes

For both months the null hypothesis (see Appendix B) for surface inversions was rejected in both tests. From the alternate hypothesis one can infer then that surface inversions were related to wind direction. The probability (\hat{p}_i) that a surface based inversion will occur with a given wind direction can be found for each month. These are presented on the next page.

TABLE 4.3
 Inversion Probabilities With a Given Wind Category
 (Surface Inversion)

		Degrees					
	0-60	60.1-120	120.1-180	180.1-240	240.1-300	300.1-360	CALMS
Jan	.649	.509	.330	.613	.308	.549	.700
Feb	.519	.272	.518	.507	.692	.742	.878

For each month several direction categories stood out as having higher inversion probabilities. Looking at Figure 4.1, it is recognizable that the higher probabilities were related to the more frequent wind regimes with the highest in February (excluding the calm category) at the northwest direction. One could infer then that this supports the physical mechanism of cool katabatic drainage winds and/or cool north winds flowing into the Poudre Valley enhancing the growth of stable layers. The high probability of inversion occurrence noted in each month with variable winds can be related to the low wind speeds usually associated with variable wind directions.

Referring to Table 4.2 it can be seen that the null hypothesis for January was not rejected while for February it was for the elevated cases. In order to check the theory that the occurrence or non-occurrence of an elevated inversion was independent of month, another χ^2 test was performed comparing the two months.

TABLE 4.4

January-February Contingency Table for Elevated Inversions

	Inversion	No Inversion	Totals
Jan	151	304	455
Feb	199	473	672
Totals	350	777	1127

χ^2 was 1.62 for this test. For 1 degree of freedom at the 5% level the null hypothesis (H_0 : The occurrence or non-occurrence is independent of the month) was accepted (χ^2_{critical} equals 3.84). No difference by month then can be shown.

A further χ^2 test was carried out in order to check the winds independently of month. The resultant χ^2 was 3.68 while χ^2_{critical} for this test at the 5% level was 12.59. It was, therefore, accepted that there was no dependency of wind regimes on month. Without further evidence it can only be inferred that elevated inversions in January were less wind dependent in occurrence than those in February.

ANOVA of Wind Directions and Inversion Thickness

Since surface inversion association with wind direction for both January and February was somewhat positive as inferred from the tests of the previous section, a further test was carried out to see if these inversions had thicknesses associated to wind direction. The sample was divided into two categories, "inversion thicknesses less than 150 meters" and "those equal to or greater than 150 meters and less than 500 meters". Wind directions were divided into categories as before. Several of the

cells in the table were 3 or less and so categories of wind direction were combined (see Table 4.5).

The null hypothesis was that thicknesses of inversions occurring from some wind direction were not related to that wind direction. At the 5% level of significance χ^2_{critical} was 9.49. For January χ^2 was 5.31 and the null hypothesis was accepted, but for February χ^2 was 9.62 and the null hypothesis was rejected. The apparent difference says that in February inversion thicknesses can be related to the wind field while in January the chance of getting a thin or thick inversion was equally probable in each wind direction category. However, the difference might also be related to the occurrence of calm winds this particular year for January and February.

Early Evening Association of Wind Direction and Inversions

From previous examples it is evident that the two main wind regimes are the southeast in the daytime and northwest at night. In order to show that the northwest drainage wind actually does accentuate inversion formation it is necessary to examine associated winds and inversions. Thicknesses of inversions will be primarily looked at as they are the main inversion characteristic that will change.

All cases of winds from 300° - 360° and 120° - 180° were plotted versus average thickness changes in Figs. 4.2a and b and 4.3a and b. All figures were constructed from 1600 to 2400 hours M.S.T. This was done because near 1600 hours daily winds are southeast and by 2400 hours winds have shifted to the northwest. Winds from 1600 to 2400 were plotted for all wind and inversion cases from the southeast and northwest. In this manner it can be seen that if the wind persisted from a

TABLE 4.5

Thickness vs. Wind Direction for Surface Inversions
 [Observations (Expected Values in Parenthesis)]

Inversion Thicknesses (m)	Wind Directions (Degrees)					Totals	d.f. = 4
	0-120	120.1-180	180.1-300	300.1-360	Calms		
<u>January, 1975</u>							
<150	43 (40.60)	23 (27.07)	27 (26.22)	64 (62.59)	24 (24.53)	181	
>150, <500	5 (7.40)	9 (4.93)	4 (4.78)	10 (11.41)	5 (4.47)	33	
TOTALS	48	32	31	74	29	214	46
<u>February, 1975</u>							
<150	37 (39.73)	38 (40.60)	71 (67.37)	143 (136.47)	47 (54.83)	336	
>150, <500	9 (6.27)	9 (6.40)	7 (10.63)	15 (21.53)	13 (8.17)	53	
TOTALS	46	47	78	158	60	389	

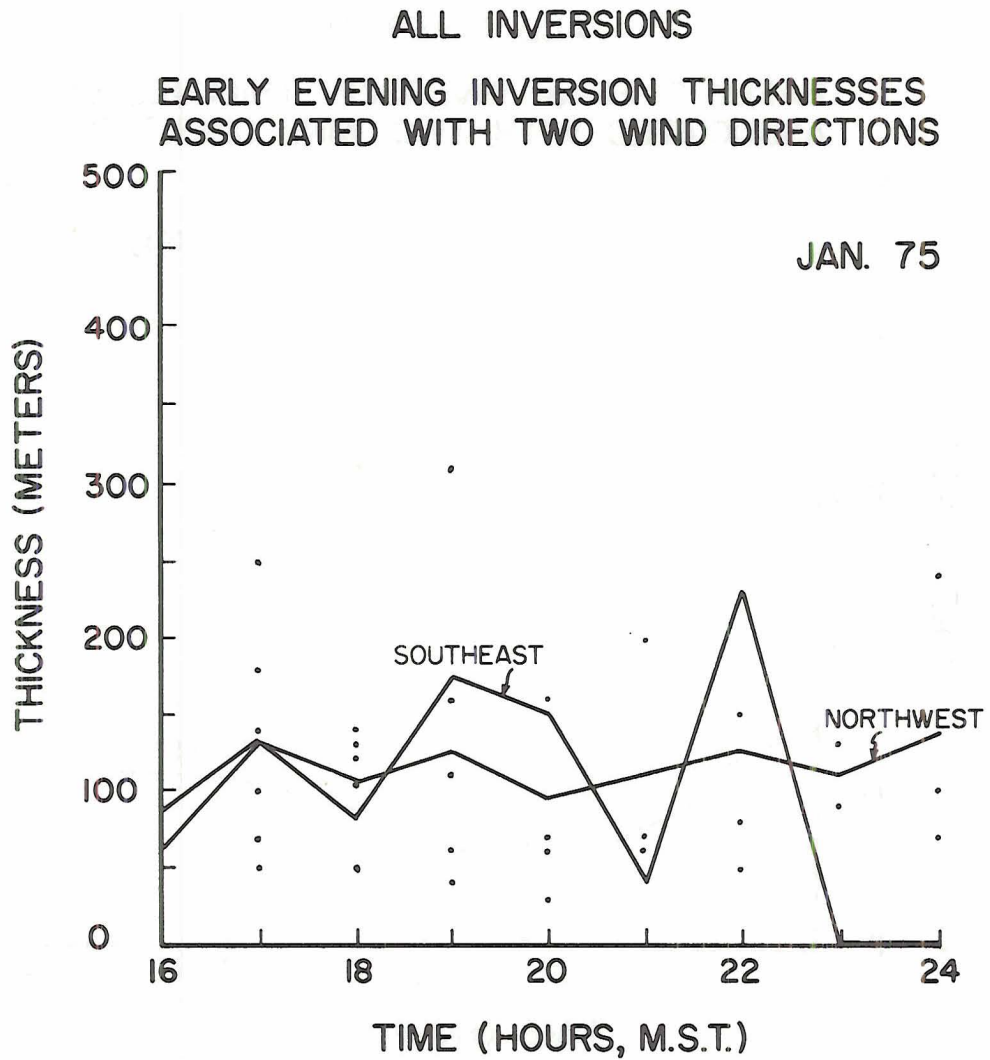


Figure 4.2a. All inversions counted by associated wind direction and averaged, January, 1975.

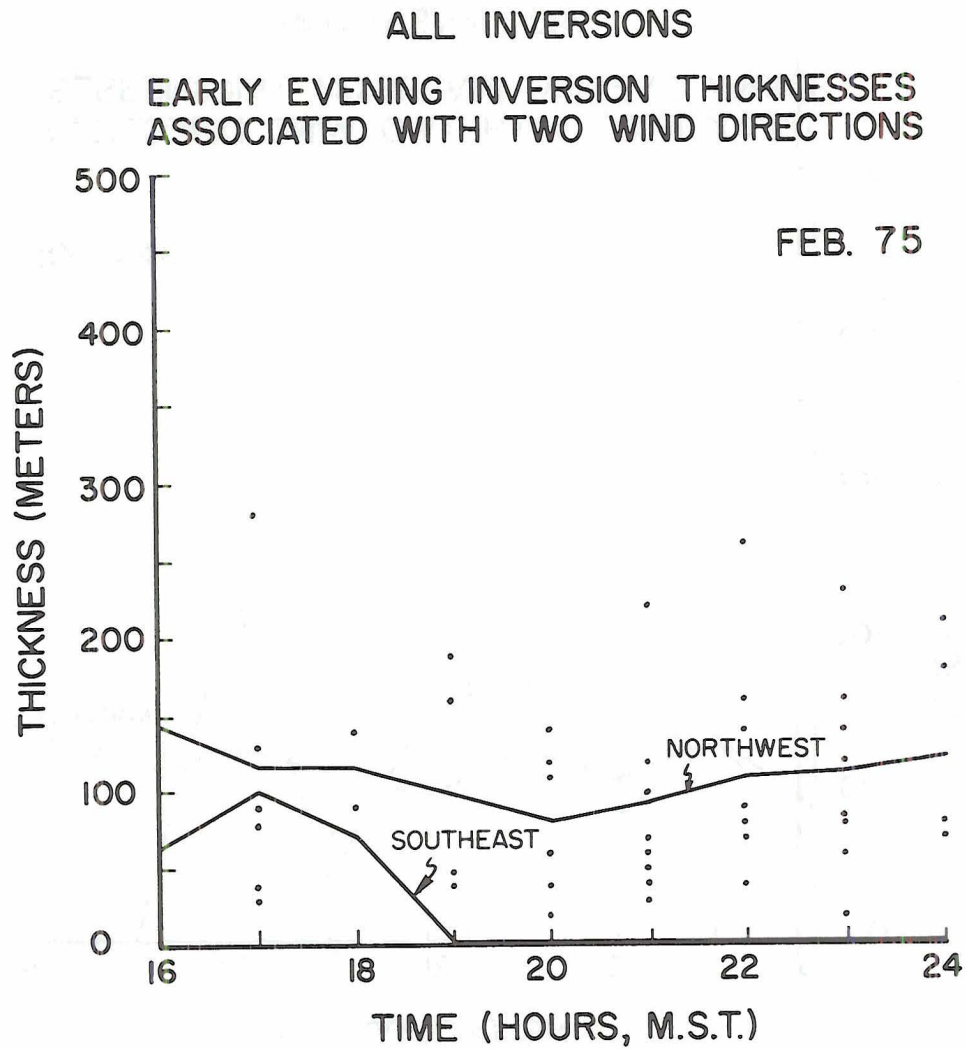


Figure 4.2b. All inversions counted by associated wind direction and averaged, February, 1975.

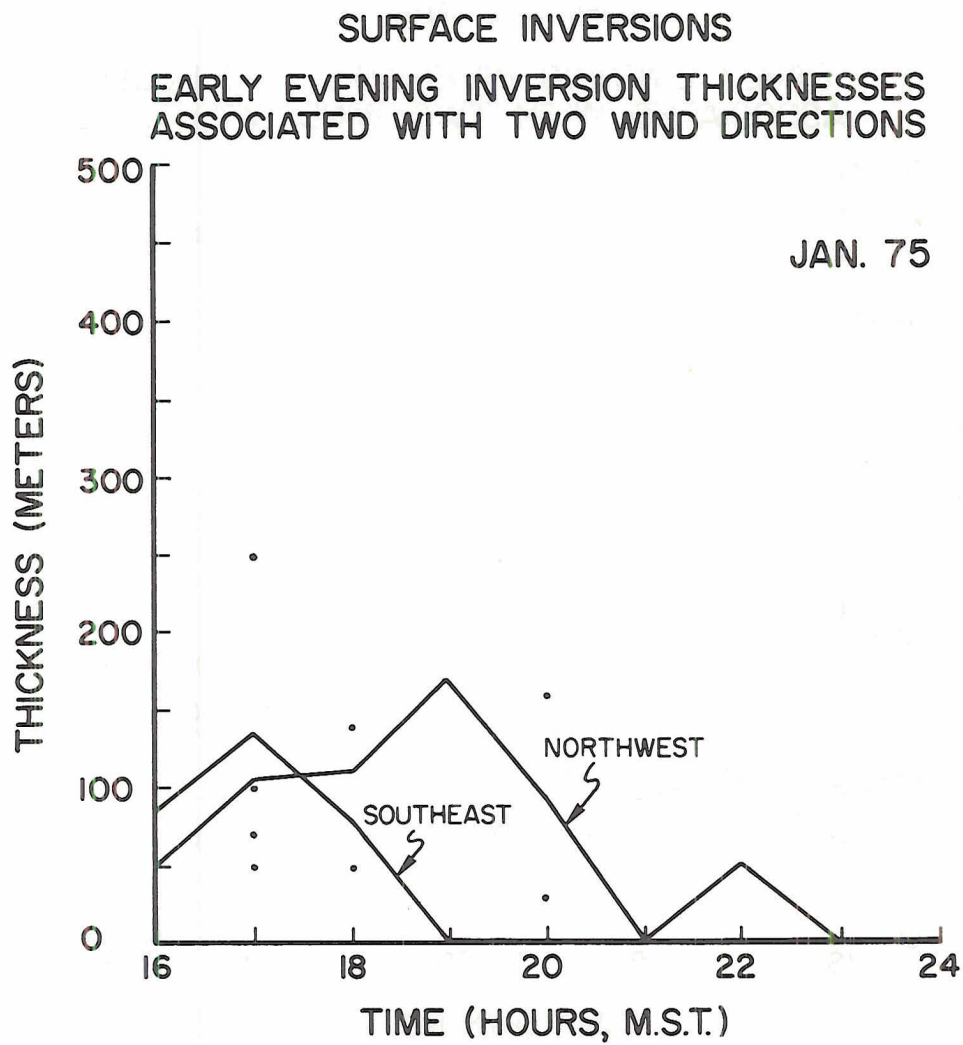


Figure 4.3a. Surface inversions counted by associated wind direction and averaged, January, 1975.

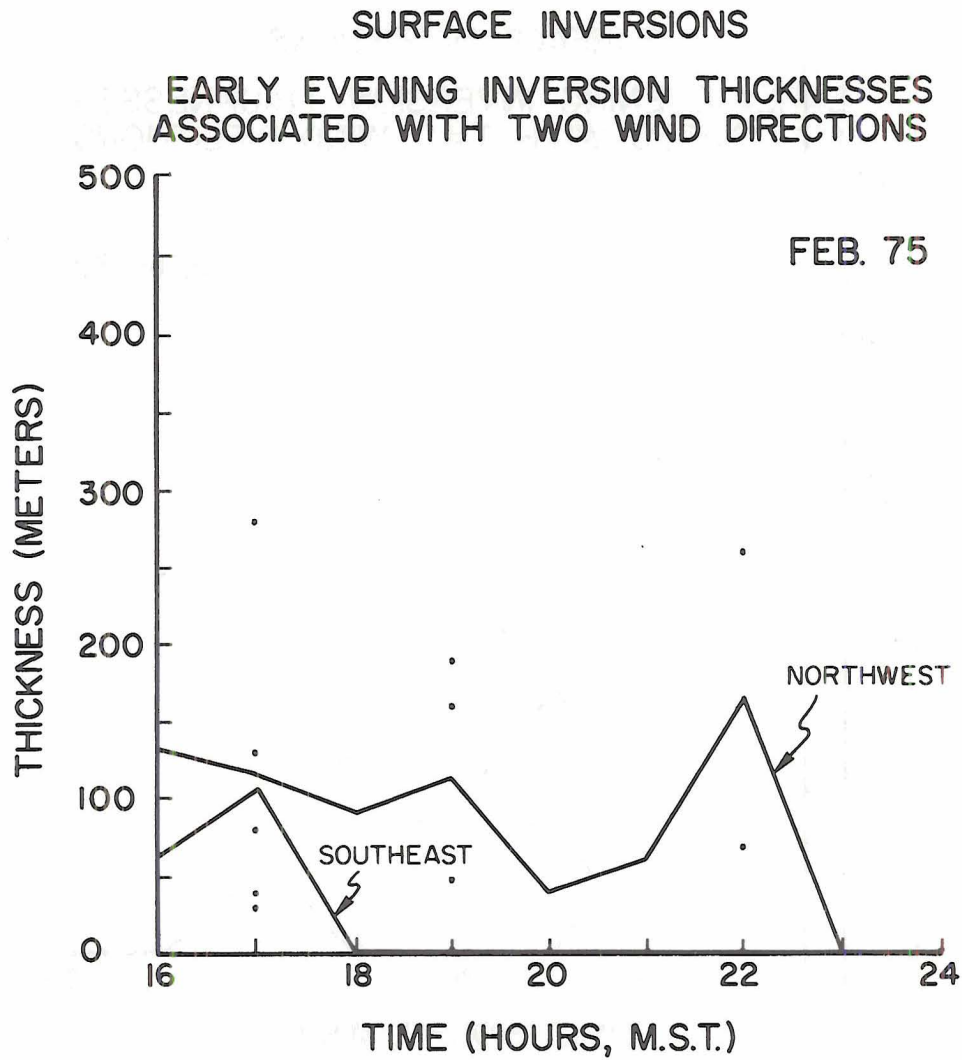


Figure 4.3b. Surface inversions counted by associated wind directions and averaged, February, 1975.

certain direction from 1600 to 2400 the inversion thickness change could be observed.

In Figure 4.2a and b all inversions (surface and elevated) that occurred between 1600 and 2400 were counted that were associated with southeast or northwest winds. In February a definite difference in inversion thicknesses between the two wind directions is evident. The northwest or drainage wind inversions are thicker and much more frequent than the southeast inversions, which no longer occur after 1900 hours. The northwest inversions for January are similar to February, except that the southeast inversions also occur and only die out after 2300.

In order to see more of the influence of wind direction on surface based inversions, elevated inversions were subtracted from the sample. Now in Figures 4.3a and b, January and February agree to a greater extent, with southwest surface inversions not present after 1900 hours and northwest inversions dominating until 2300.

The early evening dependence of inversion formation at the surface on wind direction (for the two major regimes) has therefore been shown along with the time dependent change of thickness and occurrence.

Association of Inversions With Wind Speed

The association of light winds with inversions is well documented. A familiar comparison, reproduced by Sutton (1953) as his Figure 25, of wind-speed profiles for inversion, neutral, and superadiabatic conditions shows that the lightest winds occur with inversions. In an investigation at the Hanford works area by Jenne and Hilot (1950) of the association of inversions and wind speed, it was found that between calm

and 5 m/s there was a definite trend of decreasing stability with increasing wind speed.

Using available surface wind speeds and acdar records, evidence was sought that inversions at Fort Collins were more frequent with light winds than strong winds. Two by two contingency tables were prepared for each month. Wind speed categories were "calm to less than 5 m/s" and "greater than or equal to 5 m/s"; inversion categories were "inversion" and "no inversion" with contingency tables for all inversions, surface inversions and elevated inversions being prepared.

The χ^2 for a two by two table was used testing the null hypothesis that inversion occurrence is independent of wind speed. Table 4.6 is an example of one such contingency table and related parameters.

From the previous discussions it can be noted that most surface inversions occur in the nighttime hours and elevated inversions in the daytime. In differentiating surface and elevated inversions it was shown in Table 4.7 that surface inversions were related to wind speeds (the null hypothesis was rejected). Elevated inversions on the other hand are not related to surface wind speeds in January as they are in February. This could be attributed to the fact that elevated inversions were much higher in height than the winds measured near the surface and could be in a slightly different wind field.

From the entries in the surface inversion contingency tables, the frequency of inversions with less than 5 m/s and greater than 5 m/s were 54% and 27% for January and, 64% and 42% for February respectively.

The influence of surface inversions can be seen on the all-inversion χ^2 's that were calculated. January and February for this case were

dependent on wind speeds, so that under certain wind conditions an inversion can be expected to occur. The frequencies of occurrence with speeds less than 5 m/s and greater than 5 m/s were 65% and 39% for January and, 71% and 42% for February, respectively.

Association of Inversions with Two Meteorological Variables

In the previous two chapters it was shown separately that inversions in Fort Collins are related to certain wind direction and wind speed patterns. In order to describe more fully the possible dual relationship of inversions to two meteorological variables simultaneously, the 3-way analysis of variance is utilized.

Cloud Cover, Wind Speeds and Inversions

January and February cloud cover data (from the Fort Collins weather station), wind speeds (10 meters above surface) and radar recordings of inversions, were related by a χ^2 test. A graphical presentation is given in Figure 4.4.

In order to first see if any valid relationship existed, a χ^2 test was applied to each set of data. Values of "less than 3 m/s" and "greater than 3 m/s" were used for wind speed classes, and cloud cover classes were "0-2 tenths", "3-6 tenths", "7-10 tenths". χ^2 was then calculated with the following results:

CLOUD COVER VS. WIND SPEEDS VS. ASSOCIATED INVERSION FREQUENCY
 SURFACE INVERSIONS ONLY (0000 - 2400MST) FEBRUARY 1975

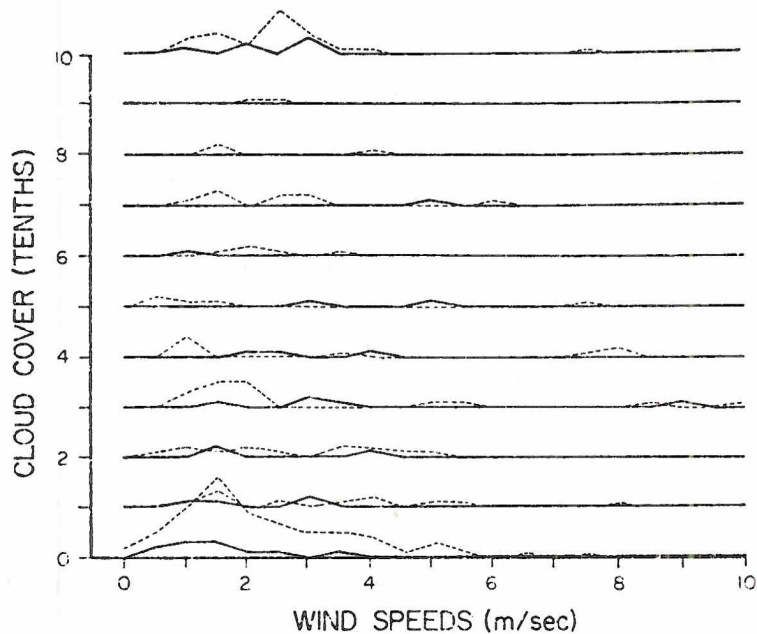


Figure 4.4. Cloud cover, wind speeds and frequency of inversion occurrence. Between each cloud cover category are 10 frequency categories so that the peak at 1.5 m/s for 0 cloud cover on the dotted line represents 16 cases of inversion less than 150 meters thick.

Note: In Figures 4.4 through 4.10:
 --- indicates inversions < 150 meters thick, and
 — indicates inversions \geq 150 meters thick.

TABLE 4.8

χ^2 Results for 3-Way ANOVA of Wind Speeds, Cloud Cover
and Inversion Occurrence

d.f. = 6

 $\chi_c^2 = 12.59$

	Date	χ_c^2	Reject?
All	Jan	8.329	No
All	Feb	11.813	No
Surface	Jan	8.601	No
Surface	Feb	14.197	Yes
Elevated	Jan	4.262	No
Elevated	Feb	8.634	No

Only the February surface inversion cases rejected the null hypothesis. This says that wind speeds, cloud cover and inversion occurrence were mutually independent, that is, when light winds and clear skies occur, an inversion may or may not occur simultaneously. Having used observations available only on a two hour basis, the number of values used in this analysis was only half of that used in subsequent analysis (next two sections). Further analysis of cloud cover should be carried out when further data are available.

Figure 4.4 gives the results of February surface inversions associated with cloud cover and wind speeds. It can be seen that both thin (dotted line, < 150 meters thick) and thick (solid line, \geq 150 and < 500 meters thick) inversions were more frequent with clearer skies and lighter wind speeds.

Wind Direction, Wind Speed and Inversion Occurrence

It was shown previously that inversion occurrence and wind directions are dependent, with a high probability that inversion occurrence is dependent on wind direction rather than vice versa. In this section the added factor of wind speed was tested along with wind direction and inversion occurrence. Again the χ^2 test was used with wind speed classes as before and wind direction classes, "0°-120°", "120.1°-180°", "180.1°-300°", "300.1-360°", and "calm". These wind direction classes were used to allow for the maximum number of values in each cell of the contingency table. The test for independency yielded the following results:

TABLE 4.9

χ^2 Results for 3-Way ANOVA for Wind Speeds, Wind Directions
and Inversion Occurrence

d.f. = 12

 $\chi^2_c = 21.026$

Inversions	Date	χ^2	Reject?
All	Jan	72.754	Yes
All	Feb	219.738	Yes
Surface	Jan	79.250	Yes
Surface	Feb	218.767	Yes
Elevated	Jan	46.116	Yes
Elevated	Feb	188.152	Yes

In all cases the null hypothesis was rejected and the alternate hypothesis accepted, that is, wind speed, wind direction and inversion occurrence are mutually dependent.

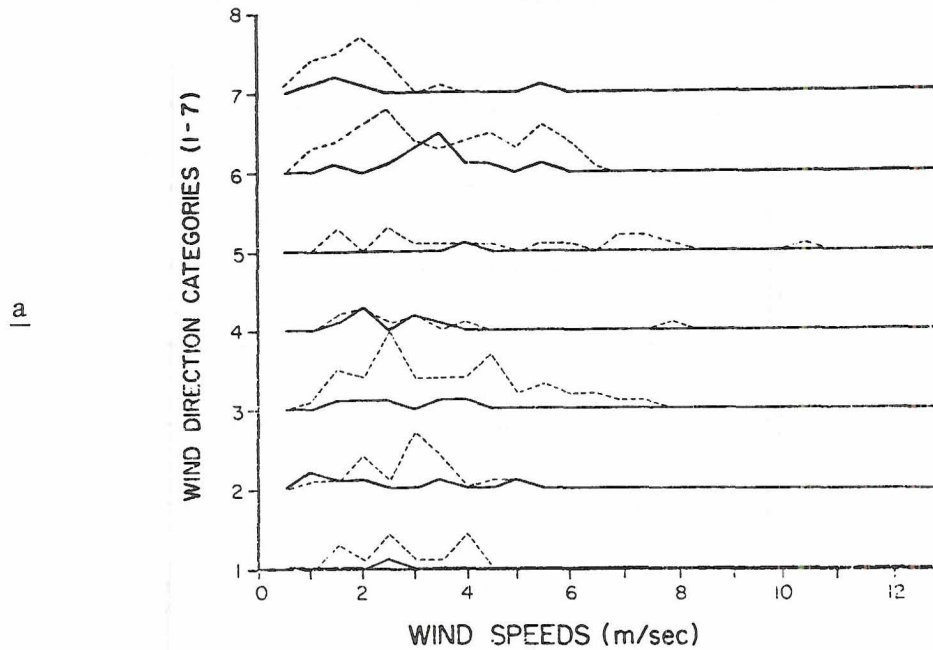
The inversions of greatest interest in regard to climatological control were the surface inversions, since it was proposed in earlier chapters that northwest drainage winds could enhance inversion formation. Plots of surface inversions "all day" do not yield much in the way of supporting this idea, though they do show the predominance of inversions with northwest, east, and southeast winds with wind speeds below 7.5 m/s (Figs. 4.5a,b). Categories of plotted wind directions used in these and subsequent figures were:

0 - 60°	-- 1
60.1-120	-- 2
120.1-180	-- 3
180.1-240	-- 4
240.1-300	-- 5
300.1-360	-- 6
Calm	-- 7

Plots, however, of night surface inversions (Figs. 4.6a,b) show in general more cases of surface inversions with northwest winds and light wind speeds than southeast wind cases, especially in February (4.6b). Thin inversions (dotted lines) occurred more than thick inversions (solid lines), for both months, but a peak in January with thick inversions can be seen for the 300°-360° category at 3.5 m/s.

Calm winds (category 7) in all cases exhibited a peak of inversion occurrences with wind speeds below 2.5 m/s. This confirms the hypothesis that light winds associated with no particular wind direction are indicative of stable or near stable air conditions.

WIND DIRECTIONS VS. WIND SPEEDS VS. ASSOCIATED INVERSION FREQUENCY
 SURFACE INVERSIONS ONLY (0000 - 2400MST) JANUARY 1975



WIND DIRECTIONS VS. WIND SPEEDS VS. ASSOCIATED INVERSION FREQUENCY
 SURFACE INVERSIONS ONLY (0000 - 2400MST) FEBRUARY 1975

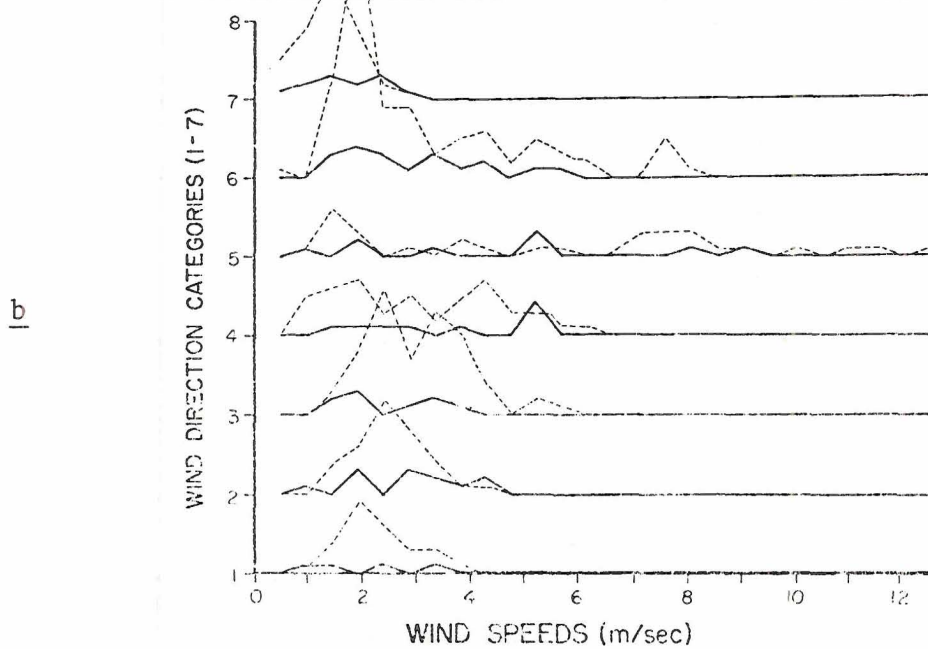
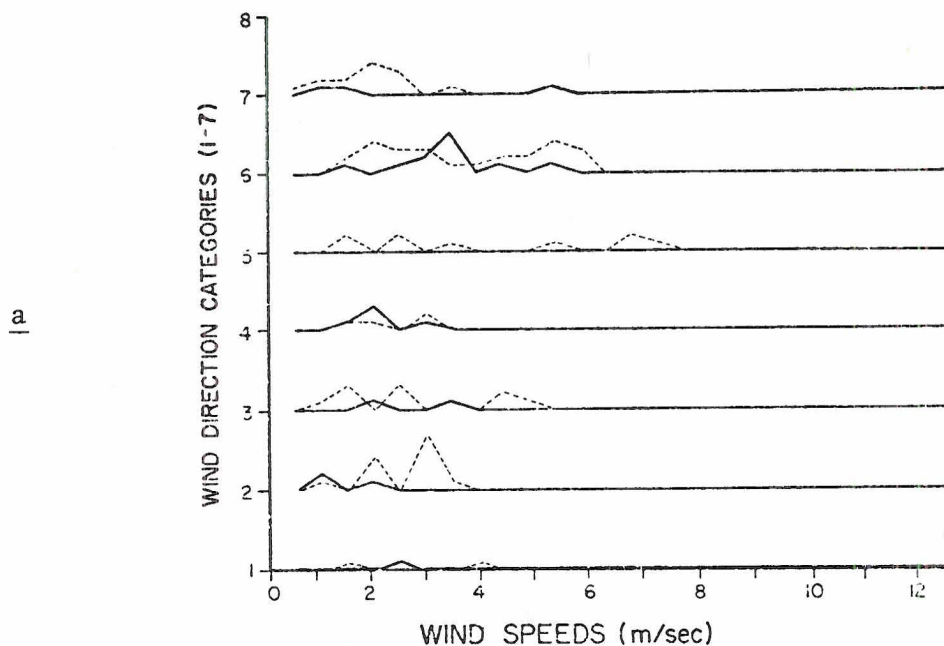


Figure 4.5a,b. Windspeeds, wind directions and frequency of occurrence of thin (< 150 m) and thick (\geq 150 m) inversions associated with them. Surface inversions only for: a. January, 1975, and b. February, 1975.

WIND DIRECTION VS. WIND SPEEDS VS. ASSOCIATED INVERSION FREQUENCY
 SURFACE INVERSIONS ONLY (1700-0800MST) JANUARY 1975



WIND DIRECTION VS. WIND SPEEDS VS. ASSOCIATED INVERSION FREQUENCY
 SURFACE INVERSION ONLY (1700-0800MST) FEBRUARY 1975

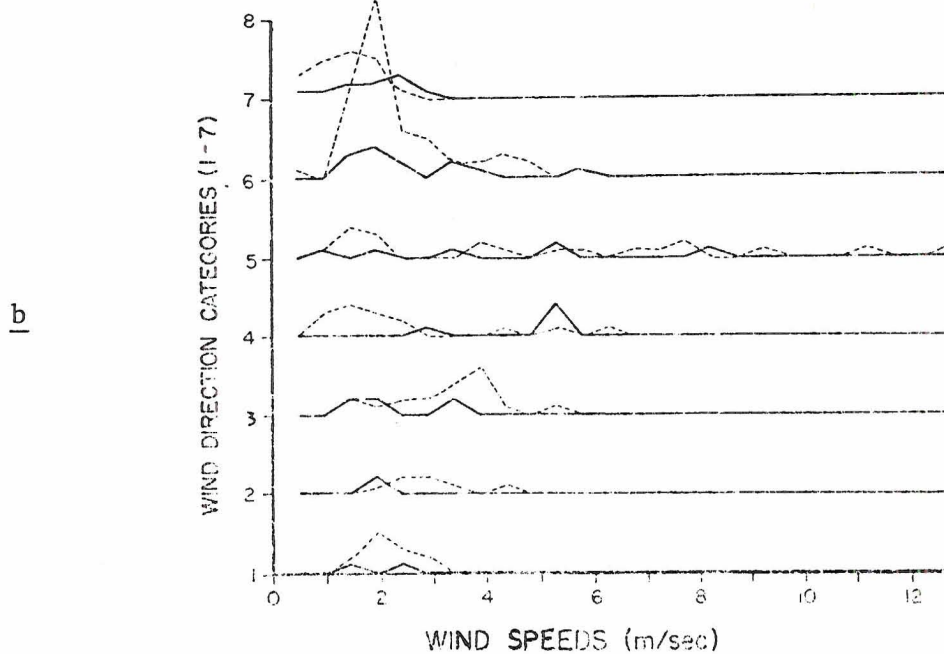


Figure 4.6a,b. Windspeeds, wind directions and frequency of occurrence of thin (< 150 m) and thick (≥ 150 m) inversions associated with them from 1700 to 0800 MST. Surface inversions only for: a. January, 1975, and b. February, 1975.

CO Concentrations, Wind Speed and Inversion Occurrences

As a final 3-way ANOVA test, CO concentrations taken on an hourly basis (on the roof of the courthouse in Ft. Collins) were compared to inversions and wind speeds.* CO classes were "1 to < 5 ppm" and "5 to \leq 18 ppm" with wind speed classes as before. χ^2 results for all elevated and surface inversions were:

TABLE 4.10**

χ^2 Results for 3-Way ANOVA of CO Concentrations, Wind Speeds
and Inversion Occurrences

d.f. = 3

 $\chi_c^2 = 7.81$

Inversions	Date	χ^2	Reject
All	Jan	9.254	Yes
Surface	Jan	8.249	Yes
Elevated	Jan	17.695	Yes

** CO data only available for January in Ft. Collins

For January in all cases the null hypothesis of independency was rejected and the alternate hypothesis accepted. With these results we can say that there is some mutual relationship of CO concentrations, wind speeds and inversion presence.

Plots of contingency tables for surface inversions occurring with light winds, showed peaks of CO between 1.5-2 m/s in the daytime and nighttime (Figs. 4.7 and 4.8) for concentrations below 5 ppm. Higher concentrations occurred more frequently in the daytime (Fig. 4.8)

* Only Monday through Friday CO values were used because of the continuity from day to day of CO peaks. Data from 1-19-75 to 1-26-75 was missing.

CO CONCENTRATION CATEGORIES VS. WIND SPEEDS VS. INVERSION OCCURRENCES
 SURFACE INVERSIONS ONLY (1700-0800MST) JANUARY 1975

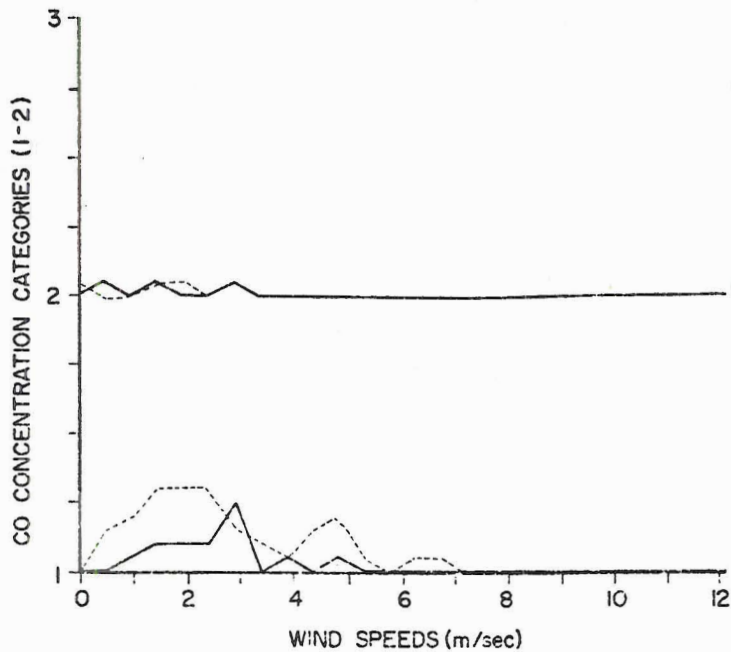


Figure 4.7. Association of [CO], wind speeds and surface inversion occurrences (thin < 150 m; thick \geq 150 m) from 1700 to 1800 MST, for January 1975.

CO CONCENTRATION CATEGORIES VS. WIND SPEEDS VS. INVERSION OCCURRENCES
 SURFACE INVERSIONS ONLY (0800-1700MST) JANUARY 1975

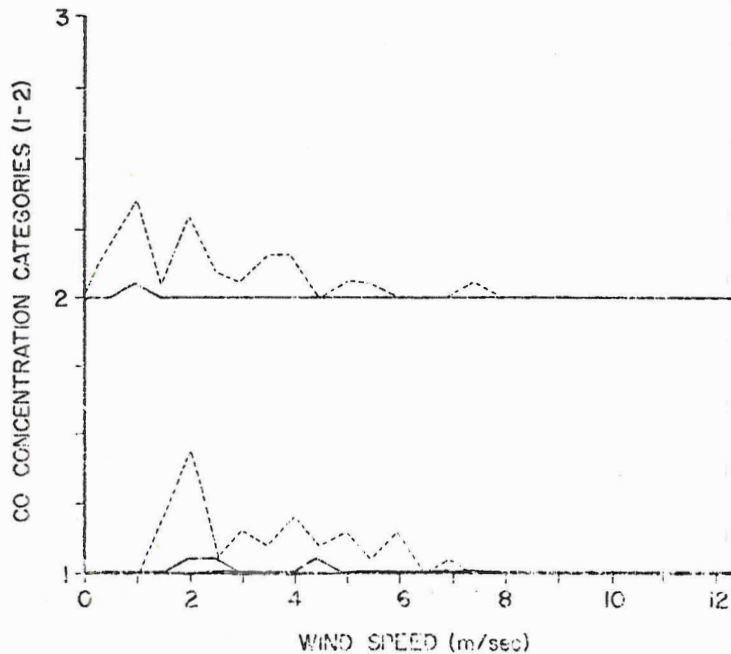


Figure 4.8. Association of [CO], wind speeds and surface inversions (thin < 150 m; thick \geq 150 m) from 0800 to 1700 MST, for January, 1975.

probably as a result of the greater input of CO at this time (automobile combustion).

With elevated inversions, however, the opposite occurred. At low and high concentrations more elevated inversions occurred at night than in the daytime (Fig. 4.9 and 4.10). These results were somewhat perplexing in that CO concentrations were generally higher in the daytime. We can only suggest that possibly CO levels were great enough that evening elevated inversions trapped CO left from daytime combustion sources.

CO CONCENTRATION CATEGORIES VS. WIND SPEEDS VS. INVERSION OCCURRENCES
ELEVATED INVERSIONS ONLY (0800 - 1700MST) JANUARY 1975

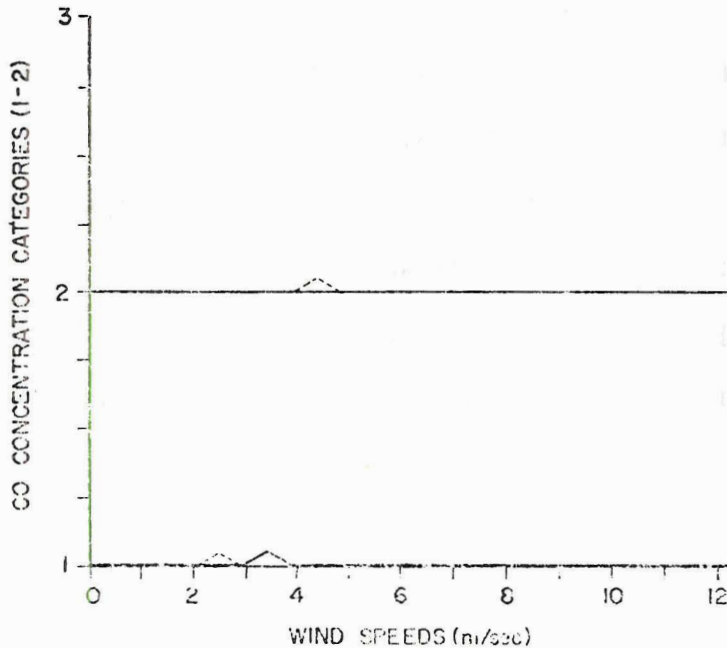


Figure 4.9. Association of [CO], wind speeds and elevated inversions (thin < 150 m; thick \geq 150 m) from 0800 to 1700 MST, for January, 1975.

CO CONCENTRATION CATEGORIES VS. WIND SPEEDS VS. INVERSION OCCURRENCES
ELEVATED INVERSION ONLY (1700 - 0800) JANUARY 1975

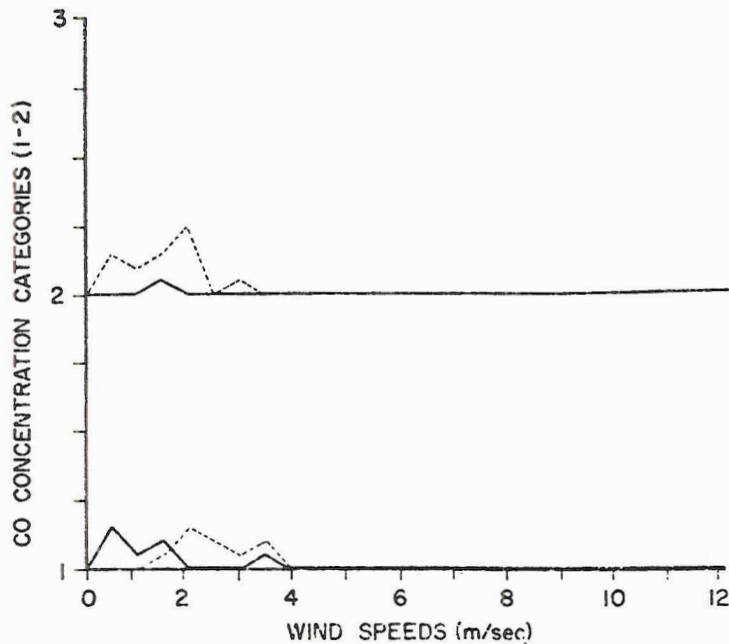


Figure 4.10. Association of [CO], wind speeds and elevated inversions (thin < 150 m; thick \geq 150 m) from 1700 to 0800 MST, for January, 1975.

5. CASE STUDY

To this point most inversion and meteorological features at Ft. Collins were generalized to show trends. In order to gain some insight into the combined effects on the air pollution problem, a case study is presented. The episode chosen for study was from 1600 M.S.T. on January 31 to 0800 M.S.T. February 1, 1975. CO concentrations for Ft. Collins were utilized as before. The daily cycle (Monday through Friday) of CO in Ft. Collins is for a peak near 0800 hours with the morning rush hour at 6-7 ppm, and another peak near 1700 hours when traffic again is heavy from 10-12 ppm (personal communication with Dr. Myron Corrin, Department of Atmospheric Science, Colorado State University).

On the evening of January 31 concentrations were as high as 8 ppm at 1900 hours. Looking at the surface maps for January 31 and February 1 we can see that the central Rocky Mountain region was dominated by a high pressure system (Figures 5.1, 5.2). With no strong cyclonic activity in the vicinity of Ft. Collins, light drainage winds and relatively clear skies were present on this night. The formation of a surface nocturnal inversion was probable under these conditions with the resultant trapping of CO at low levels.

In Figure 5.3 CO concentrations (the circles connected by a solid line), inversions (shaded areas), and wind speeds and directions (wind barbs at the bottom) were plotted as a function of time. From 1600 to 1730 an elevated inversion was present between 325 and 400 meters. CO concentrations increased with the evening traffic but did not decrease until 2200 hours. This could be attributed to the fact that traffic was present throughout the early evening because this was a Friday night. In

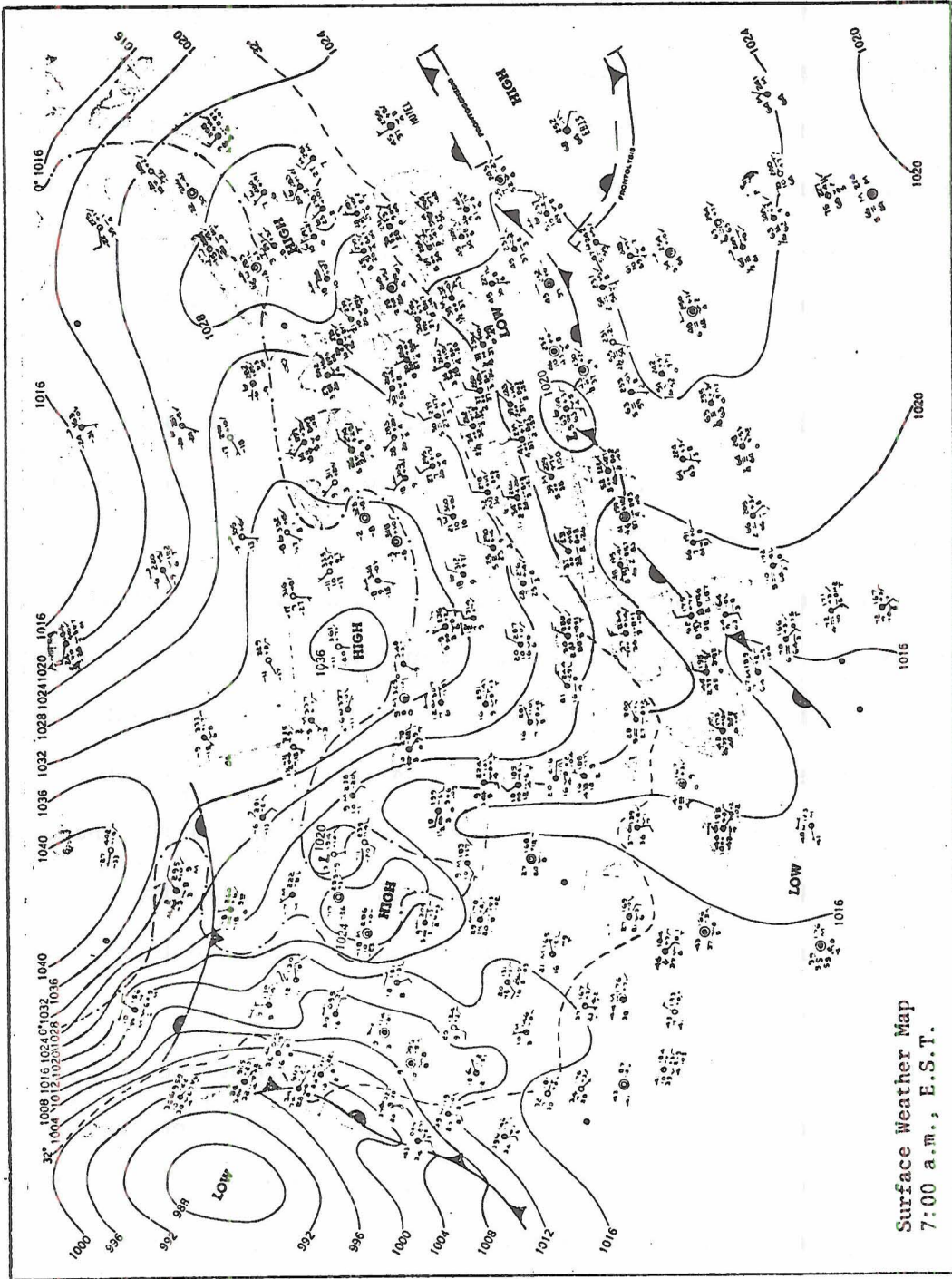


Figure 5.1. Friday, January 31, 1975. (From Daily Weather Maps, NOAA Environmental Data Service.)

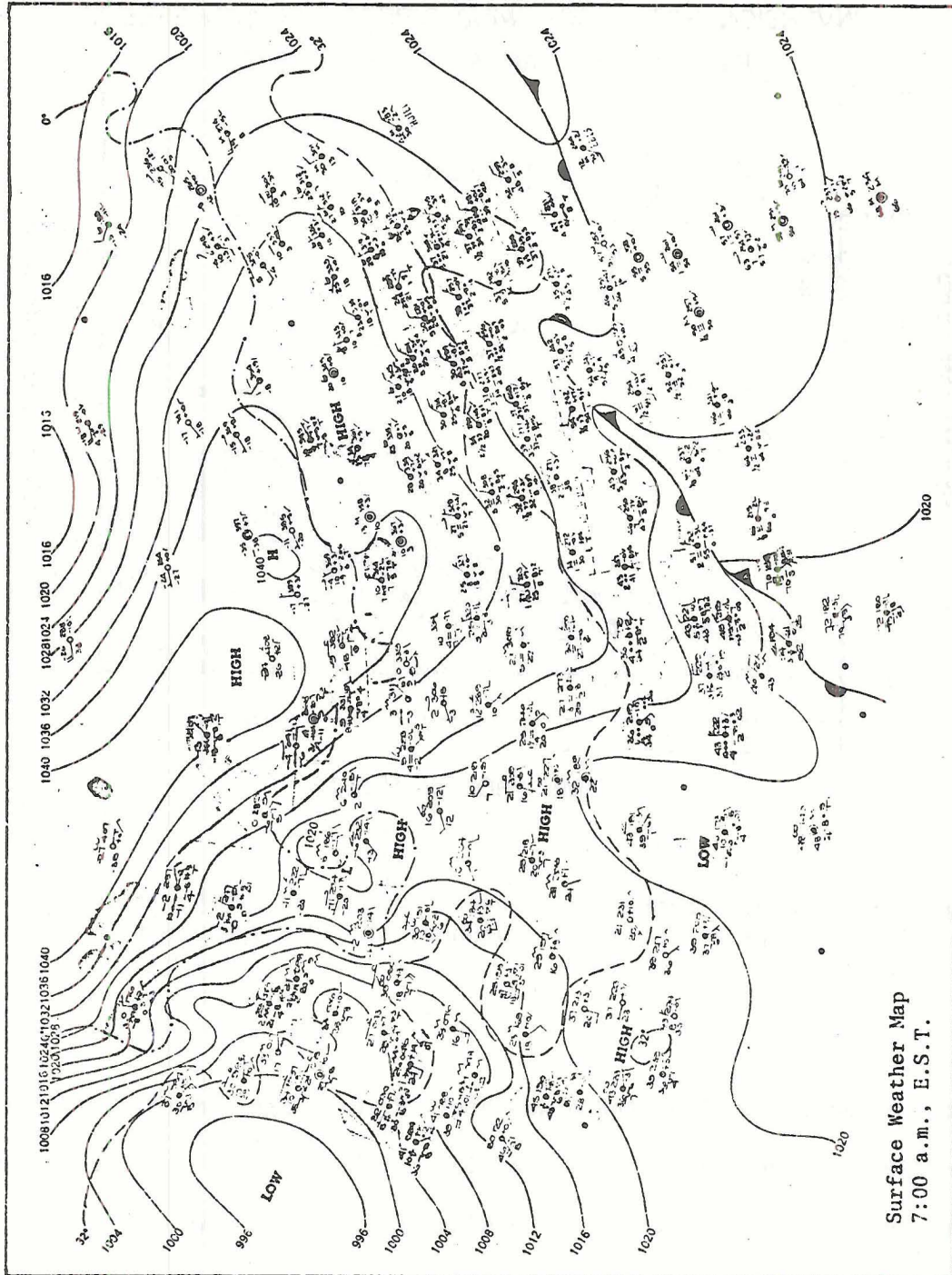


Figure 5.2. Saturday, February 1, 1975. (From Daily Weather Maps, NOAA Environmental Data Service.)

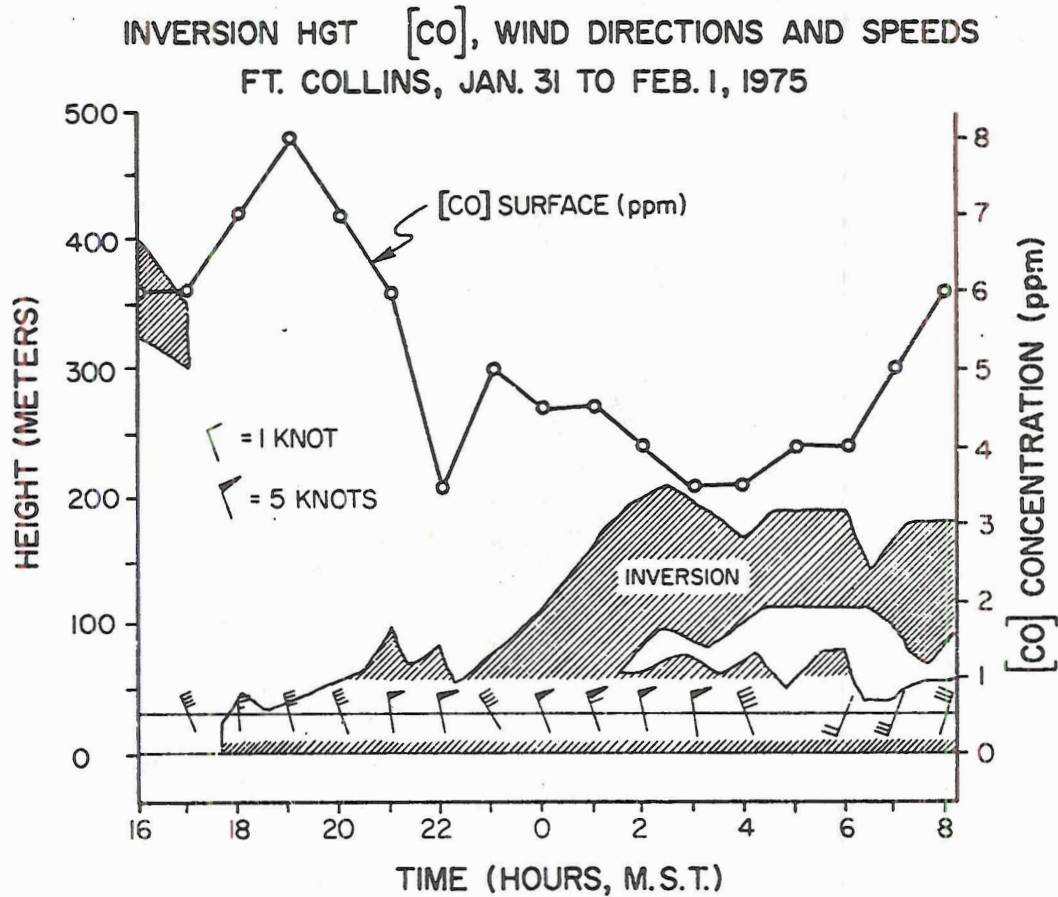


Figure 5.3. CO concentrations, inversion (shaded area), and wind field (barbs at bottom) for January 31, 1975 from 1600 to February 1, 1975 at 0800.

fact, an indication that there was heavy Friday night traffic was that near 2300, as the surface inversion intensified, the CO concentrations increased. From 0000 to 0400 the wind speeds increased slightly causing some turbulence in the layer even to the extent of dividing the stable layer into two.

The stable layer of air at the surface and the elevated inversion both persisted during the whole time period. Because February 1 was a Saturday morning, we would expect the peak of morning CO concentrations to be shifted two or three hours toward the middle of the day, but peaks equal to the weekly values were reached by 0800! One explanation offered is the overnight persistence of the nocturnal inversion which had effectively trapped much of the CO from the previous day and night, along with the presence of light winds. Both of these factors could deter the diffusion of CO out of Ft. Collins and possibly contributed to this slightly anomalous peak on February 1, 1975.

6. DISCUSSIONS AND CONCLUSIONS

In drawing together the information presented in the foregoing sections, we must first look at the main objective of this study. Basically this was to utilize a relatively new remote sensing device, the acoustic radar, in a "prototype" climatological study. The greatest value of the system was its ability to continuously monitor the structure of the lowest atmospheric layers.

Effectively this objective was reached to some degree. Inversion data for January and February was broken down into time and space occurrences and catalogued into various classes. In summary, Ft. Collins had a high incidence of inversions in the wintertime months of January and February. Many of these inversions were nocturnal surface inversions which formed after sundown and were associated with clear skies and light breezes. It was also found that nocturnal inversions were enhanced as cold air drainage added to the stable layer formation.

In addition to nocturnal inversions, elevated inversions occurred. However, they were not present in the daytime as frequently as expected. Generally when strong subsidence was present during the day, elevated inversions persisted through the morning hours. But with subsidence, clear skies and much solar radiation dominated. Generally, afternoon inversions were broken by the strong convective cells at the surface or pushed to heights above the range of the acdar system (500 meters).

CO concentrations were then positively associated with the high occurrence of inversions and inversion-favoring meteorological conditions. Positive associations of inversions and wind direction, and

inversions and wind speeds were also found. Cloud cover was not mutually associated with wind speeds and inversions.

Acdar was a valid and valuable tool in continuously monitoring the lower boundary layer. These soundings used in conjunction with other meteorological parameters gave good insight into time and space changes of the lower atmosphere. Further work over longer time periods will yield much more information than this short study, especially in terms of seasonal changes and yearly variations. One other valuable parameter that could have been utilized was the intensity of returned echoes to the acdar. On a well-calibrated system these can give an extra dimension to the analysis in determining temperature structures in the PBL. Also invaluable would be the direct digitizing of acdar information on site for analysis later and the immediate interpretation of acdar-sensed inversions for short term forecasting requirements.

REFERENCES

- Banta, Robert, 1974: Monostatic and Biostatic Acoustic Sounding of the Atmosphere. Colorado State University, Ft. Collins, Colorado, (Unpublished).
- _____, G. Schewe, 1975: Mountain Valley Diffusion. Colorado State University, Ft. Collins, Colorado, (Unpublished).
- Battan, Louis J., 1973: Radar Observation of the Atmosphere. Univ. of Chicago Press, Chicago. 324 pp.
- Baynton, Harold W., Jerold M. Bidwell, Donald W. Beran, 1965: The Association of Low-Level Inversions with Surface Wind and Temperature at Point Arguello. J. Appl. Met., 4(4):509-516.
- Beran, A.W., C.G. Little, B.C. Willmarth, 1971: Acoustic Doppler Measurements of Vertical Velocities in the Atmosphere. Nature, 230(5290): 160-162.
- Buettner, Konrad, 1967: Proceeding of the Symposium on Mountain Meteorology. Colorado State University Atmospheric Science Paper 122, 221 pp.
- Cox, E.F., 1957: Sound Propagation in Air. Handbuch der Physik, Bd. XLVIII, pp. 455-478.
- _____, J.V. Stanasoff, B.L. Snavely, D.W. Beecher, J. Brown, 1949: Upper Atmospheric Temperatures from Helgoland Big Bang. J. Met. 6:300-311.
- Cronenwett, William T., Gene B. Walker, Rex L. Inman, 1972: Acoustic Sounding of Meteorological Phenomena in the Planetary Boundary Layer. J. Appl. Met., 11(8):1351-1358.
- Defant, F., 1951: Compendium of Meteorology. American Meteorological Society, p. 662.
- Gilman, G.W., H.B. Coxhead, F.H. Willis, 1946: Reflection of Sound Signals in the Troposphere. J. Acoustical Soc. Amer., 18(2): 274-283.
- Hall, Freeman F., Jr., 1972: Temperature and Wind Structure Studies by Acoustic Echo-Sounding. Remote Sensing of the Troposphere. V.E. Derr, ed., 632 pp.
- Holzworth, George C., 1971: Mixing Heights, Wind Speeds and Potential for Urban Air Pollution Throughout the Contiguous United States. Environmental Protection Agency, Division of Meteorology.
- Hosler, Charles R., 1961: Low Level Inversion Frequency in the Contiguous United States. Mon. Wea. Rev., 89:319-339.

- Hoxit, Lee Ray, 1973: Variability of Planetary Boundary Layer Winds. Colorado State University Atmospheric Science Paper 199, 157 pp.
- Jenne, D.E., G.R. Hilst, 1950: Meteorological and Climatological Investigation of the Hanford Works Area. General Electric, Hanford Works, Washington.
- Kallistratova, M.R., 1961: Study Instituta Fizika at Atmosferg, Atmosfernoya Turbulentnost. 203 pp.
- Little, C.G., 1969: Acoustic Methods for the Remote Probing of the Lower Atmosphere, Proceedings IEEE, 57:571-578.
- _____, 1972: Prospects for Acoustic Echo Sounding. Remote Sensing of the Troposphere, Chapter 19, V.E. Derr, ed., 662 pp.
- McAllister, L.G., J.R. Pollard, A.R. Mahoney, P.J.R. Shaw, 1969: Acoustic Sounding - A New Approach to the Study of Atmospheric Structure. Proceedings IEEE, 57:579-587.
- National Oceanic and Aeronautics Administration: Daily Weather Maps, Weekly Series, U.S. Gov't. Printing Office.
- Paddock, Markley W., 1959: Weather Types of the East Slope of the Colorado Front Range. Public Research for the Future, John Hopkins Univ. Press, Baltimore, 16 pp.
- Panofsky, Hans A., Glenn W. Brier, 1958: Some Applications of Statistics to Meteorology. Pennsylvania State Univ., University Park, Pennsylvania, 224 pp.
- Riehl, Herbert, Dirk Herkhof, 1970: Larimer County Colorado Air Pollution and Outlook. Department of Atmospheric Science, Colorado State University, Ft. Collins, Colorado, 42 pp.
- Samson, C.A., 1965: The Surface Winds at Ft. Collins. Colorado State University, Ft. Collins, Colorado, (Unpublished).
- Schroeder, Mark J., Charles C. Buck, 1970: Fire Weather. USDA Forest Service Agr. Handbook No. 360. 229 pp.
- Slade, David H. (ed.), 1968: Meteorology and Atomic Energy, 1968. Air Resources Lab., Department of Commerce, 445 pp.
- Snedecor, George W., William C. Cochran: Statistical Methods. 6th Edition, Iowa State University Press, Ames, Iowa, 593 pp.
- Sutton, O.G., 1953: Micrometeorology. McGraw Hill Book Co., New York, 330 pp.
- Whipple, F.J.W., 1923: The High Temperatures of the Upper Atmosphere on an Explanation of Zones of Audibility. Nature, 111:187.

APPENDIX A: ACDAR

A.1 Introduction

Quantitative estimates of atmospheric structures have been derived from refractively propagated sound signals for more than 50 years. For example, artificial and natural explosions have been used to estimate upper air temperatures and wind profiles (see Cox et al., 1949; Whipple, 1923; and Cox, 1957). Acoustic probing of the atmosphere, however, has only come to be recognized as an effective remote sensing technique in the last decade. Gilman, Coxhead and Willis (1946) used acoustic backscatter to study the structure of low-level temperature inversions as they affected propagation in microwave communication links. A loud-speaker source and microphone in a 60 cm parabolic dish were used as the source and receiver, and the backscattered echoes displayed on an oscilloscope. Patterns of nocturnal inversion formation and breakup, and convective plumes were observed, but the technique lay dormant.

Little development occurred until an acoustic sounding experiment was set up at the Weapons Research Establishment in South Australia in 1967 by McAllister (1968). It was established that it was possible to detect the backscattered energy from temperature fluctuations within turbulent regions in the lower atmosphere (up to 1.8 km). This backscattered energy could then be transformed into a three-dimensional chart record of height, time and intensity. Later McAllister et al. (1969) reported observations of several atmospheric structures, and Little (1969) showed the potential usefulness of acoustic sounding because of its high sensitivity, mobility, and low cost of equipment.

Before considering in detail the sounder used in this experiment, a brief summary of the related acoustical physics will be presented, followed by a description of the system and observable echo structures with examples.

A.2 Theoretical Background

Acoustic energy propagates through the atmosphere as a longitudinal wave of pressure variations (Hall, 1972). This energy is scattered and attenuated by several things including particulate matter, turbulent fluctuations of temperature and wind velocity, and sharp temperature gradients (density changes). Acoustic scattering in dry air has been described by Kallistratova (1961).

As the acoustic energy travels through the atmospheric medium, changes in the temperature and movement of the air cause changes in the velocity of the waves of energy. The velocity \vec{V} of sound deduced by a stationary observer will be the sum of the velocity of sound \vec{C} relative to the air, plus the velocity of the air \vec{W} relative to the observer (Little, 1969). Thus

$$\vec{V} = \vec{C} + \vec{W}$$

The velocity of sound in dry air is given by

$$C = 20.05 \sqrt{T} \text{ m/s}$$

where T is the absolute temperature of the air.

The sensitivity of sound velocity to changes in wind, temperature and humidity is such that the humidity fluctuations can almost always be ignored. For remote probing then the problem of separating wind and temperature fluctuations can be accomplished since the wind is a vector quantity and temperature is scalar.

As in conventional radar when the acoustic energy wave encounters an echo-rich region scattering in various directions of the sound energy occurs; the amounts and directions of scatter vary with the intensity of microscale temperature and velocity gradients, and with the scattering angle relative to the incident beam (denoted as θ). The intensity of this returned signal can be expressed as an equivalent area of "back-scattering cross section" which is defined by Battan (1973) as "the area intercepting that amount of power, which if scattered isotropically, would return to the receiver an amount of power (equal) to that actually received". This backscattered cross section $\sigma(\theta)$ can be related to the meteorological variables in the expression for the acoustic index of refraction and, if one assumes a Kolmogoroff spectrum of turbulence, the resulting relationship is (Hall, 1972; Little, 1972):

$$\sigma(\theta) = 0.055\lambda^{-1/3} \cos^2\theta \left[\frac{C_v^2}{C^2} \cos^2 \frac{\theta}{2} + .13 \frac{C_T^2}{T^2} \right] (\sin \frac{\theta}{2})^{-11/3}$$

where C_v^2 is the velocity structure parameter and C_T^2 is the thermal structure parameter defined by:

$$C_v^2 = \left[\frac{u(x) - u(x+r)}{\sigma^{1/3}} \right]^2, \quad C_T^2 = \left[\frac{T(x) - T(x+r)}{\sigma^{1/3}} \right]^2$$

Wind speed is u at position x in the positive x direction, and r is measured along the x axis.

The above equation shows that:

- 1) the scattered acoustic power resulting from assuming a Kolmogorov spectrum of turbulence varies relatively weakly with wavelength [$\sigma(\theta) \propto \lambda^{-1/3}$];

- 2) this scattered acoustic power is the sum of two terms, one due to the wind fluctuations (normalized by the mean velocity of sound in the medium) and one due to the temperature fluctuations (normalized by the mean temperature of the medium);
- 3) both wind- and temperature-scattering terms are multiplied by $\cos^2\theta$, which means that no power will be scattered at an angle of 90° ;
- 4) The wind term includes a $\cos^2\left(\frac{\theta}{2}\right)$ multiplying term, which means that the wind fluctuations produce no scatter in the backward direction ($\theta = 180^\circ$); and
- 5) both the wind and temperature components of the scatter are multiplied by a $(\sin \frac{\theta}{2})^{-11/3}$ factor, i.e., most of the scatter is in the forward direction (Little, 1969).

Figure A.1 points out the angle dependence of the acoustic backscattering cross section from a Kolmogorov spectrum of temperature and velocity fluctuations as mentioned in points 3) and 4).

In a monostatic (transmitter and receiver collocated) configuration the wind terms in $\sigma(\theta)$ disappear and the equation takes the form:

$$\sigma(\theta) = .007\lambda^{-1/3} \left(\frac{C_T^2}{T^2} \right)$$

which shows that the only fluctuations producing detectable backscattered signals are temperature gradients and fluctuations. The functional equation then for relating transmitted and received power for the monostatic system is:

$$P = P_t \sigma(\theta) \frac{Ct}{2} \frac{A}{r^2} \tau^2 G$$

where P is the received power, P_t is the transmitted power, A is the collecting area of the receiving antenna, t is the time duration of the acoustic pulse, τ is the transmittance of the atmosphere for acoustic energy from the antenna to the scattering volume, and G is a gain factor which accounts for the antenna beam pattern characteristics. For a perfect piston source this gain factor G is $\sim .24$.

The fundamental theoretical limit of the acoustic noise power is that generated by the random thermal motion of atmospheric particles (Hall, 1972). For a standard atmosphere and a 100 Hz receiver bandwidth, this is 4×10^{-19} watts (Little, 1969). The acoustic power return, P_r , for a transmitted pulse of 20 watts, may range from this theoretical noise limit, at range of 100 m to 1 km for non-turbulent atmospheric regions, to values near 50 or 70 db above the noise limit for an atmosphere with a strong thermal structure at a range of 50 m. So the acdar system must respond over a wide dynamic range as well as responding to the $\frac{1}{r^2}$ distance dependence of the echo regions.

The fundamental electronic components will be discussed in the next section in regard to the Aerovironment 300 system. The antenna design, however, should be discussed here. The acoustic antenna is an important component in the system in that it serves to collimate the transmitted signal and refocus the received echoes. A very good antenna system is one in which the transducer is actually mounted at the focus of a parabolic dish (Hall, 1972). One problem with this setup, however, is the presence of side lobes of acoustic power and the effect that environmental noise has directly on the receiver. In order to improve antenna performance, an absorbing cuff can be arranged around the antenna. This

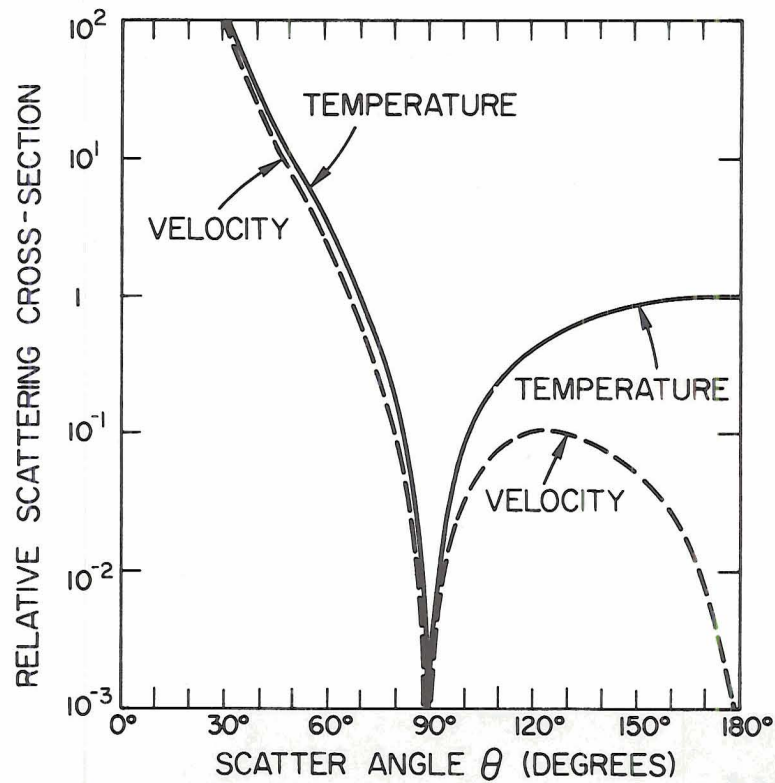


Figure A.2.1. Angle dependence of the acoustic backscattering cross section from a Komogorov spectrum of temperature and velocity fluctuations. (After Little, 1969).

gives additional side lobe attenuation and cuts down environmental noise (enough in fact to allow use in a crowded city area).

A.3 Acdar System

The Acoustic Radar (aerovironment Model 300) used in this experiment is a monostatic unit (same antenna transmitting as receiving). The system provides continuous information on a cross section of the lower atmosphere by emitting a short pulse of sound upward, "listening" to the returned echoes from temperature variations aloft, and displaying the height and relative intensities of the echo region on a chart (see Figure A.3.1).

The instrument consists of 2 functional systems: (1) An electronic module (see Figure A.3.1) which generates a short 1600 Hz electronic pulse, and then amplifies the returned signal and records it on an integral time-height record by a cycling stylus; and (2)

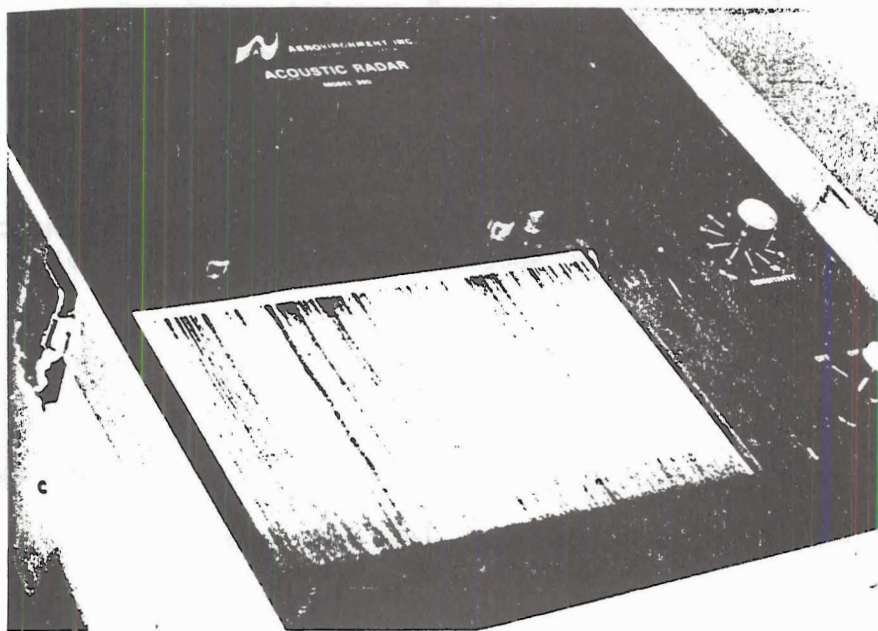


Figure A.3.1. The Aerovironment Model 300 module showing the sensitivity and power on controls. The chart paper is shown in its normal position.

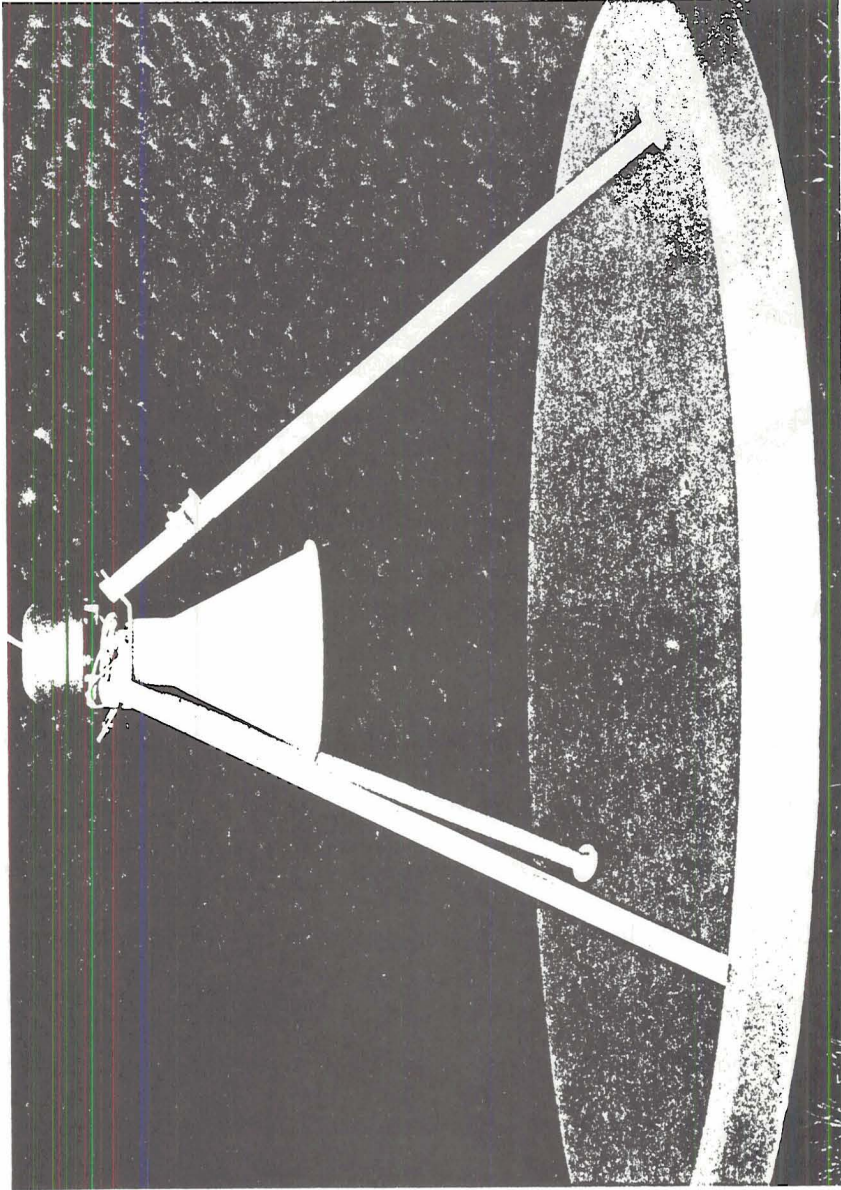


Figure A.3.2. A side view of the antenna transducer, and horn configuration.

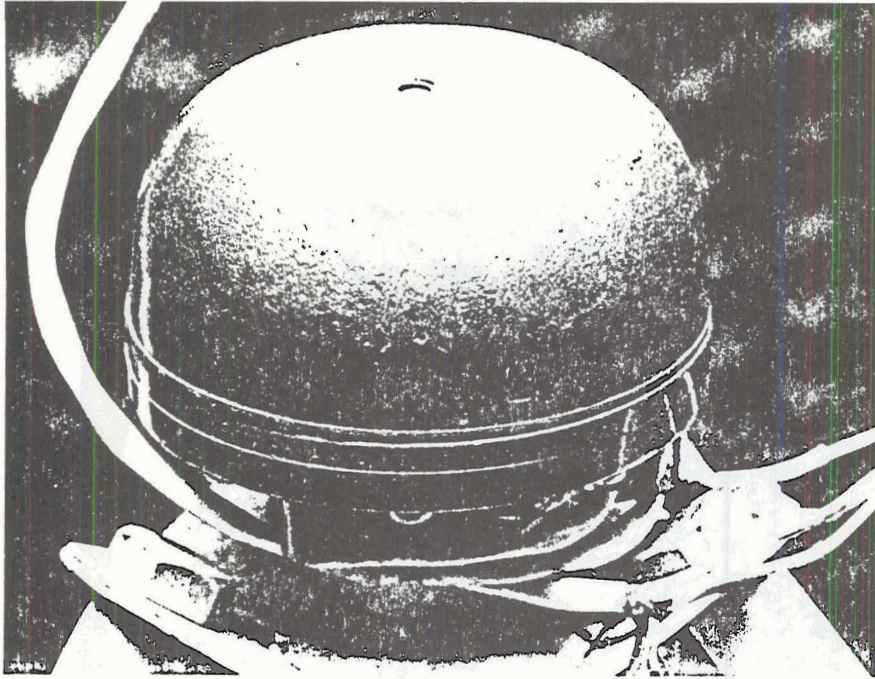


Figure A.3.3. Acoustic transducer.

an antenna (Figure A.3.2). The antenna contains an acoustic transducer (see Figure A.3.3) which generates the sound pulse and receives the echoes. Coupled closely to the transducer is a fiberglass cone (see Figure A.3.4) which helps direct the sound pulse to the 125 cm parabolic reflector. This reflector (see figures A.3.5 and A.3.6) directs the sound pulses vertically into the atmosphere and helps refocus the incoming received echoes back from the scattering region.

Because of the nature of sound waves (audible) and of antenna design, another needed part of the acoustic system for proper usage is an acoustic enclosure. This enclosure helps cut down side lobe directed sound pulses (not the main beam), shields the antenna

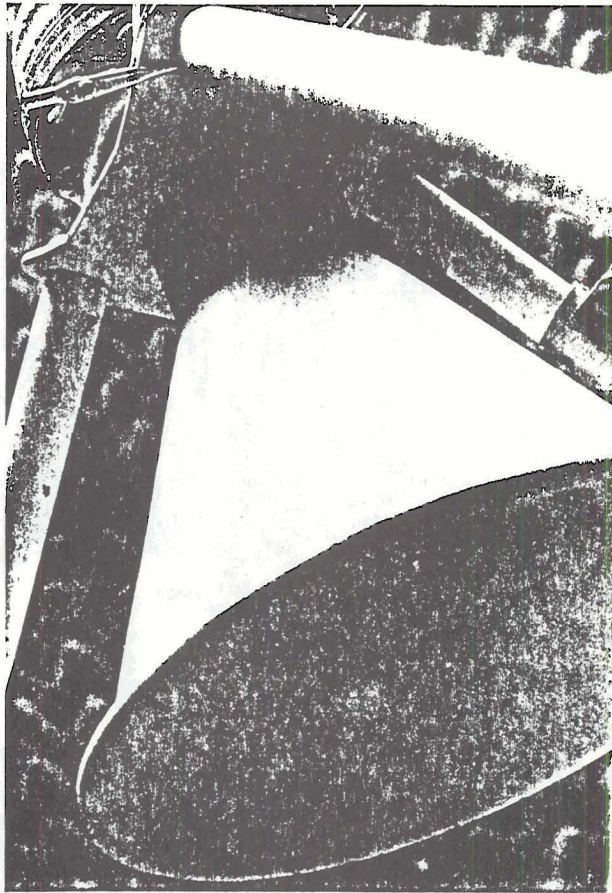


Figure A.3.4. Fiberglass cone coupled to transducer.

from ambient noise (industry, autos, etc.), and aids in keeping out local fauna (including the two-legged variety). The acoustic enclosure (see Figure A.3.6) is made up of five 122 x 244 cm panels, each of which is a 13 mm fir plywood (for structural rigidity and sound attenuation), with 15 cm-thick convoluted urethane foam (to damp out internal reflections) glued to it (see Figure A.3.7). The five panels lock into a pentagonal enclosure around the antenna (see Figure A.3.8) which provides for the shieldings listed above. A 60 m coaxial cable (see Figure A.3.8)

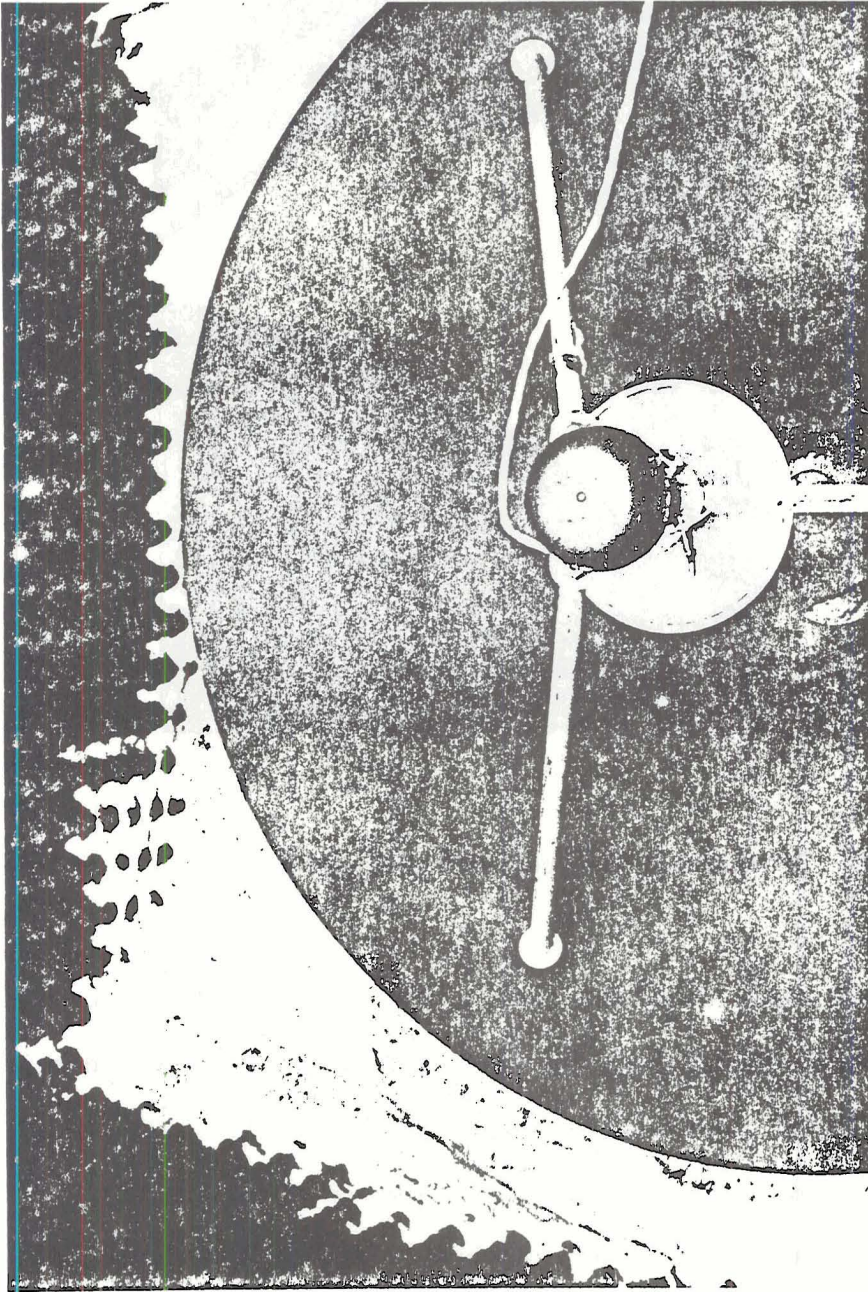


Figure A.3.5. Top view of the acoustic radar antenna which shows the direction that acoustic waves are reflected into the atmosphere.

links the transducer to the electronic module, which must be kept out of severe weather conditions to protect the electronics (especially in extreme cold and wet periods).

The various changeable parameters of the Aerovironment Model 300 include: (1) a choice of either the 500 m or 1 km height scale; (2) variations of the transmitted pulses; (3) variations in the bandwidth of received echoes; (4) an adjustable amplifier ramp start; and (5) a sensitivity potentiometer to change the amplification factor of the received echoes. The transmitted pulse lengths are 50 ms, 100 ms, and 200 ms corresponding to 35w, 70w,

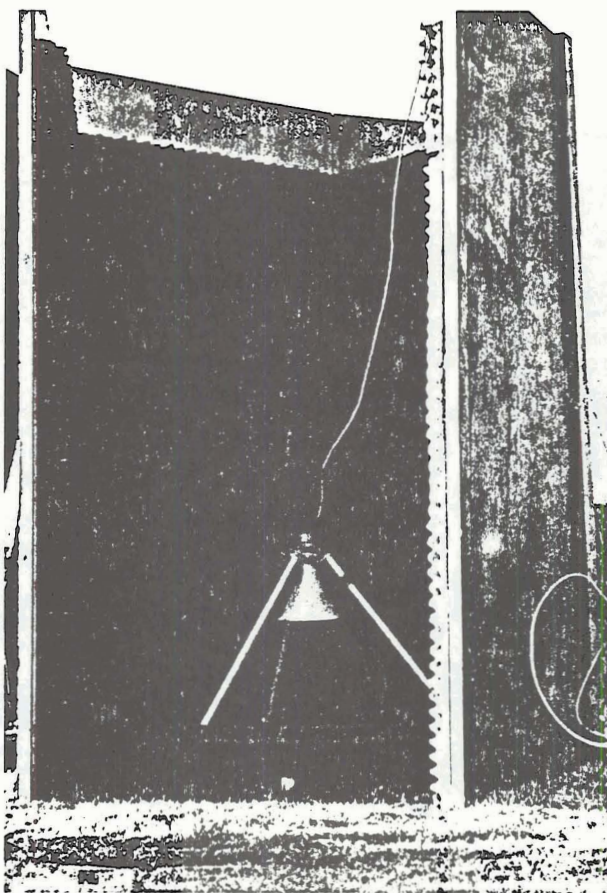


Figure A.3.6. Side view of the acoustic enclosure with one panel removed. Also shown is the urethane foam on the plywood.

and 140w of power (see Figure A.3.9). The short pulse lengths give the best resolution, but at the expense of the signal to noise ratio, while the longer pulses give greater energy input, reducing the signal to noise ratio, but consequently reducing the spatial resolution. Noise rejection is aided by the use of the filtering bandwidths. The NARROW, WIDE, and MEDIUM positions on the toggle (see Figure A.3.9) correspond to nominal system bandwidths of 20, 80, and 40 Hz centered at 1600 Hz and measured to the -3dB points. The NARROW band gives the best noise rejection, whereas the WIDE band processes a maximum of echo strength but

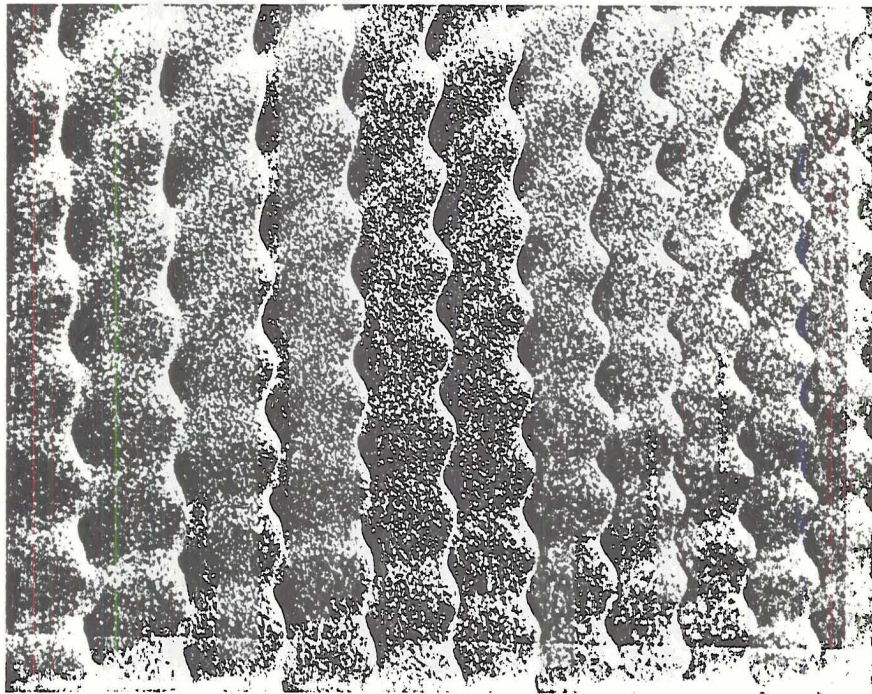


Figure A.3.7. Convoluted urethane foam used for damping.

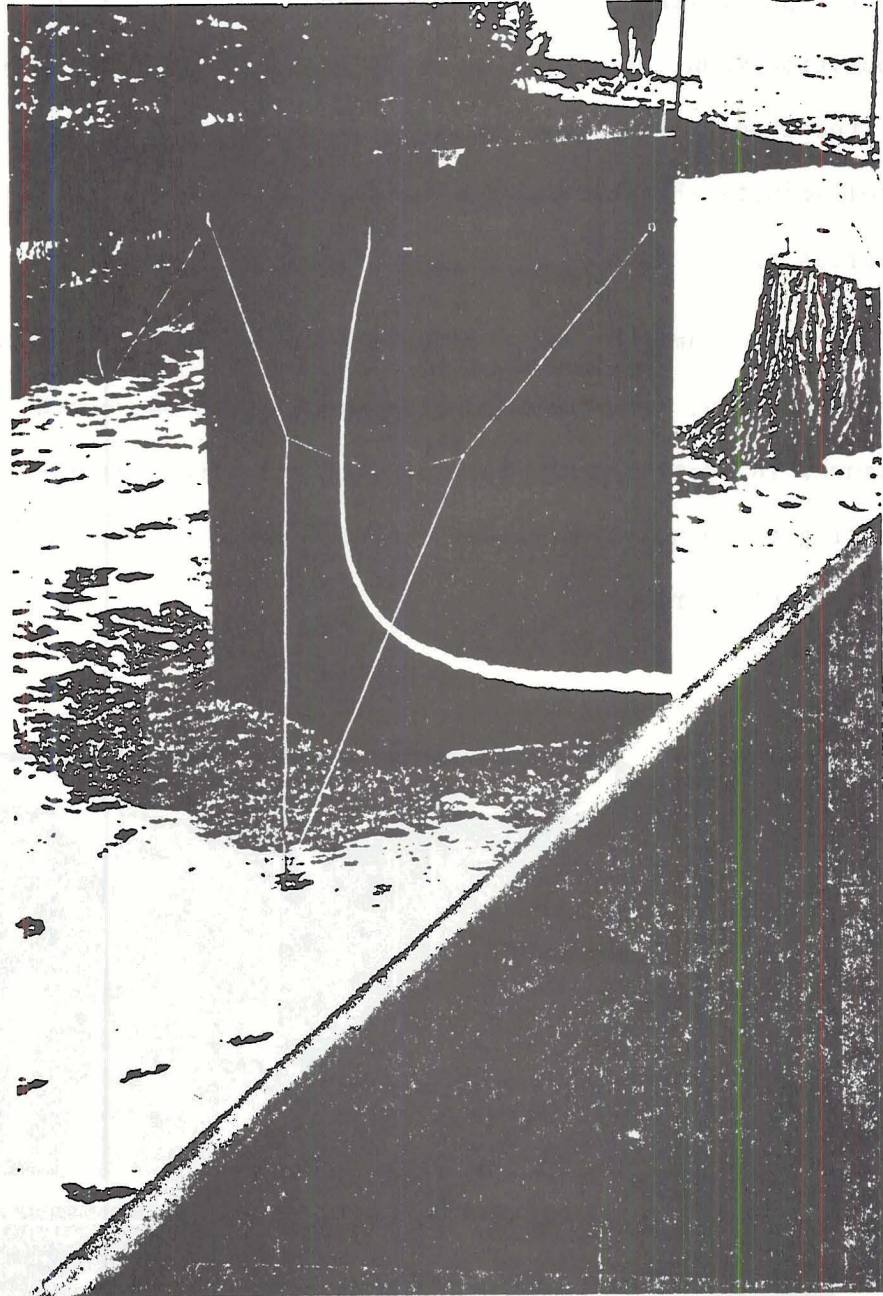


Figure A.3.8. Locked together acoustic enclosure in operational position. Coaxial cable which runs from the transducer to the electronic module.

is only usable in a noise free environment. The other control above the pulse lengths is the RAMP START. This varies the starting position when the amplifier actually begins to process echoes from the atmosphere (see Figure A.3.9). Finally the sensitivity control adjusts the darkness on the chart of the received echo and varies from 1 to 10 (see Figure A.3.1).

Other than ambient noise affecting the acdar charts by darkening them, rain, snow and wind also cause darkened records (shown in figures in Section A.4). Interpreting acdar records involves separating these non-temperature echoes from inversion and convective plume returns.

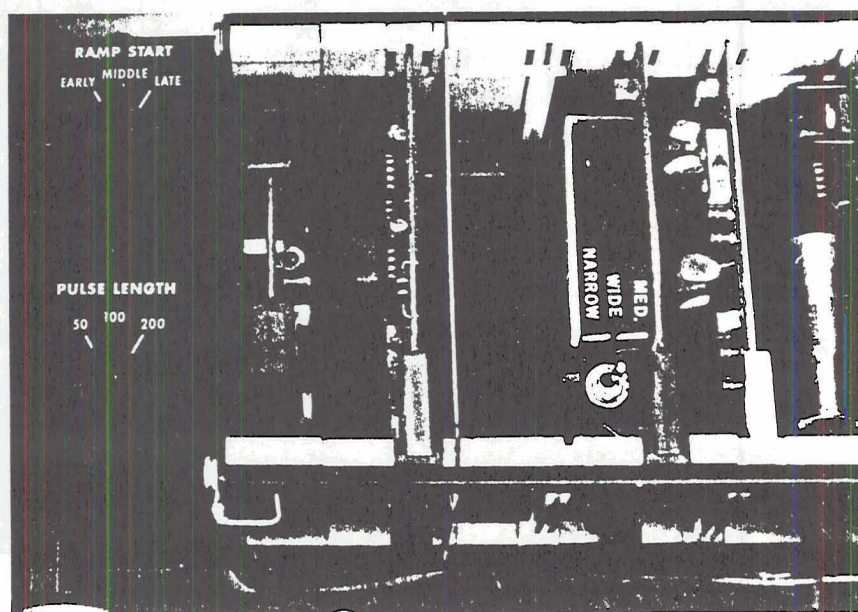


Figure A.3.9. The pulse length control is in the lowermost left hand corner. Above that is the RAMP control switch. To the right is the toggle which changes the filtering bandwidth for receiving echoes. Also shown are some of the electronics of the system which are mainly on boards for easy removal.

A.4 Monostatic Acdar Observable Echoes

Samples of observed acdar echoes are shown in Figures A.4.2 through A.4.8. These samples include thermal plumes, a radiation inversion, an elevated inversion, a subsidence inversion, a frontal inversion and an episode where a nocturnal inversion is lifted as thermal plumes push it up and mix it effectively with environmental air until it dissipates.

An acdar system operating in the monostatic mode, as mentioned before, detects only C_T , the thermal structure parameter. In a neutral (or dry adiabatic) atmosphere, C_T values are very small no matter how much mechanical turbulence is present. This is because air parcels displace vertically by velocity perturbations conserve their potential temperature and maintain the same temperature as their dry adiabatic environment. Thus, in a neutral, horizontally homogeneous boundary layer, velocity eddies do not produce thermal eddies. Large acoustic signal returns do occur in unstable conditions, however, owing to the organization of convection into structures called "thermal plumes", which have a very pronounced thermal eddy structure. Large returns are also found under stable conditions, where the presence of mechanical turbulence does produce large values of C_T because of the large variations of potential temperature with height (Banta, 1974). The different phenomena mentioned above are summarized along with changes in related parameters and acdar record changes in the following figures:

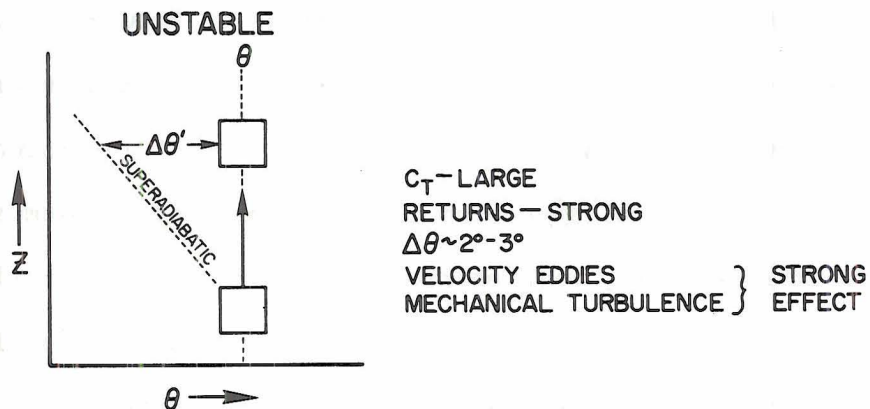


Figure A.4.1a. Superadiabatic atmosphere: Convective plumes from surface warming present with sharp temperature gradients in a short distance. Dark echo traces appear looking like spikes with dif-fused tops (where environmental air mixes in sufficiently).

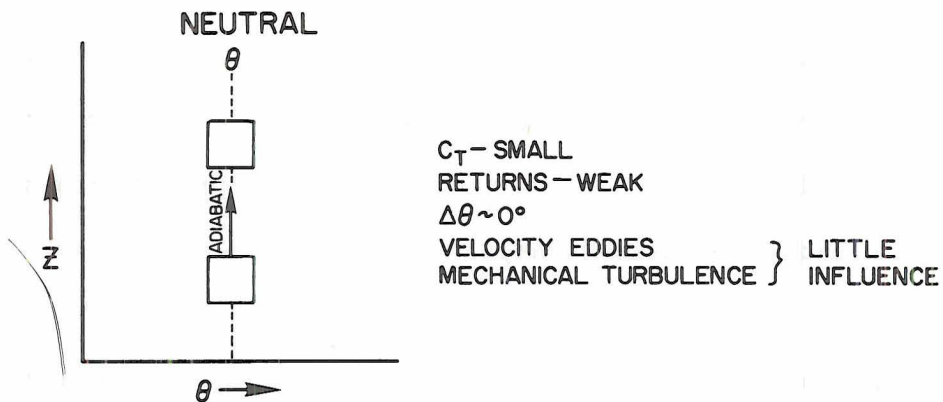


Figure A.4.1b. Neutral atmosphere: Atmosphere is in neutral buoyant state. Little or no returns on acdar chart output.

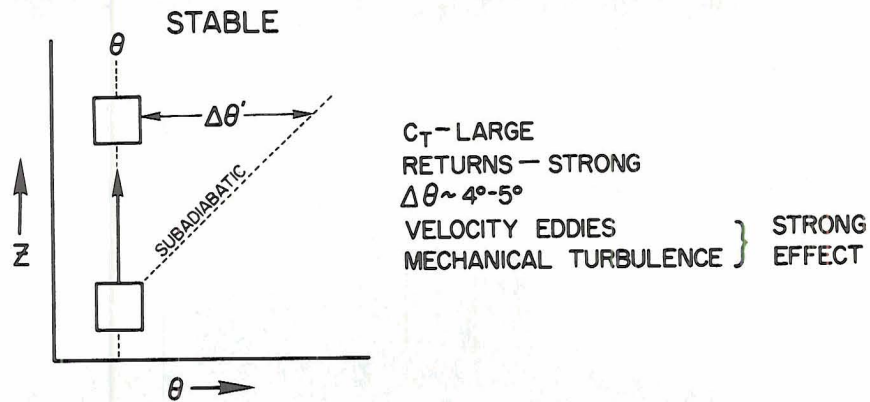


Figure A.4.1c. Stable atmosphere: Backscatter from microscale, turbulent temperature fluctuations which are caused by: 1. the rapid increase of potential temperature with height through the stable inversion layer; and mechanical eddies (induced by terrain) which can produce thermal eddies with large temperature variations; 2. the abundance of turbulent kinetic energy in the layer associated with large wind shears that generally occur across inversions.

Thermal Plumes

A thermal plume is the rise of a heated (solar surface heating), non-uniform air parcel from the ground up into the planetary boundary layer (Hali, 1972). The strongest temperature fluctuations and therefore, the regions of maximum acoustic return, are found in the areas of maximum shear between rising warm air and sinking cool air (Beran, et al., 1971). The temperature fluctuations in the core of the convective plume are also much greater than the regions between plumes. In Figure A.4.2 the dark spike-like traces near the bottom are thermal plume structures. McAllister (1969) has shown that the light areas

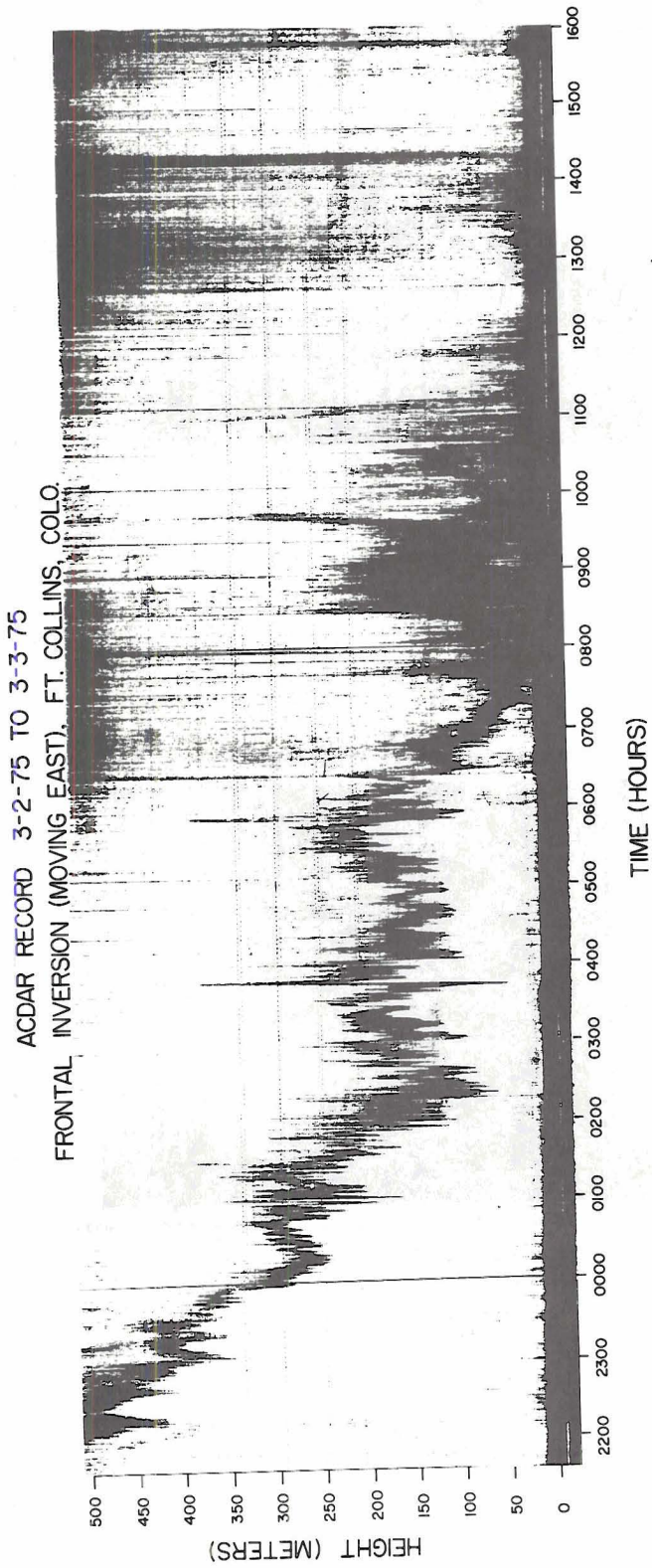


Figure A.4.7. Frontal inversion.

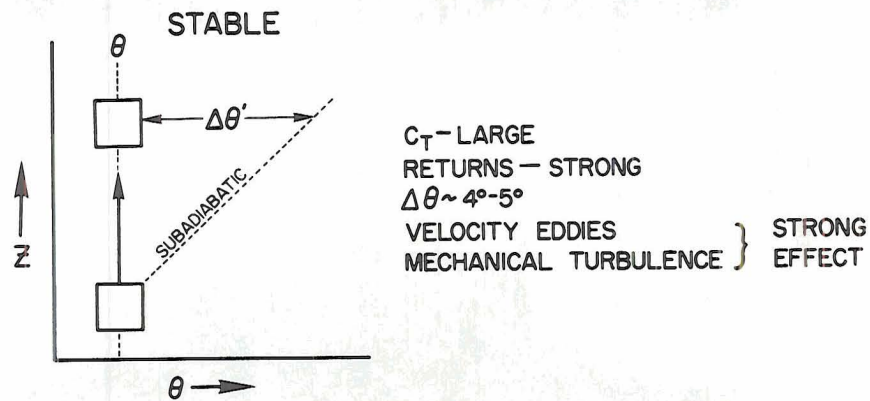


Figure A.4.1c. Stable atmosphere: Backscatter from microscale, turbulent temperature fluctuations which are caused by: 1. the rapid increase of potential temperature with height through the stable inversion layer; and mechanical eddies (induced by terrain) which can produce thermal eddies with large temperature variations; 2. the abundance of turbulent kinetic energy in the layer associated with large wind shears that generally occur across inversions.

Thermal Plumes

A thermal plume is the rise of a heated (solar surface heating), non-uniform air parcel from the ground up into the planetary boundary layer (Hali, 1972). The strongest temperature fluctuations and therefore, the regions of maximum acoustic return, are found in the areas of maximum shear between rising warm air and sinking cool air (Beran, et al., 1971). The temperature fluctuations in the core of the convective plume are also much greater than the regions between plumes. In Figure A.4.2 the dark spike-like traces near the bottom are thermal plume structures. McAllister (1969) has shown that the light areas

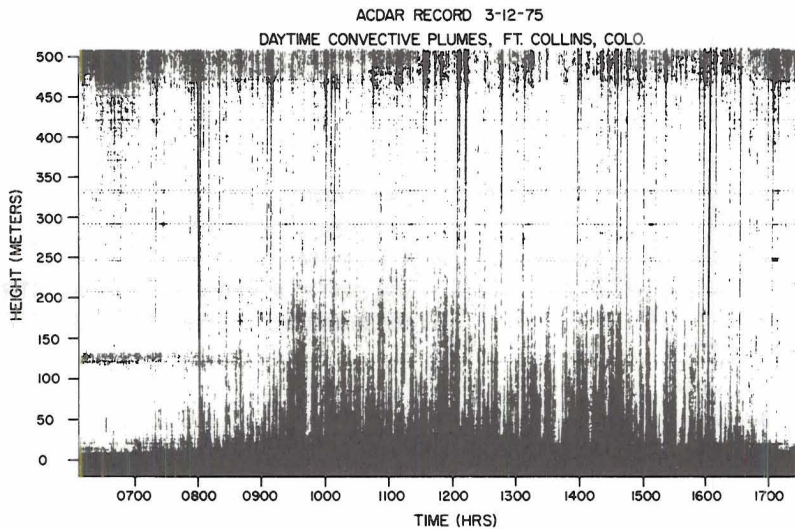


Figure A.4.2. Daytime convective plumes.

between plumes correspond to temperature traces that are relatively smooth with no rapid fluctuations. Inside the maximum gradient areas, however, where sounder returns are strong, temperatures were warmer and fluctuated rapidly.

Inversions

Inversions show up as dark, often layered, traces on the acdar display. Acoustic energy is scattered from inversion layers not because of temperature gradients, but because of the presence of microscale, turbulent temperature fluctuations within the inversion (Hall, 1972). Some of the reasons these microscale temperature fluctuations occur were alluded to in Figure A.4.1c. The development and structure of many kinds of inversions can be monitored and studied on a continuous real-time basis using the acdar system. The recordings from acdar consistently correspond well with radiosonde data and so can be used together to monitor lower atmospheric phenomena.

In Figure 2.1 presented in a previous chapter, the dark band aloft is an elevated daytime inversion. Other examples of inversion layers are shown in Figures A.4.3 and A.4.4 where examples of a surface nocturnal layer and a subsiding elevated layer can be seen. The nocturnal surface layer in Figure A.4.3 is typical after sunset on a cold, clear winter evening in Colorado, in that surfaces cool rapidly. The inversion is the dark layer deepening from about 1900 hours to 0300 where wind shear and turbulence cause a more diffuse layer to occur. In Figure A.4.4, the strong subsiding air is evident (and has been correlated to a high pressure system and little vertical motion over Fort Collins) and can be seen as a sinking dark band from around 0200 to 0900 where thermal activity begins to cause oscillating motions in the layer. Strong subsiding air layers like this are those that are most desirable to monitor in terms of air pollution forecasting.

ACDAR RECORD 1-31-75 TO 2-1-75
GROWTH OF NOCTURNAL RADIATION INVERSION, FT. COLLINS, COLO.

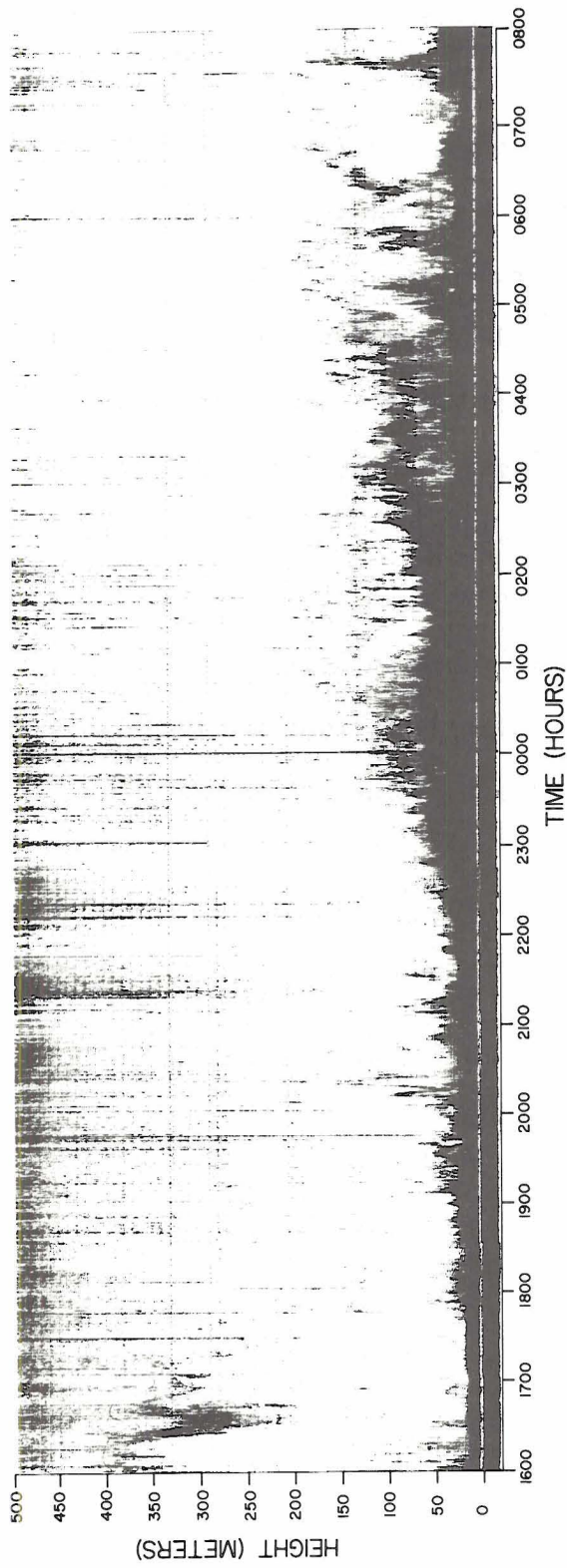


Figure A.4.3. Nocturnal radiation inversion.

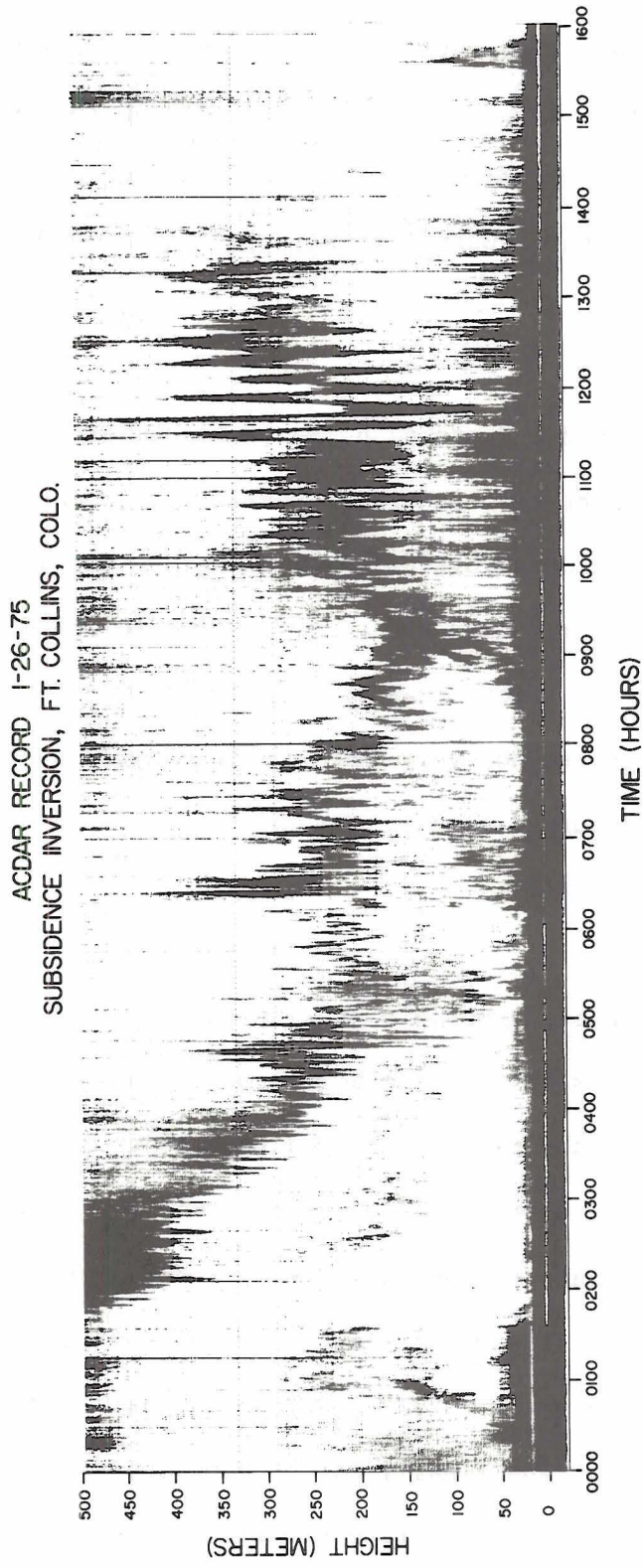


Figure A.4.4. Subsidence inversion.

Fog

Figure A.4.5 shows the acoustic echoes which were attributed to the scattering from small scale temperature fluctuations at the top of a convective layer where fog formed. The dark vertical spikes near the bottom of the chart are the result of thermal surface activity, while the fog layer is the dark band running from 150 meters at 0900 hours to 350 meters at 1500 hours.

Wind

The effects of wind and industrial noise (automobiles, airplanes, heavy industry, etc.) can be seen on almost every acdar record shown. Most appear as solid black dark vertical traces that do not last very long. Figure A.4.6, however, shows the effects of a prolonged windy period such as a chinook or strong downdraft. It is obvious that under such conditions soundings are not very fruitful in monitoring the lower atmosphere in that the returned signals are completely wiped out by the ambient noise.

Frontal Inversion

As cold air moves under warmer air as with a cold front, the interface between the two layers of air is a region of strong mixing of the two air masses. This intense temperature and turbulent structure is a strong scatter of acoustic energy and so can be seen with acdar. Figure A.4.7 shows such an interface between a warm layer of upper air and a cool layer of surface air. The layer slowly decreases with height as the cold front (identified on the 3/3/75 surface analysis 0500 MST) backs up slowly to the east and finally passes completely by about 1100. The traces after this time are convective plumes.

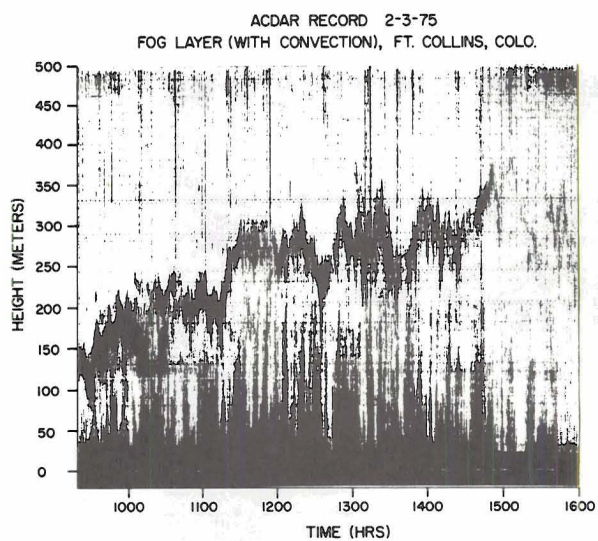


Figure A.4.5. Fog

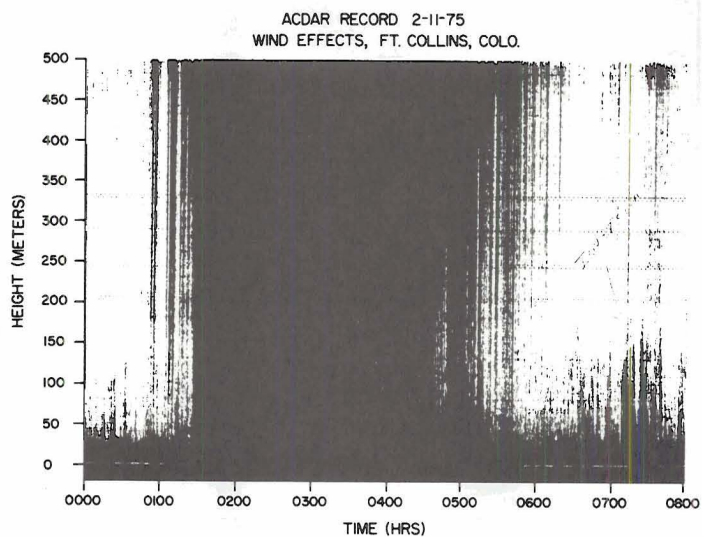


Figure A.4.6. Wind

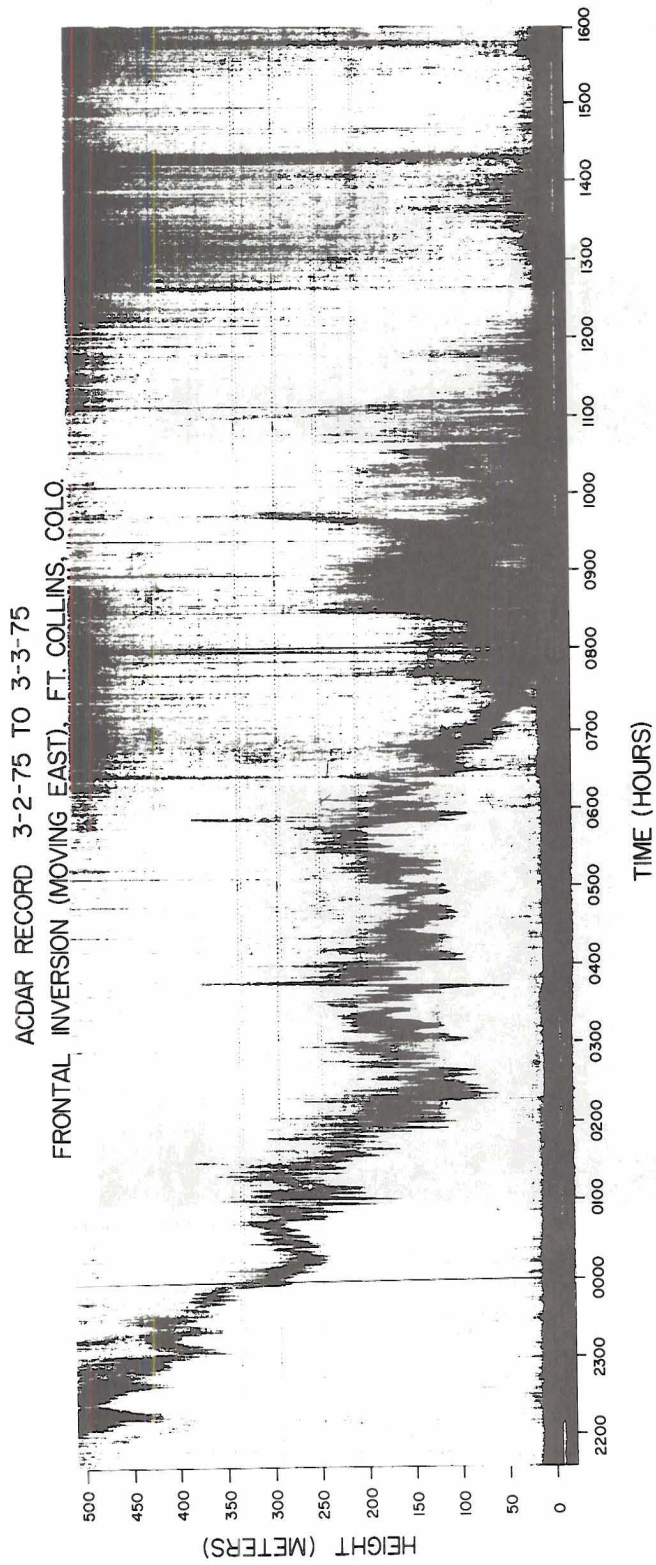


Figure A.4.7. Frontal inversion.

Diurnal Cycle (Winter)

As a final example of observable echoes in Fort Collins, a diurnal cycle is shown in Figure A.4.8. From 0800 to 1500 convective plumes can be seen with a brief elevated inversion between 1000 and 1100 near 200 meters. Slightly after the thermal plumes die down at 1500 the surface begins to cool and a layer of stable air builds up. At 1900 hours the top of the layer "blows off" as a result of wind shear but the stable layer remains intact at the surface, and the process continues through the night. The dark traces starting at 0630 are a result of increased wind speeds and morning traffic.

ACDAR RECORD 12-2-74 TO 12-3-74
TYPICAL DIURNAL CYCLE AND GROWTH OF NOCTURNAL BOUNDARY LAYER, FT. COLLINS, COLO.

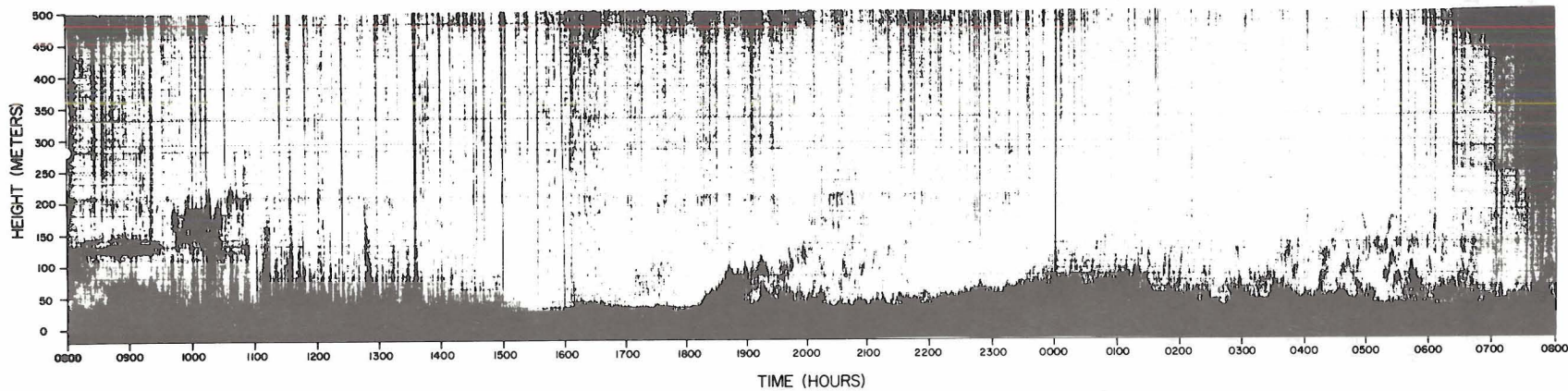


Figure A.4.8. Diurnal inversion and convective plume cycle.

APPENDIX B: χ^2_{R1} and χ^2_{RC}

Two χ^2 methods were used in Chapter 4. One method is actually "a test for homogeneity". This will be referred to as the χ^2_{R1} test. The other method is to use two inversion categories, "inversion" and "no inversion", so that combined they equal the number of wind cases from a given direction. This will be called the χ^2_{RC} test. Representative examples of each contingency table with associated equations are given in the following tables. The null hypothesis (with its alternate hypothesis) for each test is:

$H_0(\chi^2_{R1})$: An inversion has equal probability of being associated with all wind directions.

$H_\alpha(\chi^2_{R1})$: An inversion has unequal probability of being associated with all wind directions.

$H_0(\chi^2_{RC})$: Inversion and not inversion occurrence is not related to wind direction.

$H_\alpha(\chi^2_{RC})$: Inversion and not inversion occurrence is related to wind direction.

TABLE B.1

χ^2_{R1} All Inversions February 1975

	Wind Direction (Degrees)						TOTALS 672=m
	0-60	60.1-120	120.1-180	180.1-240	240.1-300	300.1-360	
Wind Cases	54	81	112	73	65	213	74
Inversions OBS	29	33	71	45	46	163	67
EXP	36.48	54.72	75.67	49.32	43.91	143.90	49.99
							454
							453.99

$$\hat{p} = \frac{\sum \text{Inversions}}{\sum \text{Cases of Wind}} = \frac{\sum o_i}{\sum w_i}$$

$$e_i = w_i \hat{p} \quad \hat{p}_i = \frac{o_i}{w_i}$$

$$\chi^2_{R1} = \sum_{i=1}^n \frac{(o_i - e_i)^2}{e_i}$$

d.f. = 6 $\alpha = .05$

$\chi^2_6 = 12.59$ critical region is $\chi^2_{R1} \geq \chi^2_6$

$\chi^2_{R1} = 19.24$ Reject Null Hypothesis

	0-60	60.1-120	120.1-180	180.1-240	240.1-300	300.1-360	VARIABLE
\hat{p}_i	.537	.407	.634	.616	.707	.765	.905

- α' - confidence level
- o_i - observed inversion cases in cell
- e_i - expected inversion cases in cell
- \hat{p} - probability total sample
- w_i - observed wind cases in each cell
- \hat{p}_i - probability of inversion in each cell
- n - total sample size
- d.f. - degrees of freedom

TABLE B.2

 χ^2_{RC} All Inversions February 1975

Wind Direction (Degrees)								
Obs (Exp)	0-60	60.1-120	120.1-180	180.1-240	240.1-300	300.1-360	VARIABLE	TOTALS
Inversions	29 (36.48)	33 (54.72)	71 (75.67)	45 (49.32)	46 (43.91)	163 (143.90)	67 (49.99)	454 (453.99)
No Inversions	25 (17.52)	48 (26.28)	41 (36.33)	28 (23.68)	19 (21.09)	50 (69.10)	7 (24.01)	218 (218.01)
TOTALS	54 (54.00)	81 (81.00)	112 (112.00)	73 (73.00)	65 (65.00)	213 (213.00)	74 (74.00)	672

$$E_{ij} = \frac{R_i C_j}{n}$$

$$\chi^2_{RC} = \sum_{i=1}^n \frac{(O_{ij} - E_{ij})^2}{E_{ij}}$$

$$d.f. = 6 \quad \alpha = .05$$

$$\chi^2_6 = 12.59 \quad \chi^2_{RC} \geq \chi^2_6 \text{ is the critical region}$$

$$\chi^2_{RC} = 59.32 \quad \text{Reject Null Hypothesis}$$

R_i - row total

C_j - column total

n - total sample size

d.f. - degrees of freedom

O_{ij} - expected in each cell (in parenthesis)

α - confidence level

